# Stress Assisted Diffusion in Polymers

Thesis by

Sy R. Shimabukuro

In Partial Fulfillment of the Requirements

for the Degree of

Doctor of Philosophy

California Institute of Technology
Pasadena, California

1991

(Submitted August 9, 1990)

# Acknowledgments

There are many undertakings that, though one person may receive all the accolades, require the efforts of a great number of people and I feel a Doctorate in Philosophy is one of them. In this small section I would like to acknowledge a few of the people that have made my stint here at Caltech a memorable one.

First and foremost I would like to acknowledge my advisor, Professor Knauss, whose patience, time, and energy has finally gotten me out of here.

To the new and old members of The Society of Professional Students (SOPS) who provided a respite from the work at Caltech. Thank you Paul and Linda Nowak, George Yates, and Bill and M.P. Donlon for all the fun times we had together.

Moving away from home can sometimes be a lonely experience and I would like to give a big "mahalo" to my displaced Hawaiian friends for helping me make the transition to the mainland lifestyle. A special "Aloha" to Keith and Kris Abe, Wini Otaguro, Carol Aoki, and Ruby Takushi for being there when I needed a hand.

Finally I would like to thank my family, especially my parents, for the support they have given me over these many years.

# Abstract

A model for diluent diffusion into a polymer which includes mass flux contributions from both a concentration gradient and pressure gradient is proposed. The pressure is a result of the diluent-induced swelling of the polymer and a constitutive law is incorporated that is analogous to that used in nonlinear thermo-viscoelasticity. The concept of free volume is used as the common basis to relate the relaxation processes for a viscoelastic material to the diffusion of the diluent molecules. The resultant strains (swelling) and stresses must satisfy a strain-displacement relationship and equilibrium equations, respectively.

The governing equations are solved using the finite element technique. An iterative scheme is developed to solve the stress-coupled diffusion process as two separate problems: one for the diffusion process and one for the mechanical response. The two problems are solved individually where the solution from one problem is used as input to the other.

Numerical simulations are performed for both one-dimensional and two-dimensional axisymmetric problems in which the diluent is assumed to diffuse along the axis of the cylinder. The results suggest that certain anomalous experimental diffusion results can be explained through the relaxation behavior of the polymer. There are indications that Case II behavior is included in the model by an appropriate choice of material parameters. The results also indicate that typical diffusion experiments may be inadequate to uniquely define the physical model for the diffusion process when more than one type of diffusion driving force exists.

# Table of Contents

# List of Figures

# List of Tables

# Introduction

The use of polymeric materials for structural applications has increased significantly over the past few decades. In connection with composite materials, high specific strength and stiffness allow for significant weight savings over comparable metallic parts, an attractive property for military applications (as well as in the civil sector; e.g., cars). Unlike metals, polymeric properties are often poorly characterized and not well understood even in laboratory conditions. Matters are complicated by the fact that in addition to being time dependent the properties are often affected by environmental conditions.

An illustration of possible environmentally induced problems arises in the use of polymers in structural adhesives. Adhesives are an attractive fastening alternative since the use of rivets or bolts requires that holes be introduced into the parts being joined. Introducing a hole may damage the part, for instance composite parts may delaminate when fastener holes are manufactured. Also the resulting hole will form a stress concentration region around the fastener. This is not to say that bonded joints are trouble free, the adhesion process often introduces large residual stresses and strains within the bond joint because of the elevated temperatures that are sometimes needed to cure the adhesive. Such residual stresses and strains will limit the ultimate load which the joint can sustain.

Besides residual stresses (which are basically related to manufacturing issues), if the joint is used in an environment where large temperature

variations occur or where diluents such as moisture or solvents can be absorbed, plasticization of the adhesive can occur, further reducing the ultimate load that the joint can sustain. Hence the service environment of the joint must be considered when one examines the suitability of polymers for adhesion purposes. This study will focus primarily on the environmentally induced interactions between the diluent (solvent) and the stress state in the polymer.

The effect of the diluent on the polymer is by and large dependent on its concentration. Many studies[8,15] have been performed on "conditioned" polymers (polymers containing a uniform concentration of diluent) which demonstrate the various changes in the mechanical behavior of a polymer. A particularly important result is that the concentration of the diluent may drastically change the relaxation times characterizing the time-dependent polymeric properties. As a consequence when characterizing the long-term behavior of a polymeric structure, both the rate and amount of diluent that is absorbed needs to be taken into account. Such an accounting would require that the diffusion process of the diluent-polymer system be mathematically modelled in some fashion, usually through a diffusion-type equation.

The absorption of a diluent into a polymer usually occurs over a relatively long time span, as compared to thermal conduction, and this fact often creates special problems in predicting or even studying the diffusion behavior. Depending on the state of the polymer different diffusion behaviors are observed. For rubbery polymers (polymers which are in an environment above its glass transition temperature, $T_g$) the diffusion can very often be described by a Fickian-like diffusion process. Glassy polymers

(polymer which are below their $T_g$) which undergo significant stiffness relaxation typically exhibit diffusion processes which are termed "anomalous" or "non-Fickian" and are often not readily explainable. Also other researchers[12] have shown that the stress level affects both the rate of diffusion as well as the final solvent uptake. These issues complicate the problem since it appears that, while the diluent concentration affects the mechanical properties, the mechanical response of the polymer will in turn affect the diffusion process. Hence the diffusion process (the rate of absorption of the diluent) and the mechanical response (the resultant displacements, stresses, and strains due to diluent) of the polymer are coupled together.

By providing a model for the diffusion process, which tries to incorporate current ideas on nonlinear viscoelastic material behavior, this study attempts to explain some of the experimental observations found in the literature. The study is broken down into four chapters which will illustrate the model that is being studied. Chapter 1 deals with the mechanical response of the polymer due to the diluent. There a constitutive law relating the stresses, strains, and diluent concentration is proposed which draws on the ideas of nonlinear thermo-viscoelasticity.

The diffusion process is addressed in Chapter 2 and modifications are made to Fick's first law to incorporate the possibility of a pressure gradient induced mass flux. To include the effect of the mobility of the diluent and polymer molecules the diffusion coefficient is modified by a free volume based term. A basic "feel" for the terms in the proposed mass flux equation is provided by a model that portrays the diluent molecules as "balls" and the polymer molecules as "chains."

Numerical simulations of the governing equations, as proposed in the two previous chapters, are delineated in Chapter 3. The nonlinearities of the problem create difficulties in testing the computer code, but included are several numerical test cases with the aim of validating that the code is operating properly. Finally the numerical solutions to several problems involving different levels of coupling between the diffusion process and the mechanical response, material properties, and boundary conditions are presented.

Chapter 4 discusses the ramifications of the results derived in Chapter 3 and provides concluding remarks on the applicability of the proposed model.

# Chapter 1
# Mechanical Response

## 1.1 Introduction

As a diluent diffuses into a polymer, swelling strains are generated and displacement constraints lead to the development of internal, normally self-equilibrating stresses. Because the mechanical response of swelling systems is similar to materials undergoing thermal expansion, the governing field equations and constitutive behavior for diluent swelling are analogously modelled to follow nonlinear thermoviscoelasticity. In the following, the governing equations for the mechanical response of a polymer undergoing diluent swelling will be presented and discussed.

## 1.2 Field Equations

Consider a body undergoing a deformation with a displacement field, $\underset{\sim}{u}(\underset{\sim}{x},t)$, such that $\|\nabla \underset{\sim}{u}(\underset{\sim}{x},t)\| << 1$. From these deformations an infinitesimal strain field, $\underset{\sim}{\varepsilon}(\underset{\sim}{x},t)$, is defined as

$$\underset{\sim}{\varepsilon}(\underset{\sim}{x},t) = \frac{1}{2}\left( \nabla \underset{\sim}{u}(\underset{\sim}{x},t) + \nabla \underset{\sim}{u}(\underset{\sim}{x},t)^{T} \right); \qquad \|\nabla \underset{\sim}{u}(\underset{\sim}{x},t)\| << 1 \tag{1.1}$$

The strain field and diluent concentration field, $c(\underset{\sim}{x},t)$, would in general create a stress field in the body. These three quantities, stress, strain, and diluent concentration, are related to one another through a constitutive model which will be discussed in the next section.

The resultant stress field, $\underset{\sim}{\sigma}(\underset{\sim}{x},t)$, must also satisfy the equations of equilibrium

$$\nabla \cdot \underset{\sim}{\sigma}(\underset{\sim}{x},t) + \underset{\sim}{b}(\underset{\sim}{x},t) = \underset{\sim}{0} \tag{1.2}$$

where $\underset{\sim}{b}(\underset{\sim}{x},t)$ are body forces potentially applied to the body.

## 1.3 Constitutive Behavior

The computations presented here draw on a modified nonlinear small strain viscoelastic model as the constitutive law for the stress-strain behavior of the polymer. The polymer is assumed to follow a time shifting behavior as a result of the diluent in a manner that is similar to that of thermo-rheologically simple materials (TRS); the time shifting is assumed to be described through the concept of free volume.

Amorphous-type (noncrystalline) polymers typically exhibit TRS behavior and it is for this class of materials that the following constitutive law is expected to hold. A few examples of amorphous polymers are polyvinylacetate (PVAc), polystyrene (PS), polymethacrylate (PMA), and polymethylmethacrylate (PMMA).

### 1.3.1 Decomposition of the Stress and Strain Fields

Within the constitutive model two field quantities are used extensively: the pressure, $P(\underset{\sim}{x},t)$, and the (strain) dilatation, $e(\underset{\sim}{x},t)$. The pressure and dilatation are related to the scalar field of the isotropic component de-

fined by a decomposition of the stress and strain fields, respectively. The decompositions are

$$\underset{\sim}{\sigma}(\underset{\sim}{x},t) = \underset{\sim}{s}(\underset{\sim}{x},t) + \tfrac{1}{3} tr\, \underset{\sim}{\sigma}(\underset{\sim}{x},t)\underset{\sim}{I} = \underset{\sim}{s}(\underset{\sim}{x},t) - P(\underset{\sim}{x},t)\underset{\sim}{I} \tag{1.3}$$

and

$$\underset{\sim}{\varepsilon}(\underset{\sim}{x},t) = \underset{\sim}{e}(\underset{\sim}{x},t) + \tfrac{1}{3} tr\, \underset{\sim}{\varepsilon}(\underset{\sim}{x},t)\underset{\sim}{I} = \underset{\sim}{e}(\underset{\sim}{x},t) + \tfrac{1}{3} e(\underset{\sim}{x},t)\underset{\sim}{I} \tag{1.4}$$

where $\underset{\sim}{s}(\underset{\sim}{x},t)$ and $\underset{\sim}{e}(\underset{\sim}{x},t)$ are known respectively as the deviatoric stress and strain fields. In terms of the above decomposition, the pressure is related to the stress field by

$$P(\underset{\sim}{x},t) = -\tfrac{1}{3} tr\, \underset{\sim}{\sigma}(\underset{\sim}{x},t) \tag{1.5}$$

while the dilatation is represented as

$$e(\underset{\sim}{x},t) = tr\, \underset{\sim}{\varepsilon}(\underset{\sim}{x},t) \tag{1.6}$$

The dilatation can be further divided into a swelling strain, $e^{C}$, and a mechanical strain, $e^{M}$. The swelling strain is defined as the diluent-induced dilatation which the body would undergo if it were externally unconstrained. The difference between the dilatation and the swelling strain is termed the mechanical strain and may be a result of inhomogeneities in the concentration field or external body constraints (displacement boundary conditions). By using the above definitions, the dilatation field can be expressed as

$$e(\underset{\sim}{x},t) = e^{M}(\underset{\sim}{x},t) + e^{C}(\underset{\sim}{x},t) = e^{M}(\underset{\sim}{x},t) + \int_{-\infty}^{t} \alpha(t-\tau)\frac{\partial c(\underset{\sim}{x},\tau)}{\partial \tau} d\tau \tag{1.7}$$

where the swelling coefficient, $\alpha(t)$, describes the material's unconstrained strain response to the diluent concentration and is directly analogous to the time-dependent thermal coefficient of expansion.

Following the time-dependent nature of polymeric material properties, such as the bulk and shear moduli, the swelling coefficient, $\alpha(t)$, is also assumed to be time-dependent. The temporal dependency reflects that the polymer molecules cannot instantaneously reorient themselves to accommodate the diluent molecules. Further, as a result of other viscoelastic principles, the convolution in Eqn. (1.7) reflects the assumption that the effects of temporal changes in concentration contribute to the dilatation in an additive manner. Experiments to characterize the time dependence of $\alpha(t)$ are difficult to perform. The long time scale of the diffusion process, creating an inhomogeneous concentration field within the body, would corrupt the strain measurements needed for an accurate evaluation of $\alpha(t)$. As a consequence, to date there is no experimental data for $\alpha(t)$ and thus for this study $\alpha(t)$ is assumed to be a constant.

### 1.3.2 The Concept of Free Volume

Underlying the free volume concept is the idea that the viscoelastic nature of polymers is a result of the relative motion of the long polymeric molecules. This motion is achieved by having segments of the molecules "jump" between the "holes" or "spaces" within the bulk polymer. "Holes" that participate in this molecular rearrangement are called the free volume of the polymer and by normalizing the free volume by the polymer's total volume one obtains the fractional free volume or free-volume fraction, $f$. The "holes" are dependent on the environmental conditions encountered by the polymer. Thermal heating will agitate the polymer molecules creating more "holes" within the polymer, while diluent molecules accomplish

the same result by perhaps disrupting the packing order of the polymer molecules.

Voids must exist between the polymer molecular chains due to the randomness of the packing of such chains. There have been some attempts to measure the free volume within a polymer[22]. Such measurements are often questionable since the data is dependent on the type of marker used and might not truly reflect the free volume (volume which is involved with molecular reorientation in the system). The lack of direct experimental evidence has created some debate on the appropriateness of using the free volume to model the polymeric relaxation behavior. But phenomenologically the free volume concept is a simple way of explaining and predicting the polymer behavior and thus will be used in this study.

As an illustration, the concept of free volume is used to justify the material behavior of a class of polymers that are called thermo-rheologically simple (TRS) materials. A material is TRS if its time-dependent properties at different temperatures can be superimposed onto a single master curve, at a reference temperature, by shifting the curve segments along the logarithmic time axis and by accepting a small "adjustment" on the vertical axis, (see Fig. 1.1). The time shifting is phenomenologically characterized for temperatures above the polymer's glass transition temperature, $T_g$, by the WLF equation proposed by Williams, Landel, and Ferry[30]. Earlier, Doolittle[7] had introduced the idea of free volume as the parameter that governs the viscosity of simple hydrocarbon based fluids and proposed a phenomenological equation to fit his data. By assuming a relationship between the temperature-induced

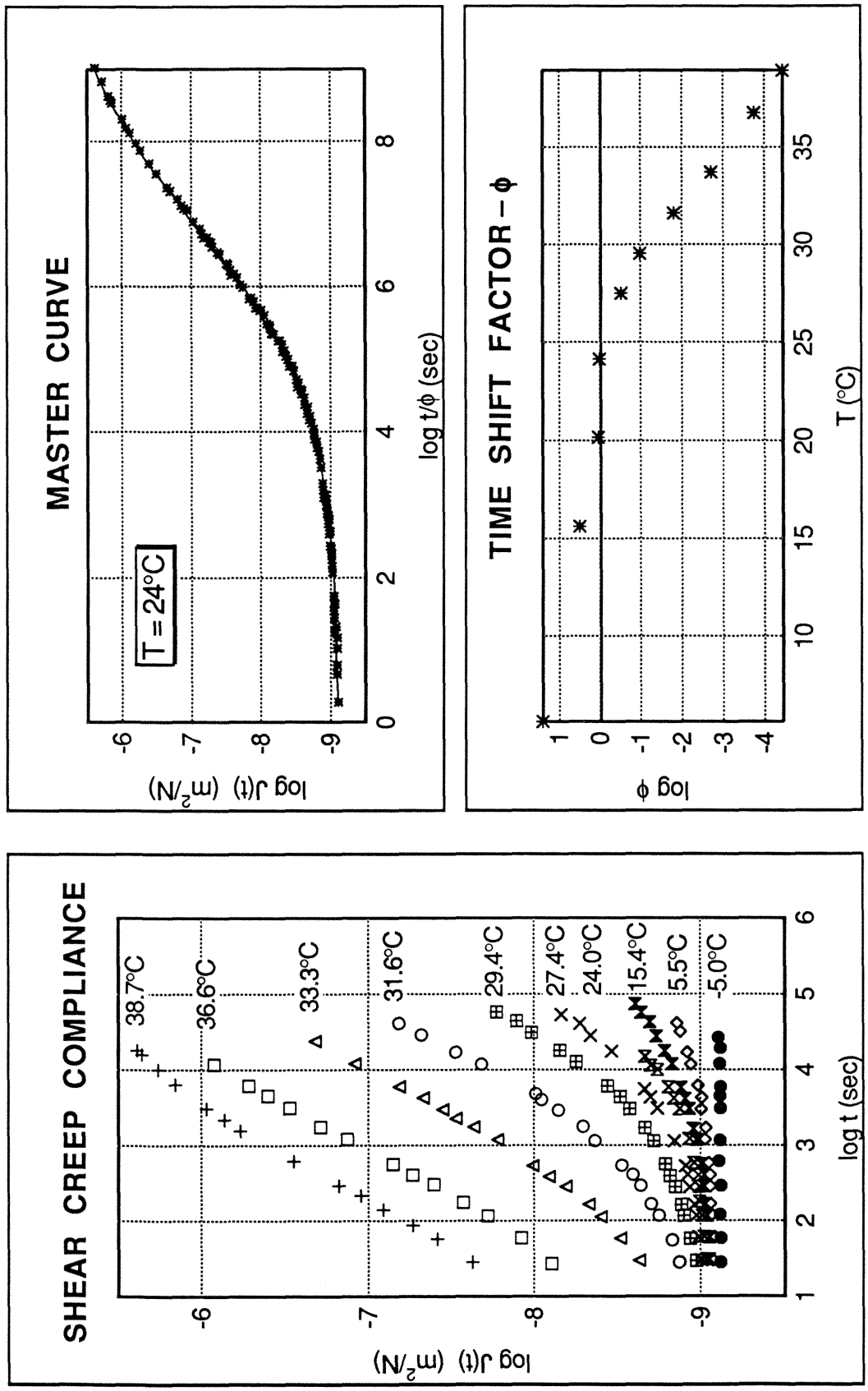


Figure 1.1 An example of a TRS material. The shear modulus of PVAc is measured at various temperatures and is time shifted to form a master curve ( $T_g$ for dry PVAc is 29°C)[15].

dilatation and the free volume fraction, the WLF equation can be shown to be equivalent to the Doolittle equation for temperatures above $T_g$. By using statistical mechanics Cohen and Turnbull[3] provided the theoretical justification linking the free volume concept to a Doolittle-type equation, further bolstering the concept of free volume.

The fractional free volume is assumed to be related to the diluent-induced swelling strains of the polymer. This assumption is based on the investigations by Knauss and Kenner[15] who studied the effects of temperature and moisture on the mechanical properties of PVAc. Knauss and Kenner found that the shear modulus for PVAc at different moisture concentrations could be shifted to form a single master curve, like that of a TRS material, (reinforcing the previous assumption of the similarity between thermal and diluent-induced dilatation). They further showed that the deduced fractional free volume could be related to the moisture-induced dilatation through a Doolittle-type equation. An important aspect in the experiments performed by Knauss and Kenner is that the PVAc specimens were externally unconstrained and had been conditioned such that the moisture concentrations were uniform within the specimen, thus the swelling strain is equal to the dilatation.

Further justification for a concentration-dependent free volume fraction, $f$, may be inferred from the literature review in Ferry's[8] text on the effect of diluents on various polymeric properties such as the glass transition and relaxation times. Ferry comments that at low concentrations a linear dependence of $f$ on the concentration can be made if the fractional free volumes of the diluent $(f_1)$ and the polymer $(f_2)$ are additive (or nearly so) and in this linear range $f$ has the form

$$f(\underset{\sim}{x},t) = f_2(T(\underset{\sim}{x},t)) + \varpi c(\underset{\sim}{x},t) \tag{1.8}$$

where $T$ is the temperature, $c$ the concentration, and $\varpi$ a proportionality constant. In structural applications, the diluent concentrations within the polymer are fairly low (<10%) and Eqn. (1.8) should suffice for the work presented here. Assuming again that the swelling strains are related to the diluent concentration the fractional free volume described by Eqn. (1.8) would be similar to that proposed by Knauss and Kenner.

If $f$ is assumed to be linearly related to the dilatation a serious conceptual flaw becomes apparent. Imagine an experiment in which the polymer is restricted in such a way as to prevent any volumetric change, hence the dilatation is zero by definition. If a diluent then diffuses into the polymer, the diluent molecules would occupy a portion of the "holes" which make up the free volume. Thus a contradiction occurs because $f$ must remain constant since the dilatation is zero but conceptually this cannot be since the diluent molecules now occupy a portion of the free volume.

Similarly, if $f$ is assumed to be linearly proportional to only the swelling dilatation, a mechanically constrained body will result in the wrong qualitative effect for the fractional free volume.

These contradictions may be eliminated by simply assuming $f$ to be linearly proportional to both the mechanical strain and the swelling strain. This proportionality leads to the representation for $f$ as

$$f(\underset{\sim}{x},t) = f_o(\underset{\sim}{x}) + Ae^{\mathrm{M}}(\underset{\sim}{x},t) + Be^{\mathrm{C}}(\underset{\sim}{x},t) \tag{1.9}$$

where the variable $f_o$ is the free-volume fraction in the reference state. Rewriting Eqn. (1.9) in terms of the dilatation strain and the swelling strain, by using Eqn. (1.7) to eliminate $e^M$, yields

$$f(\underset{\sim}{x},t) = f_o(\underset{\sim}{x}) + Ae(\underset{\sim}{x},t) + (B-A)e^C(\underset{\sim}{x},t) \tag{1.10}$$

Restrictions on the parameters $A$ and $B$ can be deduced from the arguments that lead to Eqn. 1.9 as

$$0 < B < A \tag{1.11}$$

The partitioning of $f$ does have the attractive feature that the free volume fraction is related to both the free volume fraction of the polymer, $Ae^M$, and the free volume fraction introduced to the polymer by the diluent, $Be^C$. This assumption allows the free volume fraction to be proportional to the swelling dilatation, as claimed by Knauss and Kenner, but eliminates some of the troubling features that would occur if the polymer were mechanically restrained.

### 1.3.3 Time Shift Factor

Experimentally the time shift factor is determined by the amount of shift needed to superimpose material property curves obtained at different but constant temperatures to form a master curve. Another way of looking at the time shift factor is that it allows the master curve to appear, with respect to time, to contract or elongate depending on the state of the polymer such that it corresponds to the experimental time window.

The relation between the time shift factor, $\phi(\underset{\sim}{x},t)$, and the change in the free volume fraction is given by the Doolittle result as

$$\ln\phi(\underset{\sim}{x},t) = -b\left(\frac{1}{f_o(\underset{\sim}{x},t)} - \frac{1}{f(\underset{\sim}{x},t)}\right) \tag{1.12}$$

where by Cohen and Turnbull[3] $b$ is a parameter related to the critical size of the "holes" needed for a polymer segment to "jump." The time is then scaled by the time shift factor to yield the internal or reduced time, $\xi$, of the polymer as

$$\xi(t) - \xi(\tau) = \int_{\tau}^{t} \frac{d\eta}{\phi(\underset{\sim}{x},\eta)} \tag{1.13}$$

### 1.3.4 Stress - Strain Relations

The relationship between the deviatoric stresses and strains and the pressure and dilatation can now be given by

$$\underset{\sim}{s}(\underset{\sim}{x},t) = \int_{-\infty}^{t} 2G\big(\xi(t)-\xi(\tau)\big)\frac{\partial \underset{\sim}{e}}{\partial\tau}d\tau \tag{1.14}$$

$$P(\underset{\sim}{x},t) = -\int_{-\infty}^{t} K\big(\xi(t)-\xi(\tau)\big)\frac{\partial e}{\partial\tau}d\tau + \int_{-\infty}^{t} \beta\big(\xi(t)-\xi(\tau)\big)\frac{\partial c}{\partial\tau}d\tau \tag{1.15}$$

where material properties are the shear relaxation modulus, $G(t)$, the bulk relaxation modulus, $K(t)$, and the diluent-induced pressure relaxation function, $\beta(t)$. Notice that the material properties in Eqns. (1.14) and (1.15) are evaluated at the reduced time and this fact is the major difference between nonlinear and linear viscoelasticity; where the nonlinearity results from the coupling between the shear and bulk behavior (through the assumed dilatation - free volume fraction relationship), and the interaction between the stresses, strains, and free volume which in turn affects the reduced time.

This modification of the linear viscoelastic convolutions, where the material properties are evaluated at the reduced time, should also be applied to the evaluation of the dilatation, hence Eqn. (1.7) becomes

$$e(\underset{\sim}{x},t) = e^{M}(\underset{\sim}{x},t) + \int_{-\infty}^{t} \alpha(\xi(t)-\xi(\tau))\frac{\partial c(\underset{\sim}{x},t)}{\partial \tau} d\tau \qquad (1.16)$$

### 1.3.5 Modelling of Material Properties

To aid in the numerical evaluation of the material properties the continuous material time spectra are expressed as discrete spectra in the form of a finite Prony series. For example, the relaxation moduli for $K(t)$, $G(t)$, and $\beta(t)$ are expressed as

$$K(t) = \sum_{i=1}^{m} K_i \exp(-t/\tau_{Ki});\ G(t) = \sum_{j=1}^{n} G_j \exp(-t/\tau_{Gj});\ \beta(t) = \sum_{k=1}^{q} \beta_k \exp(-t/\tau_{\beta k}) \qquad (1.17)$$

where m, n, and q need to be chosen sufficiently large to allow a reasonably smooth approximation of the moduli in question; typically 10 to 20 terms are needed for each series expansion. The long time or equilibrium value of the relaxation moduli can be achieved by having the time constant, $\tau$, for one of the series element to approach $\infty$. Similarly, to model the swelling coefficient, $\alpha(t)$, one uses a modified Prony series

$$\alpha(t) = \sum_{l=1}^{r} \alpha_l \left[1 - \exp(-t/\tau_{\alpha l})\right] \qquad (1.18)$$

where the long time behavior is modelled by having one of the time constants of a series element to approach $-\infty$. The modified Prony series is used to model the swelling coefficient since it is expected to provided a better fit to the swelling dilatation creep behavior, but as mentioned before there is no experimental data for $\alpha(t)$.

The number of elements needed to portray $\beta(t)$ depends on the number of elements that are needed to model $K(t)$ and $\alpha(t)$. The diluent-induced pressure relaxation function, $\beta(t)$, can be shown to be related to the dilatational strain creep behavior, $\alpha(t)$, and the bulk relaxation modulus, $K(t)$, through their Laplace transforms $\overline{\beta}(s)$, $\overline{\alpha}(s)$, and $\overline{\mathrm{K}}(s)$, respectively.

$$\overline{\beta}(s) = s\overline{\alpha}(s)\overline{K}(s) \tag{1.19}$$

By taking the Laplace transform of the Prony series representation of $\mathrm{K}(t)$ and $\alpha(t)$ and substituting the transformed functions into Eqn. (1.19) one can show that $\beta(t)$ can be represented as a Prony series

$$\begin{aligned}\beta(t) &= \sum_{i=1}^{m}\sum_{j=1}^{n}\frac{\alpha_i K_j \tau_{\kappa j}}{\tau_{\kappa j}-\tau_{\alpha i}}\left\{\exp\left(-t/\tau_{\kappa i}\right)-\exp\left(-t/\tau_{\alpha i}\right)\right\} \\ &= \sum_{k=1}^{q}\beta_k \exp\left(-t/\tau_{\beta k}\right)\end{aligned} \tag{1.20}$$

For the subsequent study the swelling strains will be assumed to occur elastically ($\alpha(t)$ is constant with respect to time). Under this assumption $\beta(t)$ takes the simple form

$$\beta(t) = \alpha\sum_{i=1}^{m} K_i \exp\left(-t/\tau_{\kappa i}\right) \tag{1.21}$$

These governing equations and the proposed constitutive model have been incorporated into a finite element model (see Appendix A1).

# Chapter 2
# Diffusion Model

## 2.1 Introduction

In diluent-polymer systems anomalous or non-Fickian diffusion can occur and it is this topic which will be explained now. Experimentally the absorption of a diluent into a polymer is classified as non-Fickian if the data, such as the total absorbed mass, does not possess the characteristics of Fick's diffusion equations. In this study, an attempt to explain much of the observed anomalous behavior is made by modifying the basic Fickian diffusion equation to include other driving forces (besides the concentration gradient), such as pressure and temperature gradients. Similar modifications have been suggested by other researchers[4,18,25,24,29], though in this study the full range from Fickian to non-Fickian diffusion behavior will be looked at from the point of view of viscoelastic material behavior.

This chapter begins with a brief review of the characteristics of Fickian and non-Fickian diffusion and then proceeds to outline the basis for the proposed diffusion model.

## 2.2 Fickian Diffusion

The one-dimensional form of Fick's first law, which is phenomenological in nature, states that the mass flux of the diluent, $j(x,t)$, is proportional to the diluent concentration gradient, namely

$$j(x,t) = -D(c)\frac{\partial c(x,t)}{\partial x} \tag{2.1}$$

where the diffusion (proportionality) coefficient, $D$, may be considered to be a function of concentration[6], $D(c)$. By combining Fick's first law with the equation of mass conservation one derives the one-dimensional form of Fick's second law which is more commonly known as the diffusion equation. In a one-dimensional Cartesian coordinate frame the diffusion equation can be represented as

$$\frac{\partial c(x,t)}{\partial t} = \frac{\partial}{\partial x}\left[D(c)\frac{\partial c(x,t)}{\partial x}\right] \tag{2.2}$$

The generalization to three-dimensions is straightforward and states, with $\nabla$ denoting the Laplacian operator, that

$$\frac{\partial c(\underset{\sim}{x},t)}{\partial t} = \nabla\cdot\left[\underset{\sim}{D}\nabla c(\underset{\sim}{x},t)\right] \tag{2.3}$$

Solutions to Eqn. (2.3) for various types of boundary conditions, diffusion coefficients, and spatial geometries can been found in the text by Crank[5]. In particular, the solutions for a plane sheet are especially important since most experiments draw on this geometry. For a plane sheet of thickness, $2L$, with concentration, $C_1$, prescribed on the boundary and $D_o$ the value of the (possibly) concentration-dependent diffusion coefficient at

zero concentration, the solutions are often depicted as concentration profiles where $c(x,t)/C_1$ is plotted versus $x/L$ for several nondimensional "times," $D_o t/L^2$. The solutions could also be displayed as absorption (or desorption) curves which represent the concentration profiles integrated over the spatial domain yielding the mass absorbed (desorbed), $M(t)$, plotted against $\sqrt{t}$. Often the ratio $M(t)/M_\infty$ is plotted against $\sqrt{t}/\mathrm{L}$, where $M_\infty$ is the long time or equilibrium amount that is absorbed (desorbed); this type of plot is known as the "reduced" absorption (desorption) curve. One often uses the generic term the "sorption curve" to refer to either the absorption or desorption curve.

The following are a few of the characteristics that are commonly used to identify a Fickian diffusion process from the experimental results for sorption curves and concentration profiles.

(a) Sorption curves are linear in the region of small values of $\sqrt{t}$.

(b) Above the linear portion, sorption curves are always concave towards the $\sqrt{t}$ axis.

(c) The shape of the absorption curve is not very sensitive to the dependence of $D$ on concentration. On the other hand, the desorption curve is rather markedly affected by the $D$ versus $c$ relationship.

(d) When the initial and final concentrations are fixed, the reduced absorption (desorption) curves for films of different thickness all coincide yielding a single master curve.

(e) The single absorption curve so obtained is always above the corresponding single desorption curve when $D$ is an increasing function of $c$.

(f) The functional form of $D(c)$ greatly influence both the absorption and desorption concentration profiles[10].

Diluent-polymer systems, where the polymer is in its rubbery state, typically exhibit Fickian behavior. An example is the absorption and desorption curves for methyl acetate into polymethylacrylate (PMA). Experiments[6] were conducted at 35°C (the $T_g$ of dry PMA is approximately 5°C) for three different thicknesses and the results are indicated in Fig. 2.1. By replotting the data on the "reduced" time scale, $\sqrt{t}/L$, as in Fig. 2.2, it can be seen that conditions (a), (b), (d), and (e) are satisfied and this particular diluent-polymer system would be classified as Fickian.

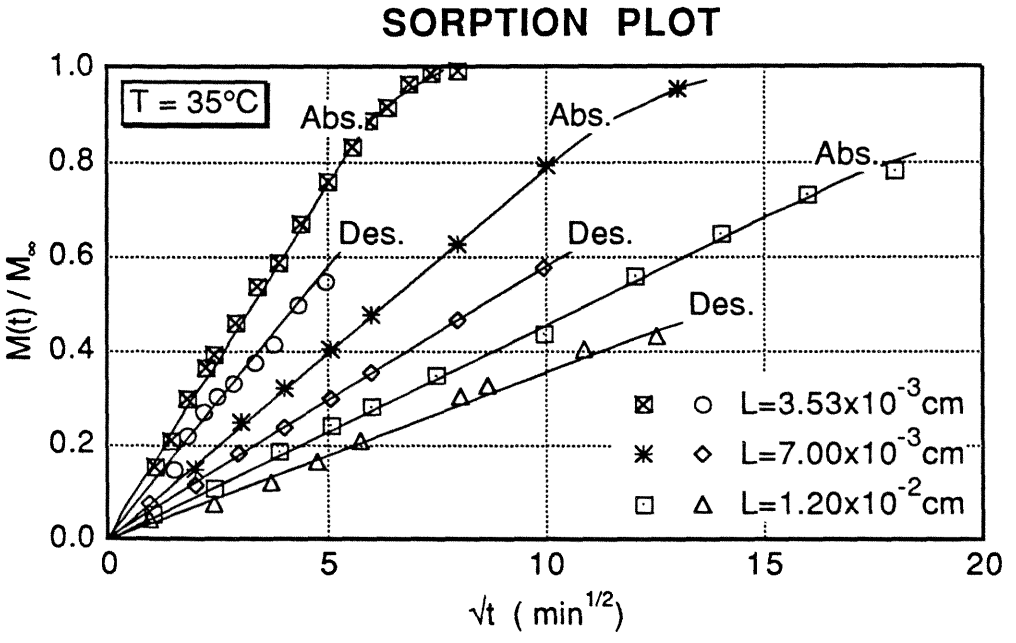


Figure 2.1 Sorption characteristics for methyl acetate into polymethylacrylate (PMA) at 35°C for three different thickness values ($T_g$ for dry PMA ~ 5°C)[6].

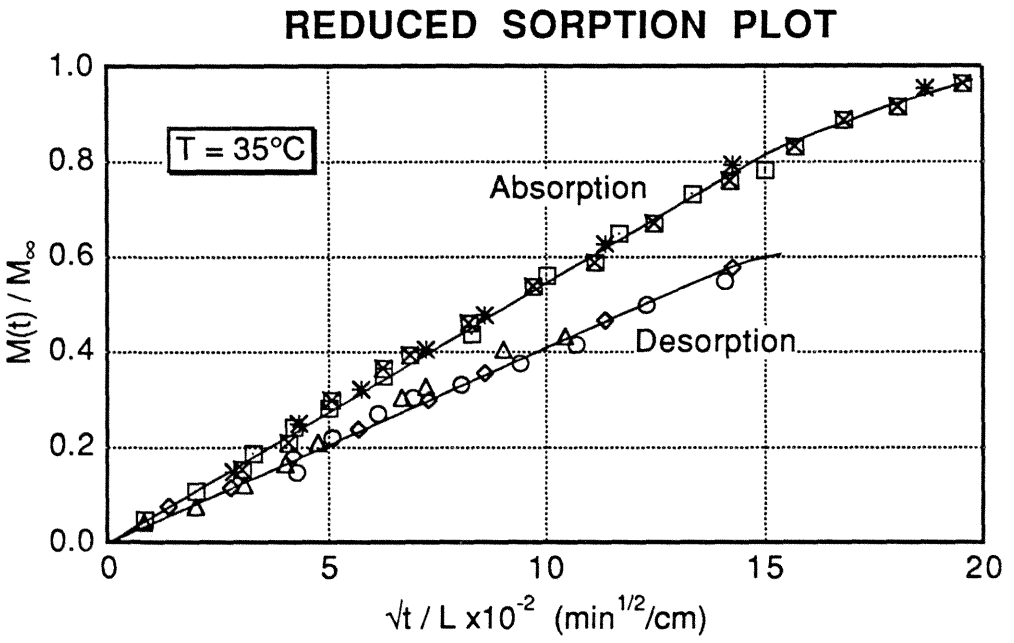


Figure 2.2 Reduced sorption curves obtained from Fig. 2.1[6].

## 2.3 Non-Fickian Diffusion

As mentioned before, Fickian diffusion usually occurs in polymer-diluent systems, which are in the rubbery state. On the other hand, glassy polymers which undergo significant relaxation during the diffusion process tend to exhibit anomalous diffusion. By comparing the ratio of the "characteristic" material relaxation time to the "characteristic" diffusion time (the Deborah number), Vrentas and Duda[28] claim to predict whether the diffusion process is Fickian or non-Fickian. A schematic of a Deborah number plot is shown in Fig. 2.3 where the outlined regions indicate areas in which different diffusion processes occur.

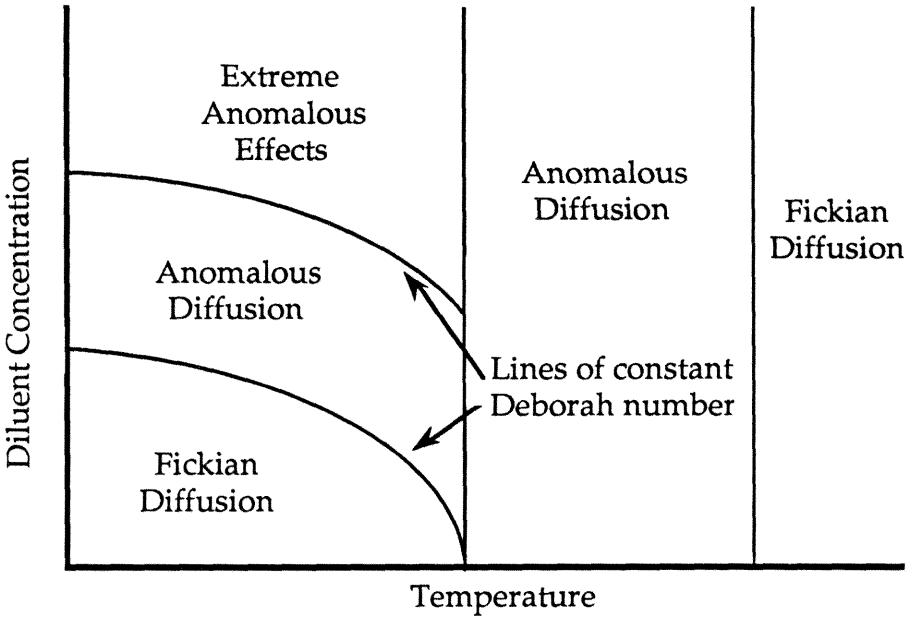


Figure 2.3 Schematic of a Deborah number plot[28].

From this figure it can be seen that at high temperatures, where the polymer is in its rubbery phase, Fickian diffusion is always expected since the polymer behaves elastically. But at low temperatures and concentrations Fickian diffusion is also expected and is a consequence of the quasi-elastic behavior of glassy polymers. At intermediate temperatures or concentrations the polymer exhibits viscoelastic behavior and the diffusion process is generally anomalous.

Many different anomalous behaviors have been observed and a partial list is presented here:

(a) In the region of small values of $\sqrt{t}$ sorption curves are not linear.

(b) The absorption curve has an inflection point.

(c) Despite the expectation that $D$ should increase with concentration, the absorption and desorption curves may intersect;

the relatively high initial rate of desorption followed by a very slow rate leads to intersection of the two curves.

(d) The absorption and desorption curves which have coincident initial slopes do not coincide over the entire region of $\sqrt{t}$.

(e) When plotted against $\sqrt{t}/L$ the absorption or desorption curves obtained from experiments on polymers of varying thicknesses cannot be reduced to a single curve[10].

An example of a type of anomalous behavior can be seen in the absorption curves for allyl chloride diffusing into polyvinylacetate (PVAc), shown in Fig. 2.4. The experiments[6] were conducted at 40°C (the $T_g$ of dry PVAc is approximately 29°C) for three different thicknesses. The absorption curves for the different thicknesses failed to coalesce when plotted on a reduced sorption plot and the characteristics of the curves range from initially linear (Fickian-like response) to sigmoidal (non-Fickian), conditions (b) and (e).

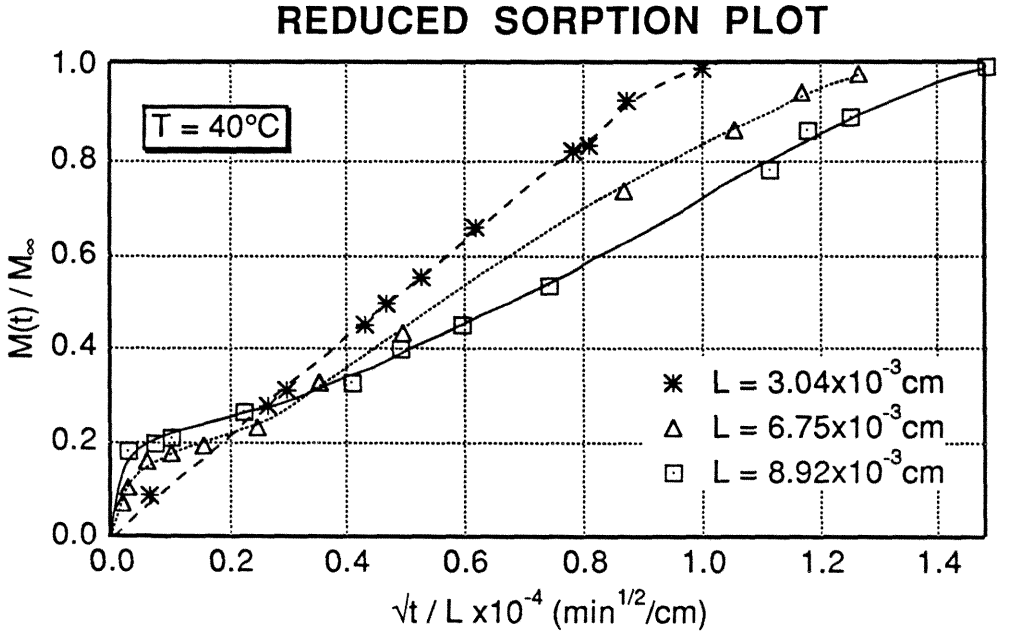


Figure 2.4 Reduced absorption curves for the allyl chloride into PVAc system at 40°C as a function of thickness ($T_g$ of dry PVAc ~ 29°C)[6].

Another important anomalous diffusion process is termed Case II diffusion. The characteristics of Case II diffusion within a plane sheet geometry are:

(a) The mass of the absorbed penetrant increases linearly with time.

(b) A sharp boundary separates the inner glassy core of unpenetrated polymer from the outer swollen shell, and there is a uniform concentration of penetrant across the swollen layer.

(c) The separation between the two states advances with constant velocity[23].

Case II diffusion has been shown in the absorption of methanol by polymethylmethacrylate (PMMA), as exemplified in Figs. 2.5 and 2.6. The experiment[23] was conducted at 10°C (the $T_g$ of dry PMMA is approximately 105°C). A typical absorption curve, Fig. 2.5, is linear with time (after a brief initial induction region) satisfying condition (a). The concentration profile in Fig. 2.6 defines the boundary that separates the glassy core from the swollen, rubbery outer shell of the polymer and conforms to conditions (b) and (c). Other systems exhibiting Case II diffusion include polystyrene with 1-iodo-n-alkanes as the diluent[11].

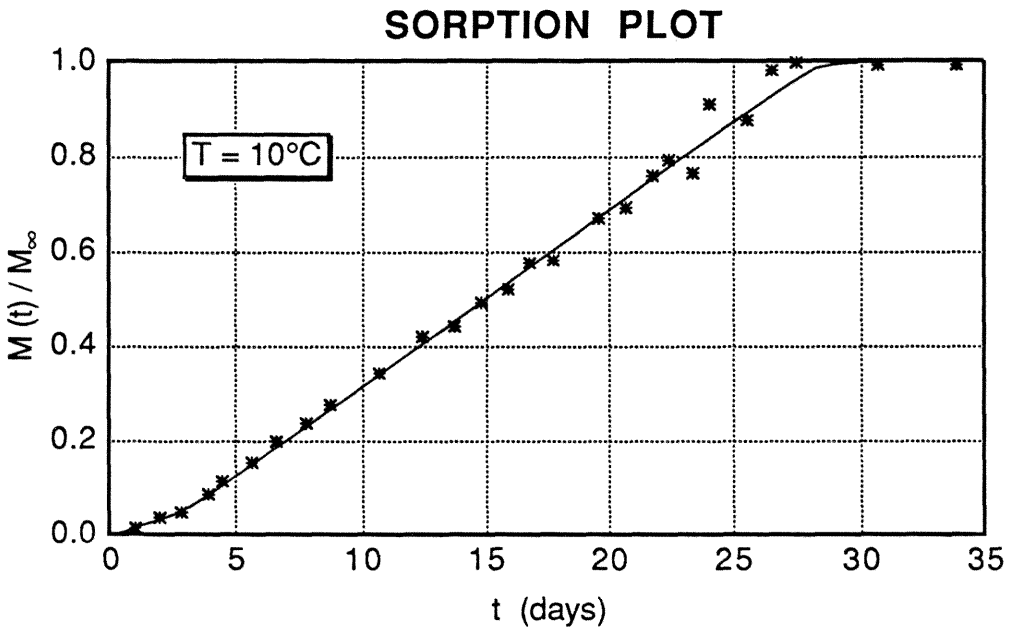


Figure 2.5 Absorption profile for methanol into PMMA at 10°C ($T_g$ of dry PMMA ~ 105° C)[23].

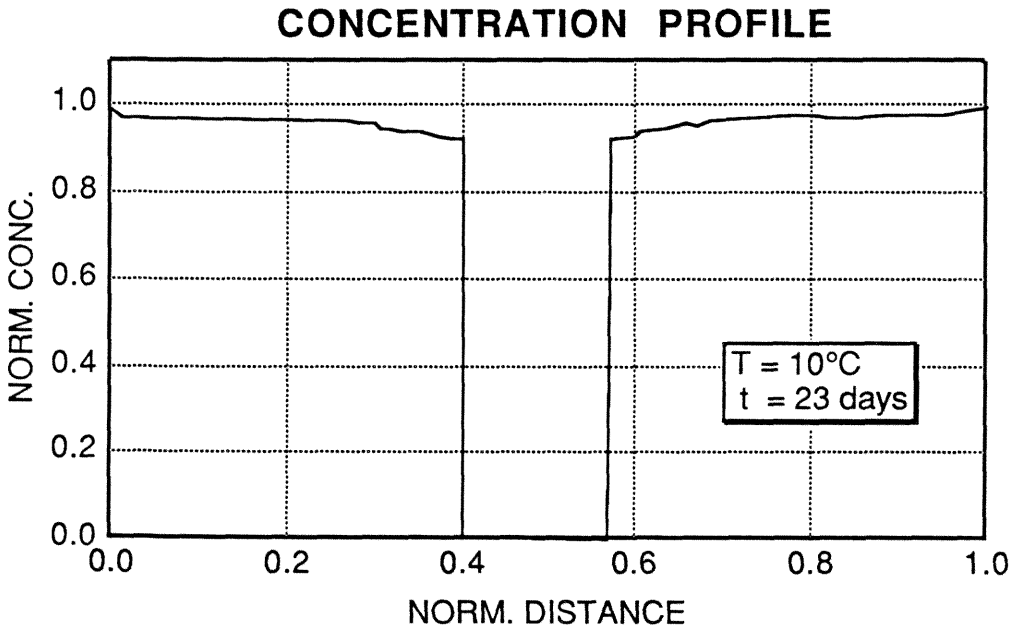


Figure 2.6 Concentration distance profile for methanol into PMMA at 10° C after 23 days of exposure[23].

## 2.4 The Diffusion Model

From a mechanistic viewpoint additional driving forces for the diluent mass flux in polymers, besides that of a concentration gradient, should be possible. As a diluent diffuses into a polymer swelling occurs and internal stresses or pressure develop which should affect the diluent mass flux in a manner analogous to a Poisseuille flow or the mass flow through a porous media. One may then, as a simple assumption, say that such a pressure-induced mass flux is additive with concentration mass flux, thus modifying the Fickian diffusion equation. Another approach is to view the diffusion problem in terms of irreversible thermodynamics and many researchers[21,26,29] have found that other driving forces, besides that of a concentration gradient, could be included in the diffusion equation. From either viewpoint potential driving forces for the diluent mass flux in a polymer can include a concentration gradient (Fick's Law), a temperature gradient (Soret effect), and/or a pressure gradient. In order to set the stage for later developments let us examine briefly a thermodynamic variable known as the chemical potential, $\mu$.

### 2.4.1 Chemical Potential

The chemical potential is classically defined (see Prigogine[21]) as an intensive variable that takes into account the change in entropy, $S$, resulting from the changes in the composition of a system. With such a definition the total differential for the entropy is given as

$$dS = \frac{dE}{T} + \frac{P}{T}dV - \sum_{i=1}^{m} \frac{\mu_i}{T} dn_i \qquad (2.4)$$

where the internal energy ($E$), pressure ($P$), volume ($V$), temperature ($T$), and the mole number for the $i^{th}$ constituent ($n_i$) describe the state and composition of the system.

Based on the thermodynamics of irreversible processes the phenomenological law governing the mass flux for the $i^{th}$ constituent, $j_i$, is given in one-dimensional form as

$$j_i = \frac{L}{T}\left( F_i - \frac{\partial \mu_i}{\partial x} \right) \tag{2.5}$$

where $L$ is a phenomenological (experimental) coefficient, $T$ the temperature, and $F_i$ a generalized force acting on the $i^{th}$ constituent.

As an example, the chemical potential of a perfect gas or a dilute solution is often expressed as

$$\mu_1(x) = \eta_1(T) + RT \ln C_1(x) \tag{2.6}$$

where $T$ is the temperature, $R$ the gas constant, and $C_1$ the diluent concentration. Substituting Eqn. (2.6) into Eqn. (2.5) yields

$$j_1 = -\frac{L}{T}\frac{RT}{C_1}\left( \frac{\partial C_1}{\partial x} - C_1 \frac{F_1 M_1}{RT} \right) = -D\left( \frac{\partial C_1}{\partial x} - C_1 \frac{M_1}{RT} F_1 \right) \tag{2.7}$$

where

$$D = \frac{L}{T}\frac{RT}{C_1} = RTB \tag{2.8}$$

is Einstein's relationship for the diffusion coefficient $D$ in terms of the mobility, $B$. $M_1$ is another phenomenological coefficient that relates the

driving force to the diluent mass flux. The mobility term, $B$, is related to the ability of the diluent molecules to move within the polymer and will be discussed later in terms of what is known as the free-volume fraction.

The form of Eqn. (2.7) where the additional driving forces are considered to be additive with the concentration gradient is usually maintained when postulating various models for the diluent mass flux equation, even if the functional form of $\mu$ is not known.

In the following sections an effort is made to explain some of these potential driving forces through a conceptual picture of the interaction between the diluent and polymeric molecules which occur during the diffusion process.

### 2.4.2 Concentration Gradient

To get started let us visualize the diluent molecules as being "ball-like" to allow a simple description of the scenario for a concentration gradient-dependent mass flux. For now the scenario assumes that both the diluent and the polymer are chemically neutral and no (electrically) polar sites exist which could affect the mobility of the molecules and thus the diffusion process. It also assumes that the polymeric molecular chains are allowed to reorient themselves, but will not undergo an appreciable motion into the diluent (the polymer provides a fixed reference frame).

A single diluent molecule or "ball" would have a Brownian motion as a result of collisions with other diluent molecules and the molecules of the polymer. It can be imagined that the side of the "ball" facing a higher density of "balls" would be subjected to, on the average, more impacts forc-

ing the "ball" to move. This view accounts for the observation that diffusing molecules will move in the direction of the negative gradient of the concentration. The fact that the "balls" would be expected to move faster the more impacts it receives per unit time represents the fact that the rate of mass transport is proportional to the magnitude of the concentration gradient. Phenomenologically, this proportionality constant is called the diffusion coefficient.

The polymer molecules form a chaotic network where molecules may be interconnected through cross-linking (chemical bonds at certain sites along the chains) or a pseudo-cross-linking may occur through van der Waals-type of bonds (polar attraction) or chain entanglements. To move through the polymeric network the "balls" are now forced to "squeeze" in between the polymer chains via the "holes" or "free spaces" that are formed by the mismatching of the chains. By relaxing the assumption that there are no polar sites, one could imagine highly polar diluent molecules replacing and thus breaking the local polar attractions that help interconnect the polymeric chains. Destruction of the interconnections would allow an increase in the rate of diffusion by providing more flexibility to the polymer chains allowing easier movement of the diffusing "balls." Alternatively, it can be imagined that the "balls" are disrupting the "order" of the polymeric chains creating more "holes", similar to defects in a crystal lattice. The "order" of polymeric chains could be the chain interconnections, the atacity of the molecules, or the structure of the molecule itself. As before, the more "holes" that are created, the greater is the mobility of both the diluent and the polymer molecules, thus increasing the diffusion rate. It is possible that polar diluent molecules, rather than forming more "holes," may bond

(due to the polar attraction) to the polymer molecules "plugging" existing "holes" and thus retarding the diffusion process. This phenomena has been observed for water molecules (which are highly polar) that interact with polymer chains that have "suitable" polar groups[6]. In any event the rate of diffusion is usually altered by concentration of the diluent and is incorporated, conventionally, through a concentration-dependent diffusion coefficient.

Environmental conditions may also affect the diffusion process. For example, the diffusion rate is usually observed to increase with temperature. A plausible explanation is linked to the higher kinetic energy, associated with the increase in temperature, of both the diluent and the polymer. Ignoring for now the possible existence of a temperature gradient, the diluent molecule would have more energy to deform the polymeric chains. Also the increase in temperature will cause the polymer chains to have a higher kinetic energy which would create more "holes" and become more flexible. The net result is that the diffusion process can occur at a faster rate and is reflected in the strong temperature dependence of the diffusion coefficient.

The functional relationship between the concentration and temperature for a given polymer-diluent diffusion coefficient are current research topics. The research is usually guided by two viewpoints: one is based on a molecular interaction (molecular-microscopic) theory and the other on the concept of free volume (macroscopic). The molecular theory tries to account for the intermolecular forces that occur between the diluent and polymeric molecules. To date the molecular theory incorporates too many simplifying assumptions so that it is unclear whether the results are appli-

cable in the present context. Hence, the less detailed model based on the free volume approach will be considered below.

As mentioned in the previous chapter, current theories for the viscoelasticity in polymers use the idea of free volume to scale the relaxation time of the material. The free volume or "holes" that allow segments of the polymer chain to rearrange are similar to the "holes" that allow for the diffusion of the diluent. The size of the "holes" may be different owing to the size difference between the diluent molecules and the segmental chain sections that participate in the diffusion or reorientation, respectively. From this viewpoint the diffusion process and viscoelasticity are related through the free volume of the polymer.

In an attempt to incorporate the effect of the polymeric chain motion Knauss and Shimabukuro[16] asserted that the time scale for the diffusion process, which is controlled by a free volume molecular rearrangement, should be terms of the internal time, $\xi$. Hence the time derivative in the diffusion equation should be written in terms of the internal time. To illustrate this idea, the one-dimensional Cartesian diffusion equation will now have the form

$$\frac{\partial c}{\partial \xi} = \frac{\partial}{\partial x}\left(\overline{D}(c)\frac{\partial c}{\partial x}\right) \tag{2.9}$$

By scaling the internal time, $\xi$, by the $\xi$ - $t$ relation in Eqn. (1.13) the diffusion equation, Eqn. (2.9), can be rewritten in terms of the actual time, $t$, as

$$\frac{\partial c}{\partial t} = \frac{1}{\phi_d(c)}\frac{\partial}{\partial x}\left(\overline{D}(c)\frac{\partial c}{\partial x}\right) \tag{2.10}$$

where $\phi_d$ is given by

$$\ln \phi_d(c) = -b_d\left[\frac{1}{f(0,T)} - \frac{1}{f(c,T)}\right] \tag{2.11}$$

The variables in Eqn. (2.11) have a similar meaning as those in Eqn. (1.13). The notable difference is that the coefficient $b_d$ reflects the critical sized "hole" needed for a diluent molecule to "jump."

An alternative viewpoint is that the mobility term in Einstein's relation, Eqn. (2.8), is governed by the free volume since this is the parameter which governs the ability of the diluent to move about the polymer. Fujita[10] uses this viewpoint and by following the work of Cohen and Turnbull[3] develops the following diffusion coefficient for polymer-diluent systems

$$\begin{aligned} \ln(D/D_o) &= b_d\left[\frac{(\gamma(T) - f(0,T))v_1}{f(0,T)\left[f(0,T) + (\gamma(T) - f(0,T))v_1\right]}\right] \\ &= b_d\left[\frac{1}{f(0,T)} - \frac{1}{f(v_1,T)}\right] \end{aligned} \tag{2.12}$$

where $f(v_1,T)$ is the free volume fraction at diluent volume fraction, $v_1$, and temperature, $T$. $D_0$ is the value of the diffusion coefficient at zero diluent concentration and $b_d$ is related to the critical sized "hole" needed so that a diluent molecule can "jump forward." Fujita expresses the free volume as

$$f(v_1,T) = f(0,T)(1-v_1) + \gamma(T)v_1 \tag{2.13}$$

where $\gamma(T)$ is a proportionality coefficient relating the free volume fraction to the volume fraction of the diluent. The form of Eqn. (2.13) is similar to

Eqn. (1.9) if the first term is viewed as the free volume fraction of the polymer. A few examples of polymer-diluent systems where Eqns. (2.12) and (2.13) correlate well with experimental results, as well as various systems for which the theory does not apply are discussed by Fujita[10].

Vrentas and Duda[27] point out that some of the deficiencies in Fujita's model are a consequence of the assumptions made in comparing experimental results to the model. A few notable assumptions were that the molecular weight of the diluent is comparable to the molecular weight of the jumping unit of the polymer chain and that the diluent concentrations are small. They also noted that Cohen and Turnbull's model is more appropriate to describe the self-diffusion coefficient rather than the diffusion coefficient for a bi-component system. Vrentas and Duda suggest that both the polymer and diluent self-diffusion coefficients, as proposed by the Cohen and Turnbull model, be used to develop the diffusion coefficient for the polymer-diluent system. To accomplish this, they make use of Bearman's molecular interaction theory[2] which relates the so-called "frictional coefficients" to the self-diffusion coefficients. The "frictional coefficient" models the movement of the polymer molecules past one another by interactive and inherent atomic forces. In this manner Vrentas and Duda derive the diffusion coefficient for a diluent-polymer system, which with the additional assumptions that the polymer contains only a trace amount of diluent yields

$$\ln(D/D_o) = -\left[\frac{b_d}{f(c,T)}\right] \tag{2.14}$$

where the variables in Eqn. 2.15 have a similar meaning as those in Eqn. (2.11).

Vrentas and Duda[28] also provide some comparison of their model with experimental results and claim to be able to extend the limitations found in using the Fujita model.

The form suggested by both Fujita[10] and Vrentas et al[28]. yield diffusion coefficients that are affected by the free volume of the system and can be recasted to a form in which the concept of time shifting and internal time comes into play. Assuming that at $D_o$ the polymer has a free volume fraction equal to the reference free volume fraction, $f_o$, the diffusion coefficient as developed by Fujita and Vrentas et al. can now be expressed in the following form

$$D(c) = \frac{D_o}{\phi_d(c)} \tag{2.15}$$

where $\phi_d$ is given by Eqn. (2.11). This leads, with an additional concentration-dependence on $D_o$, to the following one-dimensional diffusion equation

$$\frac{\partial c}{\partial t} = \frac{\partial}{\partial x}\left[ \frac{\overline{D}(c)}{\phi_d(c)} \frac{\partial c}{\partial x} \right] \tag{2.16}$$

If the spatial derivative is performed, Eqn. (2.16) can be rewritten as

$$\frac{\partial c}{\partial t} = \frac{1}{\phi_d(c)} \frac{\partial}{\partial x}\left[ \overline{D}(c) \frac{\partial c}{\partial x} \right] - \frac{\phi_d'(c)}{\phi_d(c)} \frac{\overline{D}(c)}{\phi_d(c)} \left( \frac{\partial c}{\partial x} \right)^2 \tag{2.17}$$

where the second term in Eqn. (2.17) is the only difference between Eqn. (2.10) and (2.16).

Comparisons between Eqn. (2.10) and Eqn. (2.16) were performed numerically and the resultant concentration profile and sorption plot are shown in Figs. 2.7 and 2.8. The results indicate that the solutions are similar in form to each other; hence the inclusion of the second term in Eqn. (2.17) does not significantly alter the solution (at least for the material parameters used to generate the solution). It is expected that as additional driving forces are added to the mass flux equation and as the material properties become viscoelastic the similarities would still apply.

As a consequence of the solution similarity and the effort to maintain the basic form of the mass flux equation presented in Eqn. (2.7), Fujita's model was chosen for the remainder of the study*. An additional benefit of assuming the form dictated by Fujita's model is that the comparisons made by Fujita and Vrentas et al. with experimental work would now be applicable to the proposed diffusion model.

### 2.4.3 Pressure Gradient

As the diluent diffuses into the polymer a pressure field develops in connection with the swelling of the polymer. A part of the pressure may be

---

* Besides the reasons given for choosing the Fujita model, the author had initially assumed that both models were equivalent. After much of the numerical work had been completed using the Fujita model, questions were raised about the appropriateness of that assumption. Work is currently being performed to better understand the differences between the two models though initial indications are that the two, while different, yield similar solutions.

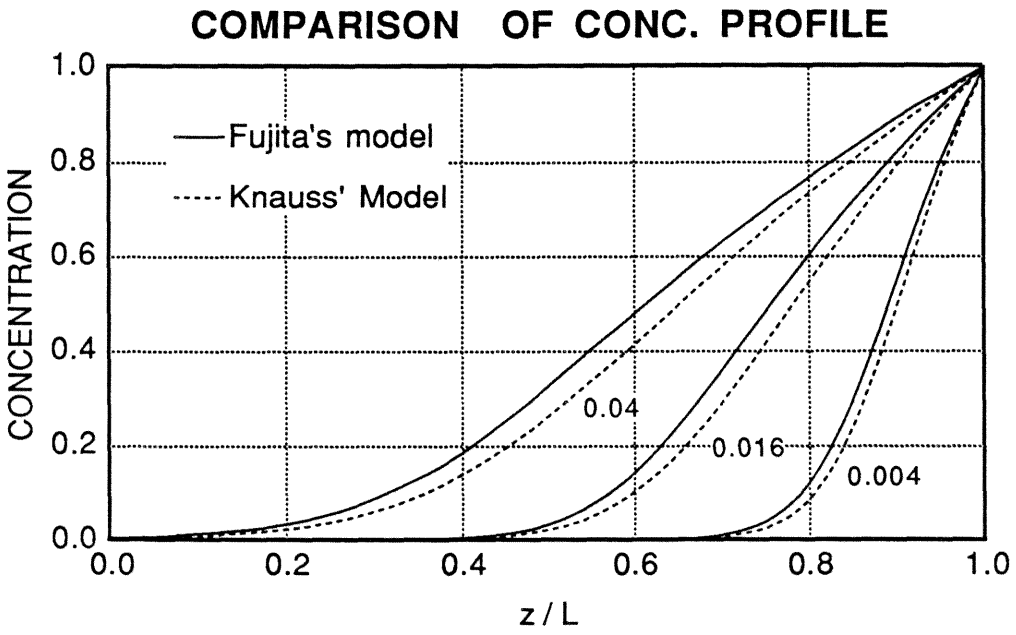


Figure 2.7 Concentration profile comparing the two diffusion models, Eqns. (2.10) and (2.17). The numbers on the curves represent a nondimensional time, $D_o t/L^2$.

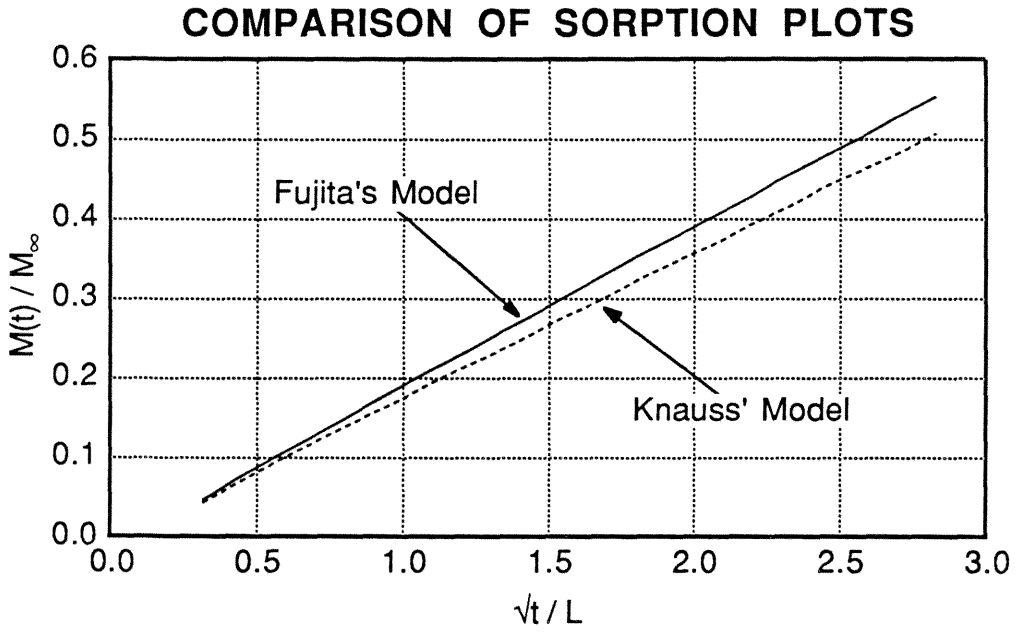


Figure 2.8 Sorption plot for the above concentration profile for the two diffusion models.

applied by the bulk polymer as a force acting on the diluent molecules. Any resultant pressure imbalance will in turn produce a net force propelling the diluent molecule in the direction of the negative pressure gradient. The result is a mass flux due to the pressure gradient, which in the spirit of Eqn. (2.7), is assumed to be an additive term in the mass flux equation.

To reinforce this additive assumption, Tirrell[25] suggests that the generalized force in Eqn. (2.7) should be the gradient of some potential field. While Weitsman[29] argues from a thermodynamic viewpoint that the potential field may be chosen to be either the Helmholtz or Gibbs free energy functions, which would yield mass flux equations dependent on the strain (dilatation) or stress (pressure) gradient, respectively. For this study, the pressure field is used since it offers the correct intuitive concept of a driving force.

The resultant swelling pressure is carried by both the diluent and the bulk polymer and the proportionality tensor, $\underset{\sim}{\Lambda}$, could be viewed as the relationship that expresses what portion of the total pressure is actually applied to the diluent. As a simplification one can assume $\underset{\sim}{\Lambda}$ to be an isotropic tensor which takes the form $\Lambda \underset{\sim}{I}$ where $\underset{\sim}{I}$ is the identity tensor. Knauss and Shimabukuro[16] provide an estimate for $\Lambda$ by modelling the diluent-polymer interaction as a thick-walled sphere (the polymer) loaded by a uniform external pressure $P$ (the resultant swelling pressure) and an internal pressure $P_s$ (the pressure on the diluent). The sphere is modelled to have an inner radius $a$ and an outer radius $b$ and is composed of a linearly elastic medium with a bulk modulus, $K$, and a shear modulus, $G$. The

diluent is assumed to have a linearly elastic bulk modulus, $K_s$. The displacement field, $u(r)$, for this problem is given by

$$u(r) = \frac{P_s a^3 - P b^3}{3K\left(b^3 - a^3\right)} r + \frac{\left(P_s - P\right) a^3 b^3}{4\mu\left(b^3 - a^3\right)} \frac{1}{r^2} \tag{2.18}$$

The pressure, $P_s$, in the cavity is related to the displacement, $u(r)$, through the bulk relationship of the liquid

$$P_s = K_s \frac{\Delta V}{V} = 3K_s \frac{u(a)}{a} \tag{2.19}$$

where use has been made of the relation

$$\Delta V = 4\pi a^2 u(a) \tag{2.20}$$

By substituting the relationship for $u(a)$ into Eqn. (2.17) and determining the ratio of $P_s$ to $P$, the relationship for $\Lambda$ can be shown to be

$$\Lambda = \frac{P_s}{P} = \frac{K_s(3K+4\mu)}{4KG(1-f) + K_s(3K+4\mu f)} \tag{2.21}$$

where the free volume fraction, $f$, is related to the two radii by

$$f = \left(\frac{a}{b}\right)^3 \tag{2.22}$$

Another estimate could be made by modelling the pressure driven mass flux as a Poisseuille flow through a thick-walled cylinder (the polymer) of inner radius $a$ and outer radius $b$. The driving pressure will be the pressure on the diluent, $P_s$, as a consequence of the resultant pressure, $P$. Following a similar procedure, as with the spherical shell, an estimate for $\Lambda$

(assuming a uniform pressure $P$ and that the cylinder ends are uncapped) can be given as

$$\Lambda = \frac{P_s}{P} = \frac{K_s(9K+6G)}{9KG(1-f) + K_s(9K+6Gf)} \tag{2.23}$$

Given this interpretation, one sees that $\Lambda$ is dependent on the free volume and in both estimates, Eqns. (2.21) and (2.23), the dependence on $f$ is the same. In general these elastic results should be replaced by their viscoelastic counterparts but one could expect that an elastic result with possibly a quasi-elastic formulation would suffice in providing an estimate for $\Lambda$.

In this study $\Lambda$ is assumed to be constant so that the effects due to the pressure gradient can be assessed more readily. This assumption is not unrealistic since typically $f$ ranges[9] between 0.025 to 0.075 and, for these values of $f$, would not affect the value of $\Lambda$ significantly.

### 2.4.4 Temperature Gradient

The phenomenon of a temperature gradient affecting the diffusion process is called the Soret effect. The Soret effect has been shown in fluid mixtures where a temperature gradient is applied to a uniform mixture; the mixture will then separate forming a concentration gradient. Following the work of Fourier and Fick, Soret suggested that the mass flux equation, Eqn. (2.1), should have an additional additive term which is proportional to the temperature gradient. The text by Tyrrell[26] provides some of the theory behind this effect and presents experimental evidence for the additive nature of the temperature gradient. As a result, the additivity of any temperature gradient-driven mass flow is also assumed.

For the purposes of this study only isothermal effects will be considered and the thermally-driven mass flux term will be ignored.

### 2.4.5 Considerations for Time-Dependent Concentration, Boundary Conditions

A possible explanation for sigmoidal shaped absorption curves has been to allow the concentration boundary condition to become time dependent[10,19]. The rational for this assumption is that the final concentration value is dependent on the ability of the polymer to deform and accommodate the diluent molecule. As the polymer absorbs more diluent the polymer begins to plasticize and the molecular chains relax allowing a higher concentration value to exist. By applying only a time-dependent concentration boundary condition, Long and Richman[19] ignore the fact that this concentration relaxation phenomenon should be applied to the whole polymer and not just the surface.

Lefebvre et al.[18] try to incorporate this phenomenon into a diffusion model by normalizing the concentration in the diffusion equations by the solubility of the diluent. The diluent concentration, $c$, is related to the solubility, $S$, through the partial pressure on the diluent, $P_s$, by Henry's Law

$$c = SP_s \tag{2.24}$$

It appears that Lefebvre et al. normalized the concentration in the diffusion equation by simply dividing the concentration values by $SP_s$. Such a normalization would hold only if $SP_s$ is not a function of the spatial and temporal variables. From their work, both $S$ and $P_s$ are functions of the free

volume (which is ultimately dependent on the spatial variables) leaving a question of the validity of the governing equations.

As indicated by the numerical solutions by Long and Richman this time-dependent boundary condition could explain much of the anomalous behavior observed in diffusion experiments. Though it may be important, this effect will be ignored in this present study so as to more readily examine the effects of a pressure-induced flow and the time shifting behavior of the diffusion coefficient.

## 2.5 Stress-Assisted Diffusion Model

A general form for the diffusion equation with the additional driving forces of pressure and temperature gradients can now be given as

$$\frac{\partial c}{\partial t} = \nabla \cdot \frac{\underset{\sim}{D}(c,T)}{\phi_d(c,T)} \left\{ \nabla c + c\underset{\sim}{\Lambda}(c,T)\nabla P + c\underset{\sim}{\Phi}(c,T)\nabla T \right\} \tag{2.25}$$

where the additional driving forces are assumed to be additive as suggested by the thermodynamics of the problem, Eqn. (2.7). The tensor functions $\underset{\sim}{D}(c,T)$, $\underset{\sim}{\Lambda}(c,T)$, and $\underset{\sim}{\Phi}(c,T)$ could be thought of as proportionality coefficients which relate the gradients of concentration ($c$), pressure ($P$), and temperature ($T$) to the mass flux, respectively.

By assuming, as mentioned in the previous section, that the material is isotropic, the proportionality coefficients are independent of concentration, and that the diffusion process occurs isothermally Eqn. (2.25) simplifies to become

$$\frac{\partial c(\underset{\sim}{x},t)}{\partial t} = \nabla \cdot \frac{D(c)}{\phi_d(c)} \left\{ \nabla c(\underset{\sim}{x},t) + c\Lambda \nabla P(\underset{\sim}{x},t) \right\} \tag{2.26}$$

### 2.5.1 Comparison with Other Stress-Assisted Diffusion Models

The form of Eqn. (2.26) has also been suggested by other investigators[4,24] in modelling Case II behavior. Thomas and Windle[24] approached the problem by using a modified Flory-Huggin's representation to model the chemical potential per mole of diluent, $\mu_1$,

$$\begin{aligned} \mu_1 - \mu_1^o &= P\bar{V}_1 N_A + RT\left\{ \frac{G\bar{V}_1}{V_i}\left[\sqrt[3]{(1-\upsilon_1)} - (1-\upsilon_1)\right]\right. \\ &\qquad \left. + \ln \upsilon_1 + (1-\upsilon_1) + \chi(1-\upsilon_1)^2 \right\} \\ &= RT \ln a_1 \end{aligned} \tag{2.27}$$

where $\mu_1^o$ is the chemical potential per mole of diluent at a reference state, $\upsilon_1$ the volume fraction or concentration of diluent in the swollen polymer, $P$ the external hydrostatic pressure or swelling pressure which acts on the polymer but not on the surrounding liquid, $G$ the molecular network parameter, $\bar{V}_1$ the molecular volume of the diluent, $V_i$ the volume of unswollen polymer, $\chi$ the diluent-polymer interaction parameter, $N_A$ Avogadro's number, and $a_1$ the activity.

The constitutive law that was chosen to relate the swelling pressure to the dilatation, $e$, is a simple viscosity relationship

$$\frac{de}{dt} = \frac{P}{\eta} \tag{2.28}$$

where $\eta$ is the viscosity of the polymer. Assuming that the dilatation is proportional to the concentration by a factor $k$, Eqn. (2.28) can be expressed as

$$\frac{d\overline{v}}{dt} = \frac{P}{\eta k} \tag{2.29}$$

Thomas and Windle derive the diffusion equation in terms of the activity rather than the concentration, but by using Eqn. (2.5) with the concentration and pressure as the independent variables the diffusion equation could be shown to take a form

$$\frac{\partial c(x,t)}{\partial t} = \frac{\partial}{\partial x}\left\{\hat{D}\left[\hat{\Omega}(c)\frac{\partial c(x,t)}{\partial x} + c\hat{\Lambda}(c)\frac{\partial P(x,t)}{\partial x}\right]\right\} \tag{2.30}$$

Cox and Cohen[4] also showed that the inclusion of a rate-dependent pressure field into the diffusion equation would lead to a Case II-type diffusion. Cox and Cohen modelled the Case II diffusion process by the following diffusion equation

$$\frac{\partial c(x,t)}{\partial t} = \frac{\partial}{\partial x}\left[\tilde{D}(c)\frac{\partial c(x,t)}{\partial x} + \tilde{\Lambda}(c)\frac{\partial P(x,t)}{\partial x}\right] \tag{2.31}$$

where the pressure field is given through the following constitutive behavior

$$\frac{\partial P(x,t)}{\partial t} = \beta(c)[g(c) - P(x,t)] \tag{2.32}$$

which is a combination of the Maxwell viscoelastic model and the Kelvin-Voigt elastic model.

The similarities between the proposed model and those by Thomas et al. and Cox et al. provide some reassurance that the full range from Fickian diffusion to Case II diffusion will be encompassed. The basic difference between the models is that the present model incorporates a more

complex constitutive model, one which is consistent with current viscoelastic theories. Both Thomas et al. and Cox et al. simply assume that the pressure field is only defined by the constitutive law while in this study a restriction is added that the resultant stresses (pressure) and strains (dilatations) must also satisfy the equilibrium equations and the strain-displacement equations.

A finite element model of Eqn. (2.26) was developed and implemented into a finite element code (the details can be found in Appendix A2).

# Chapter 3
# Numerical Analysis

## 3.1 Numerical Solution Scheme

The two problems, namely the mechanical response (MR) which deals with the solution for the displacements, strains, and stresses and the diffusion process (DP) which deals with the distribution of the diluent concentration, are coupled together in a variety of ways. Coupling between the two problems occurs through the constitutive law for the mechanical response in which case the concentration affects the stresses and strains, the stress (pressure) gradient which induces additional mass flow, and the strain modified free-volume fraction which in turn influences the behavior of the material properties. For convenience in describing various degrees of coupling, the "uncoupled" diffusion problem will be defined as that for which the MR is affected by the concentrations through the stress-strain law but the resultant pressure gradient does not affect the DP. By this definition the set of uncoupled diffusion problems could also include those cases for which the diffusion coefficient is modified by the time shifting parameter as long as the pressure gradient does not directly enter the mass flux equation.

Finding an analytical solution for the set of coupled nonlinear partial differential equations (as presented in the previous chapters) is in general unlikely; therefore the equations are solved numerically using the tech-

nique of finite elements. The equations modelling the MR and DP are converted to their numerical equivalents or, in the nomenclature of finite elements, element types. The two element types, MR and DP, each describing a matrix equation are incorporated into a finite element computer program called FEAP, an acronym for Finite Element Analysis Program. FEAP was originally developed at the University of California at Berkeley[32], enhanced at Brown University, and further modified to fit the needs of this problem. The usefulness of FEAP is that it provides the basic software needed for the finite element method, yet gives the users the flexibility to incorporate their own element types.

The iterative solution method for the coupled diffusion problem is, in principle, fairly simple; at a particular time step the diluent concentrations are solved by using the DP element and holding the displacements, stresses (pressure), and strains (dilatation) constant. Then while holding the resultant concentrations constant, the calculations for the displacement solution are performed using the MR element. Using the new displacement solution, the stresses and strains are reevaluated and the solution scheme returns to reiterate for the diluent concentration. This iterative process continues until both concentration and displacement solutions converge to within a specified tolerance. Nonlinearities associated with each problem, MR and DP, add to the complexity of the solution method since several iterations may be needed to solve each problem. This solution scheme is depicted in Fig. 3.1 where it can be seen that there are two major iterations being performed; within each individual problem and between the two problems.

As with most numerical solutions, checks must be performed to confirm the accuracy of the solution. This is especially true for nonlinear problems where approximate iterative techniques are used to find a solution. Such checks usually involve a reevaluation of the problem using different mesh (element) sizes and/or time step increments; if the new solution is "comparable" to the old solution the results are considered valid. The term "comparable" is a qualitative statement depending on the possible "errors" introduced by the solution scheme, thus error-checking with analytical solutions are important.

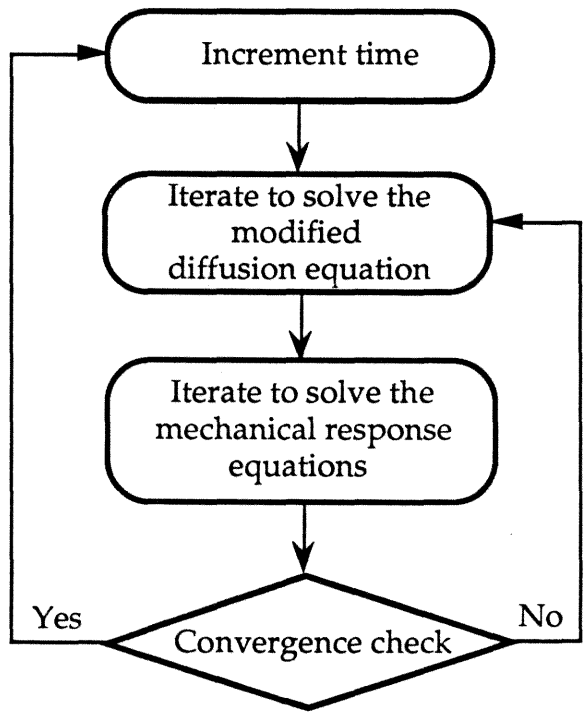


Figure 3.1 Solution scheme at a particular time step.

A separate issue is that of the uniqueness and existence of any numerically derived solution. Numerical solutions cannot answer the

uniqueness question but by incorporating the nonlinearities in a piecemeal fashion one may feel confident of a numerically derived solution.

## 3.2 Geometry and Boundary Conditions

Diffusion experiments are performed typically by exposing a plane sheet or film of thickness $2L$ to a diluent reservoir at a certain concentration. To model this situation the basic spatial geometry for the subsequent numerical analyses is chosen to be a right circular cylinder (see Fig. 3.2) of length (thickness), $2L$, and radius, $R$, undergoing axisymmetric deformation. Axial symmetry reduces the three-dimensional problem to a two-dimensional problem which still retains the basic features of the three-dimensional solution.

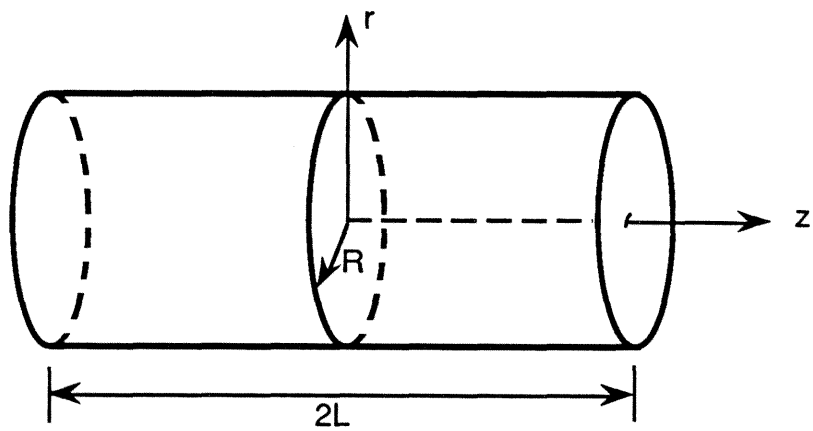


Figure 3.2 Basic geometric region for numerical analyses.

As a consequence of the axisymmetry there is no $\theta$ dependence in the problem and the spatial deformations ($u_r$, $u_\theta$, $u_z$), mass flux ($j_r$, $j_\theta$, $j_z$), and concentration ($c$) can be expressed as functions of $r$, $z$, and $t$ only.

$$u_r = u_r(r,z,t), \quad u_\theta = 0, \quad u_z = u_z(r,z,t) \tag{3.1}$$

$$j_r = j_r(r,z,t), \quad j_\theta = 0, \quad j_z = j_z(r,z,t) \tag{3.2}$$

$$c = c(r,z,t) \tag{3.3}$$

Additional boundary conditions can further reduce the problem to be fully one-dimensional and it is in these relatively simple 1-D cases where a better understanding of the interaction between the diffusion and mechanical response can be achieved. By relaxing these boundary conditions a comparison between the one- and two-dimensional cases can be made. Recall most experimental data reduction assumes the diffusion process to be one-dimensional and the 2-D comparison can be used to evaluate this assumption. In this spirit, numerical solutions and accompanying comments are presented on the validity of the proposed diffusion model in the following sections.

## 3.3 One-Dimensional Problems

The 1-D problems further restrict the spatial deformations of the cylinder be uniaxial along the $z$-axis.

$$u_r(r,z,t) = 0, \quad u_z(r,z,t) = u(z,t) \tag{3.4}$$

The tractions on the planar surfaces are assumed to be zero (no applied normal or shear stresses).

$$\sigma_{zz}(r,\pm L,t) = \sigma_{rz}(r,\pm L,t) = 0; \quad r=[0,R], \quad \forall t \geq 0 \tag{3.5}$$

The lateral surface is considered to be an impermeable boundary (the mass flux across the lateral surface is zero); while the concentration on the two planar surfaces are held constant at unity.

$$j_r(R,z,t) = 0; \quad z=[-L,L], \quad \forall t \geq 0 \tag{3.6}$$

$$c(r,\pm L,t) = 1.0; \quad r=[0,R], \quad \forall t \geq 0 \tag{3.7}$$

Angular symmetry conditions allow the cylindrical region to be modelled as a rectangular region between $r = [0,R]$ and $z = [0,L]$ with the additional boundary conditions

$$u(0,t) = \sigma_{rz}(r,0,t) = j_z(r,0,t) = 0; \quad r=[0,R], \quad \forall t \geq 0 \tag{3.8}$$

$$\sigma_{rz}(0,z,t) = j_r(0,z,t) = 0; \quad z=[0,L], \quad \forall t \geq 0 \tag{3.9}$$

The region for the 1-D problem with the associated boundary conditions is depicted in Fig. 3.3.

In the sequel, the solution behavior for various material properties are examined and compared to Fickian diffusion behavior. Several 1-D numerical solutions can be found in the text by Crank[5] and these are used to error-check the numerical scheme. Through this type of error-checking one can comprehend the accuracy of the numerical solutions produced by the iterative solution method of Fig. 3.1. Other numerical solutions are also presented to show the effects of coupling between the MR and DP problems.

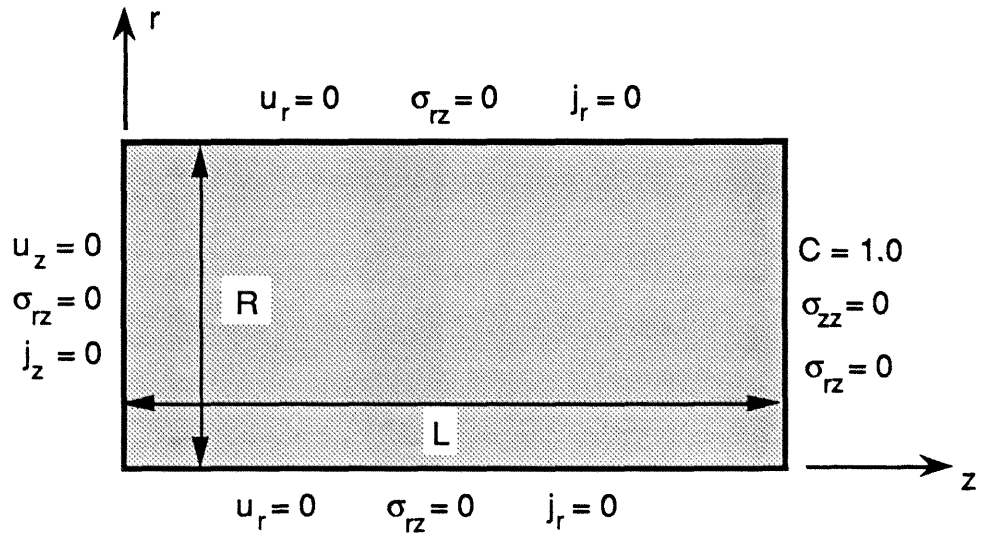


Figure 3.3 Modelled region for the 1-D problem with the associated boundary conditions.

A summary of the numerical 1-D analyses performed in this study are listed in Table 3.1.

| Summary of One-Dimensional Numerical Analyses | | | | |
|---|---|---|---|---|
| # | Description | Material Properties | Comments | Fig. |
| 1 | Uncoupled diffusion with constant D and elastic material response (Fickian). | $D$=0.1, $\Lambda$=0, $K$=1.0, $G$=0.28265, $\alpha$=0.3, $\beta$=0.3 | Examines the numerical accuracy of the two elements, MR and DP, indi-vidually. The geometry is L=0.1, R=0.002 with a minimum element size of dz=0.002. | 3.4, 3.5, 3.6 |
| 2 | Same as 1 except D is a function of concentration (Fickian). | $D$=0.01(1+100$c$), $\Lambda$=0, $K$=1.0, $G$=0.28265, $\alpha$=0.3, $\beta$=0.3 | Examines the numerical accuracy of the DP element when the diffusion coefficient is linear with concen-tration. The geometry is L=0.1, R=0.02 with a minimum element size of dz=0.002. | 3.7 |
| 3 | Coupled diffusion with constant D and elastic material properties. | $D$=0.001, $\Lambda$=100, $K$=1.0, $G$=0.28265, $\alpha$=0.3, $\beta$=0.3 | Simplest coupled diffusion problem. The problem can be uncoupled and the two solutions, (coupled and un-coupled) compared to see the effect of the iterative solution scheme. The geometry is L=0.04, R=0.02 with a minimum element size of dz=0.002. | 3.8 3.9 |
| 4 | Uncoupled diffusion with time shifting of D and elastic material properties. | $D_O$=0.001, $\Lambda$=0, K=0.6083, $G$=0.0001, $b_d$=30, $f_O$=1.0, $A$=1.0, $B$=0.9, $\alpha$=0.3, $\beta$=0.3 | The time shifting behavior of the diffusion coefficient steepens the concentration diffusion front but the results remain Fickian-like. The geometry is L=0.1, R=0.02 with a minimum element size of dz=0.002. | 3.10 3.11 |
| 5 | Coupled diffusion with time-shifting and viscoelastic material properties. | $D_O$=0.001, $\Lambda$=100, $K$ and $G$ see Fig.3.12 $b$=30, $b_d$=30, $f_O$=1.0, $A$=1.0, $B$=0.9, $\alpha$=0.3, $\beta$=$\alpha K$ | An example of the effect of proposed coupled diffusion model. The viscoelastic properties relaxes the pressure field thus slowing the rate of diffusion into the body. The geo-metry is L=0.1, R=0.02 with a min-imum element size of dz=0.002 | 3.13 3.15 |

Table 3.1 Summary of the 1-D numerical analyses that were performed.

### 3.3.1 Problem 1: 1-D Uncoupled Diffusion; Constant D; Elastic Material Properties

For this problem analytical solutions exist and a comparison between the analytical and numerical solutions will provide a baseline for future "error" comparisons. Crank[5] records an analytical solution for diffusion in a planar sheet of thickness, $2L$, having a constant diffusion coefficient, $D$, an initial concentration, $c_0$, and constant concentration boundary condition, $c_1$. The concentration profile is given as an infinite series in the following form

$$\frac{c-c_o}{c_1-c_o} = 1 - \frac{4}{\pi}\sum_{n=0}^{\infty}\frac{(-1)^n}{(2n+1)}\exp\left[\frac{-D(2n+1)^2\pi^2 t}{4L^2}\right]\cos\frac{(2n+1)\pi z}{2L} \qquad (3.10)$$

The corresponding sorption curve is also represented as the infinite series

$$\frac{M(t)}{M_\infty} = 1 - \frac{8}{\pi^2}\sum_{n=0}^{\infty}\frac{1}{(2n+1)^2}\exp\left[\frac{-D(2n+1)^2\pi^2 t}{4L^2}\right] \qquad (3.11)$$

A comparison of the analytical concentration profiles Eqn. (3.10) and the analytical sorption curve Eqn. (3.11) to the corresponding numerical solutions are shown in Fig. 3.4 and Fig. 3.5, respectively. In both plots the solutions are comparable to within plotting accuracy, indicating that at least for this simple case the numerical analysis for the DP element can yield accurate results.

The one-dimensionality of the displacement field and the elastic material properties allows one to solve the mechanical response problem explicitly, independent of the diffusion process, yielding the pressure, $P(z,t)$, and dilatation, $e(z,t)$, in terms of the concentration, $c(z,t)$, as

$$P(z,t) = \frac{4\alpha GK}{3K + 4G} c(z,t) \tag{3.12}$$

$$e(z,t) = \frac{3\alpha K}{3K + 4G} c(z,t) \tag{3.13}$$

where $\alpha$ is the swelling coefficient, $G$ the shear modulus, and $K$ the bulk modulus. Thus the pressure and dilatation profiles should be equivalent to the concentration profile provided they are scaled by the material properties in the manner shown by Eqns. (3.12) and (3.13), respectively. This relationship between $P$ and $c$ allows a check of the MR element and in Fig. 3.6 the scaled pressure corresponds to the concentration profile, to within plotting accuracy, indicating that the MR element is functioning correctly for elastic material properties.

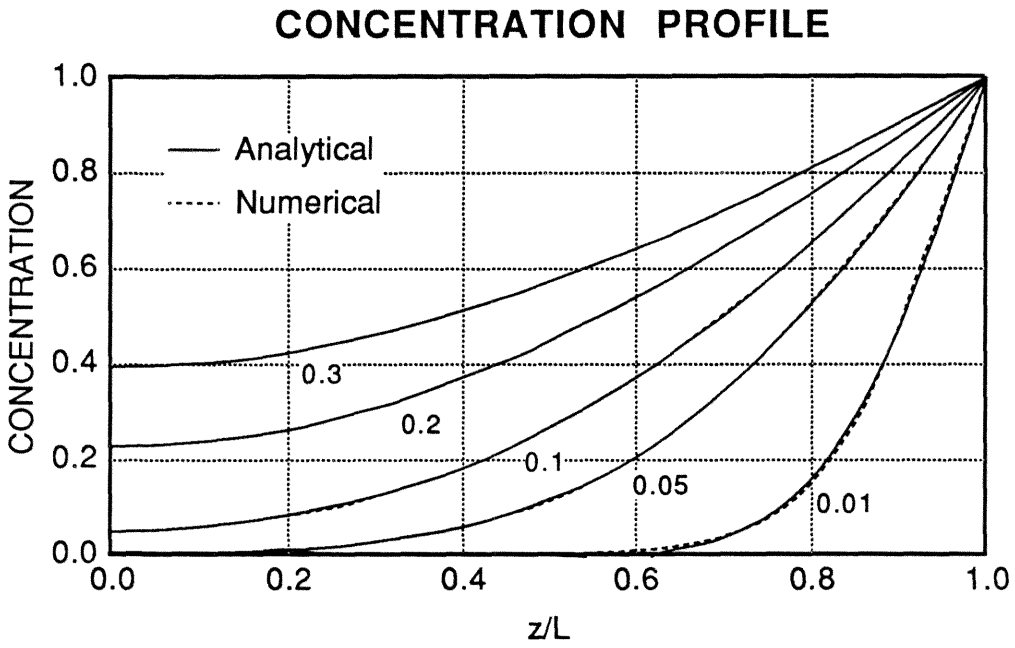


Figure 3.4 Comparison of concentration profiles given by the analytical solution, Eqn. (3.10), and the corresponding numerical analysis. Numbers on the curves are values of a nondimensional time, $Dt/L^2$.

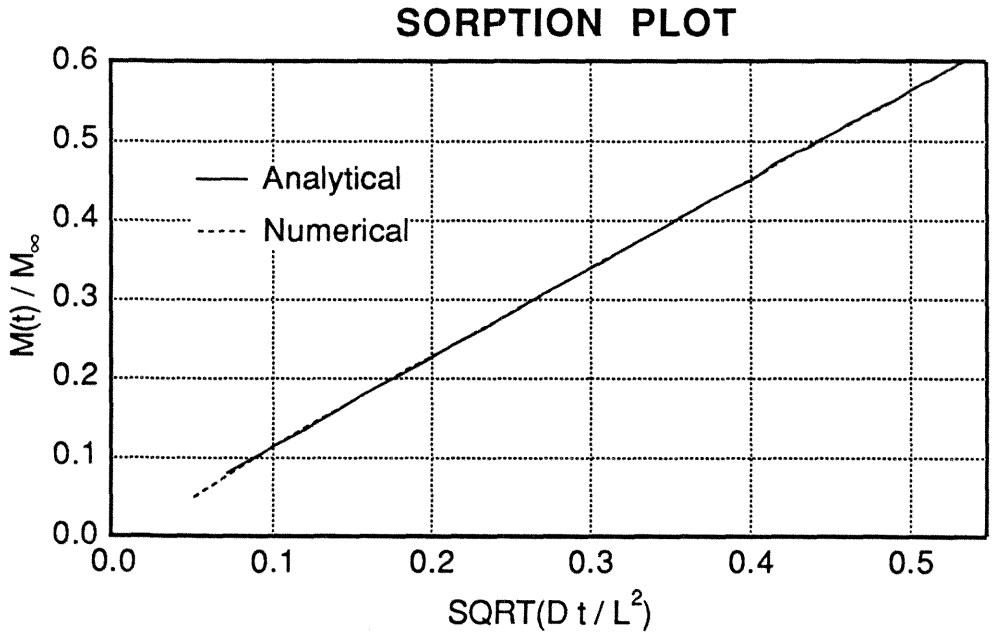


Figure 3.5 Comparison of the sorption profiles given by Eqn. (3.11) and the corresponding numerical analysis.

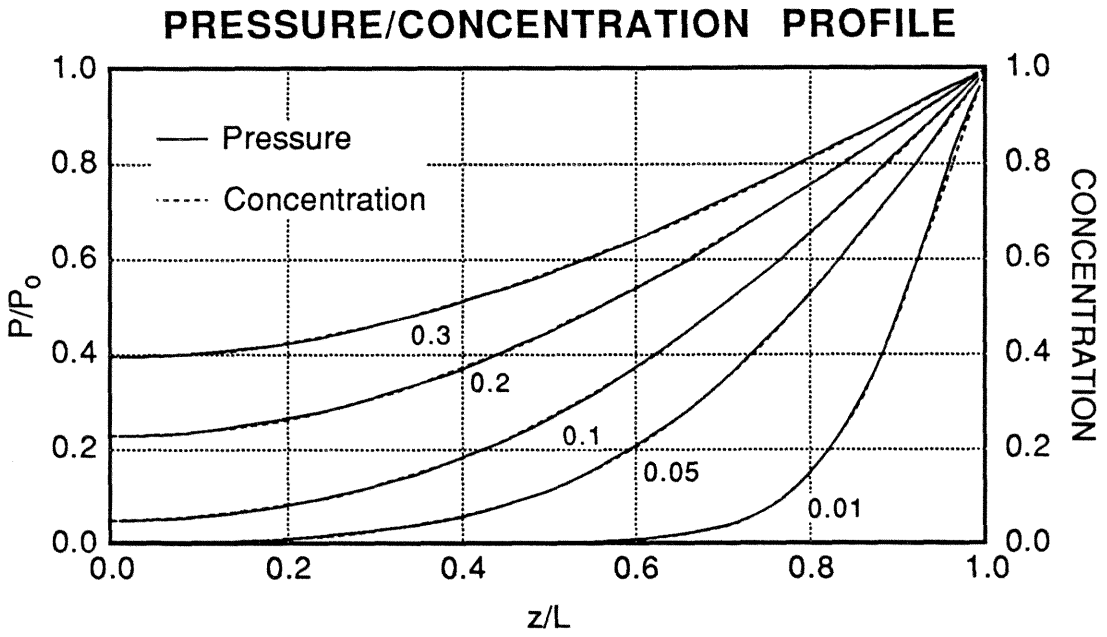


Figure 3.6 Normalized pressure profile compared to the concentration profile. For the material properties used in this calculation, $P_0 = 0.08211$. The numbers on the curves are values of a nondimensional time, $Dt/L^2$.

Though not shown here, other tests were performed where viscoelastic material properties were incorporated by using a single Prony series element for either $K(t)$, $G(t)$, or $\beta(t)$. The MR element calculated the stresses and strains which resulted from a uniform concentration applied to the entire cylindrical region at time equal zero (step function) and the numerical results compared well with analytical solutions. Such results gave further assurance that the MR element is performing correctly.

### 3.3.2 Problem 2: One-Dimensional Uncoupled Diffusion; Concentration-Dependent D; Elastic Material Properties

In many instances the diffusion coefficient, as determined by experiments, are found to be concentration-dependent and this effect has been included in the development of the DP element. In general no exact analyt-

ical solution can be found for a transient Fickian diffusion problem characterized by a concentration dependent diffusion coefficient. However, Crank[5] provides a few solutions, using either approximate analytical methods or numerical methods (finite differences), which can be used to compare with the solutions generated by the numerical code in this study.

The problem selected for comparison is that of a linearly varying diffusion coefficient of the form

$$D(c) = D_0( 1 + 100c ) \tag{3.14}$$

In Fig. 3.7 Crank's solution for the concentration profiles is compared with the finite element generated solution. The two solutions are similar although there is an initial difference that fades as time progresses. Finite element solutions for diffusion coefficients having other concentration dependences (e.g., exponential) have also been compared to corresponding solutions provided by Crank. Comments for these comparisons are similar to the linearly dependent diffusion coefficient problem*.

This test case shows that for a variable diffusion coefficient the DP element does not compare, against an analytical solution, as well with the test case having a constant diffusion coefficient. The errors introduced are probably a consequence of the digitization of the concentration profiles in Crank's text, the nonlinearities of the problem (the need to iterate and converge to a solution), and the time initialization approximations needed to

---

* The other diffusion coefficient used to check the finite element code is

$$D(c) = D_0\exp(az).$$

The results again had dissimilar initial solutions that faded with time.

start the numerical scheme. Though these apparent errors are not major, the curves are comparable, the last two possible error contributions would probably be enhanced as the nonlinearities of the problem increase. The initialization error indicates that for nonlinear problems caution must be used in interpreting the results at "early times" especially when comparing two solutions with different material parameters.

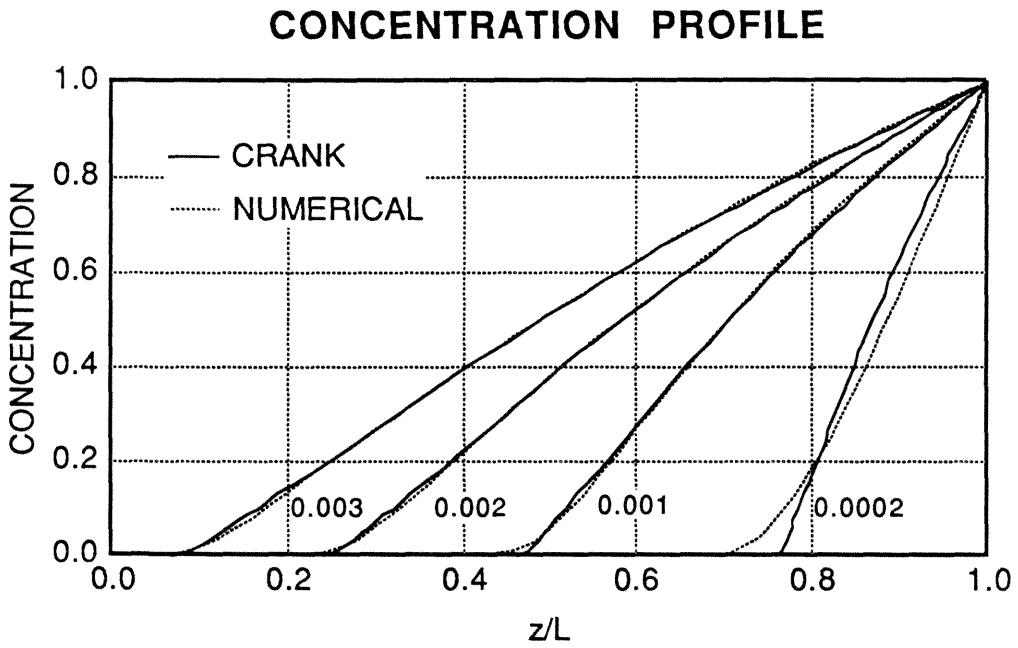


Figure 3.7 Comparison between the results provided by Crank[5] and the numerical analysis in this study. The numbers on the curve are values of the nondimensional time, $D_o t/L^2$.

### 3.3.3 Problem 3: 1-D Coupled Diffusion; Constant D; Elastic Material Properties

For this example the diffusion coefficient and the material properties are again assumed to be constant, but here the diffusion process is coupled to the mechanical response. The elimination of the time shifting effect is implemented by holding the free-volume fraction equal to the reference

free-volume fraction causing the time shifting parameter, $\phi_d$, to be equal to unity.

A special feature of this problem allows a direct assessment of the accuracy of the numerical code. To see this, first note that the pressure field for this case is also given by Eqn. (3.12). By substituting that pressure field into the 1-D form of the diffusion equation, Eqn. (2.16), a Fickian diffusion equation with a concentration-dependent diffusion coefficient is derived, namely

$$\frac{\partial c(z,t)}{\partial t} = \frac{\partial}{\partial z}\left( D(c)\frac{\partial c(z,t)}{\partial z} \right) \tag{3.15}$$

where

$$D(c) = D_o\left(1 + \frac{4\alpha GK\Lambda}{3K + 4G}c(z,t)\right) \tag{3.16}$$

Hence the coupled diffusion problem can be recast into an uncoupled diffusion problem, similar to that for Problem 2. By being able to uncouple the two problems a check of the proposed iterative solution method, §3.1, can be performed. This is accomplished by comparing the solutions generated by coupled case where the pressure from the mechanical response problem is fed back to the diffusion process and the uncoupled solution where there is no feedback. Through such a comparison, the concentration profiles at various times and the corresponding sorption plots, any "errors" that are introduced through the iterative solution method may be identified. Recall from the previous sections that solution checks have been performed for both the MR and DP elements separately and the results correspond well to analytical solutions, provided one does not look too

carefully at "early time" solutions. Consequently, the solution to the uncoupled problem can be assumed to be acceptably accurate. From Fig. 3.8, the concentration profiles for the two solutions are again comparable though at initial times a slight divergence occurs. This observation again reflects the initialization problem, but again the "shape" of the concentration profiles are similar and the "error" disappears with time. On the other hand the comparison between the resulting sorption plots for the two problems, Fig. 3.9, are comparable, since numerical integration has a "smoothing" effect, and considering that at initial times the mass is still small, resulting in a smaller absolute error. Subsequent numerical analyses must bear in mind this type of "error" while interpreting the results.

The difference probably arises from the added "stiffness" in the finite element formulation of diffusion process as a result of the pressure term. This "stiffness" would account for the initial difference since there could be insufficient flexibility between elements, to accurately capture the features of the solution (the high initial gradients). If this explaination were true the error could probably be corrected by adding more elements near the boundary to increase the flexibility of the mesh in this region. Another possibility may be the fact that since the solution for the concentration and displacements are not solved simultaneously, the solution is determined by iterating between the two problems until both are satisfied to within a specified tolerance. Thus the iterative procedure will have at least twice the possible error (as provided by the tolerance) then that of a procedure which solves both problems simultaneously (which is what occurs for the uncoupled cases). Because of the inherent numerical errors that occur in a numerical solution the tolerance level cannot be set arbitrarily small (for in

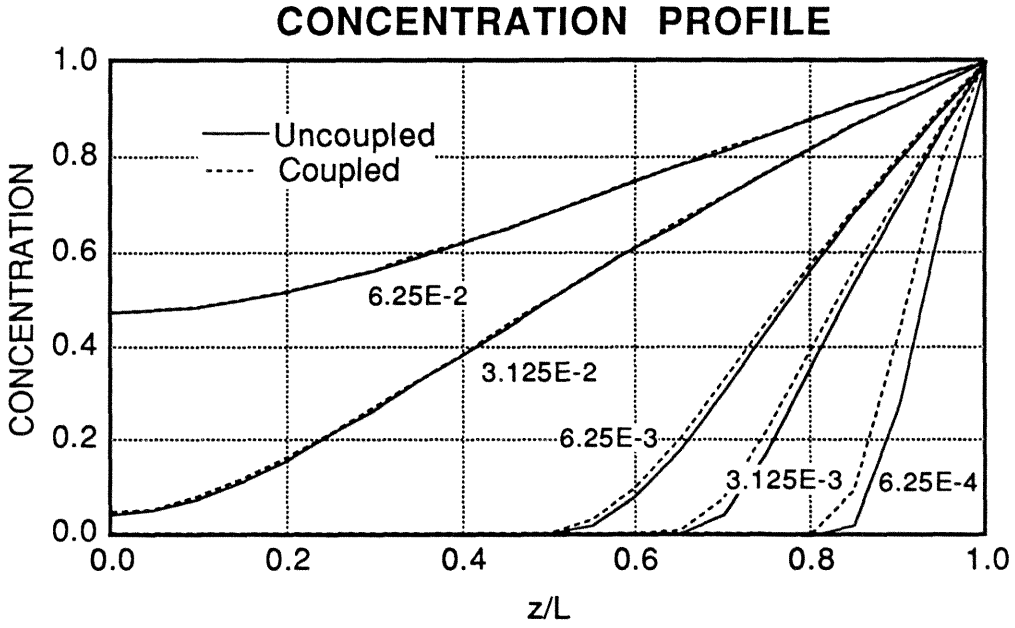


Figure 3.8 Concentration profile at various "times" comparing the uncoupled solution to the solution (coupled) to the iterative scheme. The numbers on the curve represent a nondimensional time, $D_0t/L^2$.

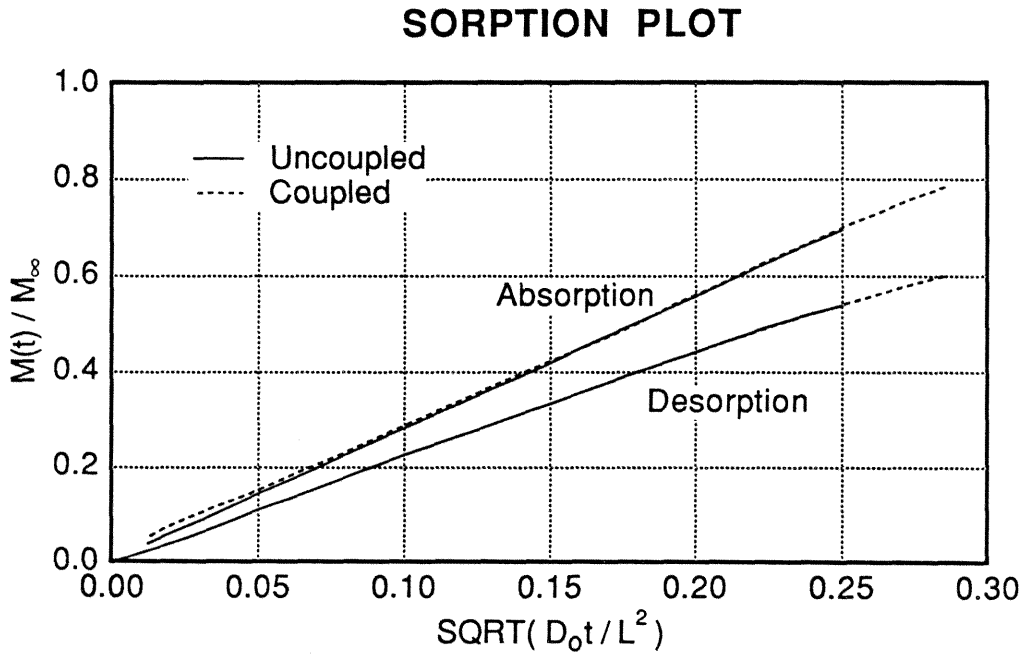


Figure 3.9 Sorption plot for Fig. 3.8 comparing the uncoupled solution to the coupled solution.

stance zero) and thus one must accept some numerical error. Here again the high initial gradients will enhance the numerical errors that are generated and could explain the initial differences.

Besides the ability to provide a "self-consistent" check for the discrete model, this problem points to an important lack of uniqueness in mathematically modelling a physical system. As an example, the experimental results by Hayes and Park[13] for the diffusion of benzene into a cross-linked rubber can be explained by a diffusion coefficient which is linear with the diluent concentration. Similar findings are also found by Aitken and Barrer[1] for the diffusion of butane and pentane into cross-linked rubbers. To deduce that the diffusion coefficient is linearly dependent on the concentration Hayes et al. and Aitken et al. assumed that the process was Fickian (the mass flux is driven only by a concentration gradient). From the 1-D solution presented here it follows that for the coupled model (the mass flux is driven by both a concentration and a pressure gradient) with elastic material properties, the diffusion coefficient could actually be constant and that the "apparent" concentration dependence is actually a consequence of a diffusion-induced pressure field within the rubber. From an experimental point of view this non-uniqueness is significant since results from typical sorption experiments would not be able to distinguish between the two models. It follows that the mechanical response could be responsible for some of the "observed" concentration-dependent diffusion coefficient.

### 3.3.4 Problem 4: 1-D Uncoupled Diffusion; Time Shift Modified Diffusion Coefficient; Elastic Material Properties

Again the one-dimensionality and elastic material properties allow the problem to be recast as an uncoupled problem. For the uncoupled problem the diffusion coefficient can be expressed in the following functional form

$$\begin{aligned} D(c) &= \frac{D_o}{\phi_d(c)}\left(1 + \frac{4\alpha KG\Lambda}{3K + 4G}\right) \\ &= D_o \exp\left[ b_d\left(\frac{1}{f_o} - \frac{1}{f(c)}\right)\right]\left(1 + \frac{4\alpha KG\Lambda}{3K + 4G}c\right) \end{aligned} \tag{3.17}$$

where

$$f(c) = f_o + \frac{3BK + 4(B-A)G}{3K + 4G}\alpha c \tag{3.18}$$

with $D_o$ the diffusion coefficient at zero concentration, time shift factor $\phi_d$, the swelling coefficient $\alpha$, bulk modulus $K$, shear modulus $G$, $\Lambda$ the constant relating pressure gradient to the diluent mass flux, $b_d$ the parameter related to the hole size need to accomplish a "jump," reference free-volume fraction $f_o$, free-volume fraction $f$, $A$ the mechanical dilatation participation factor for the free-volume fraction, and $B$ the swelling dilatation participation factor for the free-volume faction.

This case should be able to model the approximate diffusion behavior above the glass transition temperature where the material is near its rubbery stage. If the polymer is uncrosslinked the shear modulus in this

temperature region would approach zero and hence the resultant pressure would also tend to zero. This fact simplifies Eqn. (3.17) to

$$D(c) = D_o \exp\left[\frac{b_d}{f_o}\frac{B\alpha c}{f_o + B\alpha c}\right] \tag{3.19}$$

Numerical solutions for the coupled diffusion problem, with $\Lambda = 0$ and a nearly zero shear modulus ($G/K \sim 0.00016$), are shown in Figs. 3.10 and 3.11; and would correspond also to the uncoupled problem with the diffusion coefficient given by Eqn. (3.19). As a result of the time shift parameter the diffusion coefficient shows a strong concentration dependence. This dependence causes the concentration profiles to develop a sharp diffusion front (see Fig. 3.10) in comparison to the elastic problem where the diffusion coefficient is not modified by the time shift parameter (see Fig. 3.8). The sharp concentration gradients appear to be similar to what is expected for a Case II diffusion process, but the sorption plot (Fig. 3.11) still retains the initial $\sqrt{t}$ linearity (rather than the linearity with respect to $t$ for a Case II process) and thus would normally be classified as Fickian.

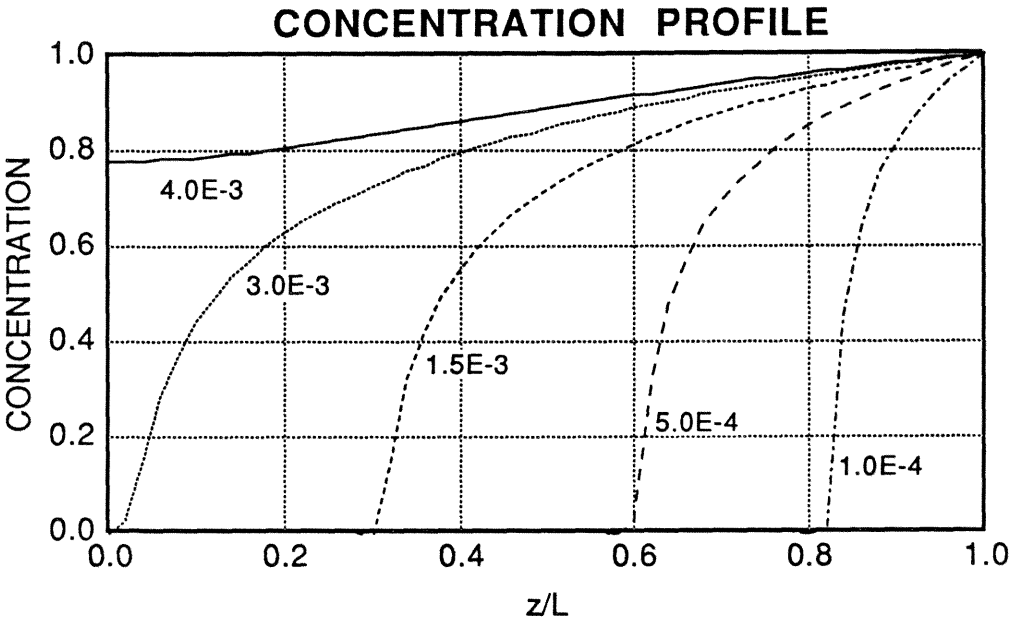


Figure 3.10 Concentration profile at various times for the elastic case with the diffusion coefficient affected by the time shifting parameter. The numbers on the curve represent a nondimensional time, $D_0t/L^2$.

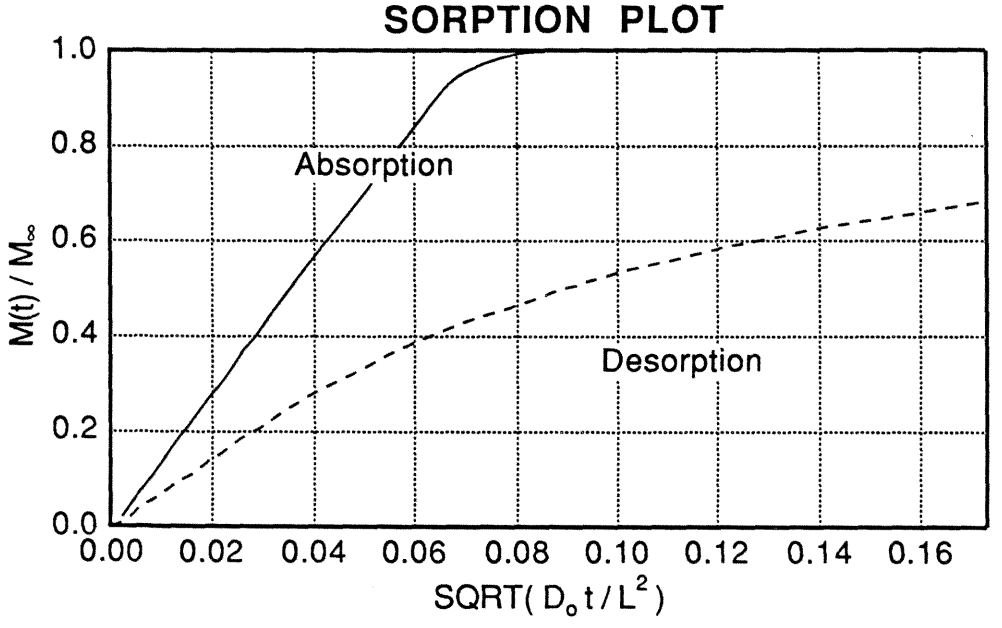


Figure 3.11 Sorption plot for Fig. 3.10; note that the initial linearity of the absorption curve would cause this problem to be classified as a Fickian diffusion process.

### 3.3.5 Problem 5: 1-D Coupled Diffusion; Time Shift Modified Diffusion Coefficient; Nonlinear Viscoelastic Material Response

The full effects of the nonlinear viscoelasticity and the proposed diffusion model are examined in this problem. The viscoelastic bulk and shear moduli are modelled using PVAc data, where the moduli have been scaled such that the glassy bulk modulus equals unity (see Fig. 3.12). The swelling coefficient was taken to be constant and equal to 0.3 and the pressure-induced relaxation coefficient, $\beta$, which is related to the swelling coefficient and the bulk modulus is given by Eqn. (1.21).

The results for the concentration profile are shown in Fig. 3.13. A significant feature is that at initial times the profiles are similar to those in Fig. 3.10, but as time progress the profiles become sigmoidal in shape. An explanation for the sigmoidal behavior can be put forth by examining the pressure profile, delineated in Fig. 3.14. The pressure profile shows a significant relaxation behavior leading to an inverse pressure gradient which inhibits the mass flux into the region. This causes the concentration profile to appear to "stall" creating the sigmoidal feature.

An absorption plot for the same material properties, but for two different thicknesses, are shown in Fig. 3.14. Note that the length scaling has failed and the process would be considered non-Fickian. A simple explanation can be put forth for this phenomenon: at "smaller" thicknesses the pressure field has less time to relax before a significant amount of diluent has diffused into the body thereby extending the Fickian behavior of the sorption plot. As the thickness is increased the pressure field can relax

causing the sigmoidal appearance of the sorption curve. The results are similar to the situation presented by the diffusion of allyl chloride into PVAc, shown in Fig. 3.3, suggesting that a similar phenomenon may be occurring for this diluent-polymer system*.

In the published literature sigmoidal behavior in sorption plots are often explained on the basis of a time-dependent (usually assumed exponential) concentration boundary condition, (see §2.4.5). It is noteworthy that the present model is also able to capture the sigmoidal behavior without resorting to a time-dependent boundary condition. The addition of a time-dependent concentration boundary condition would probably enhance the sigmoidal behavior, but for reasons mentioned in §2.4.5 this effect is not included in this study.

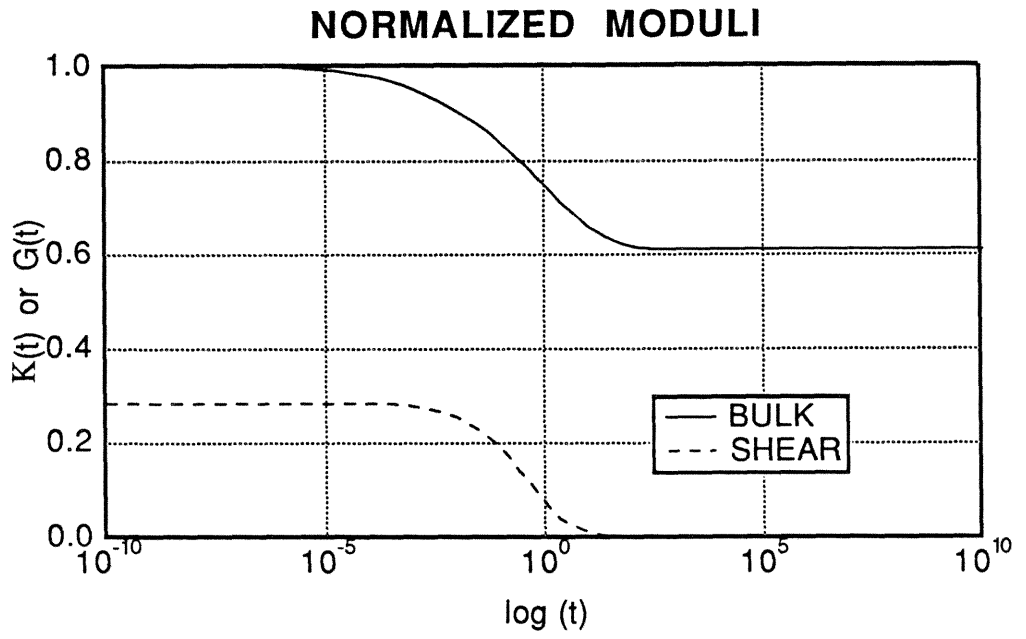


Figure 3.12 Material properties for the bulk and shear behavior used in the following numerical analysis. The properties are for PVAc normalized such that the bulk moduli is 1.0 in the glassy region.

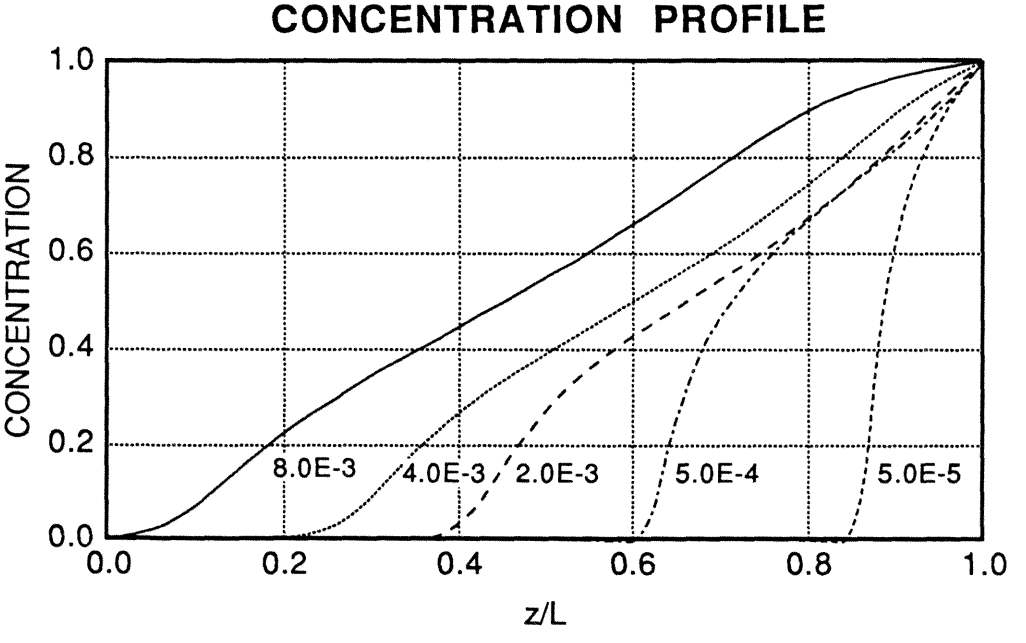


Figure 3.13 Concentration profile at various time steps for the fully viscoelastic case. Note the relaxation of the pressure field may cause the observed sigmoidal shape. The numbers on the curves reflect the nondimensional time, $D_0 t/L^2$.

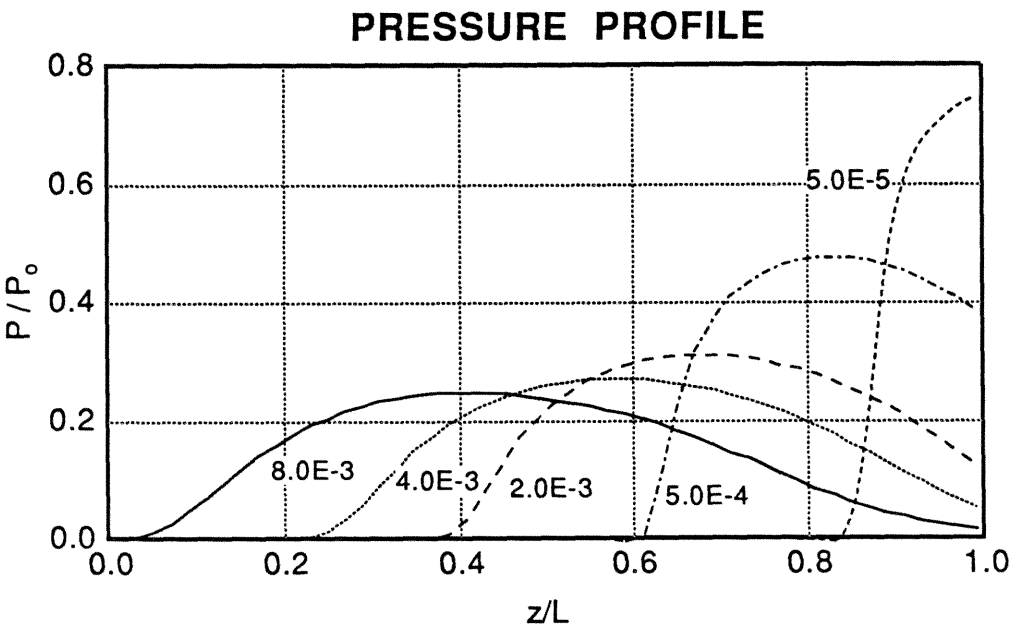


Figure 3.14 Pressure profile corresponding to Fig. 3.8. The significant pressure relaxation accounts for the sigmoidal nature of the concentration profile. The numbers on the curves represent a nondimensional time, $D_o t/L^2$.

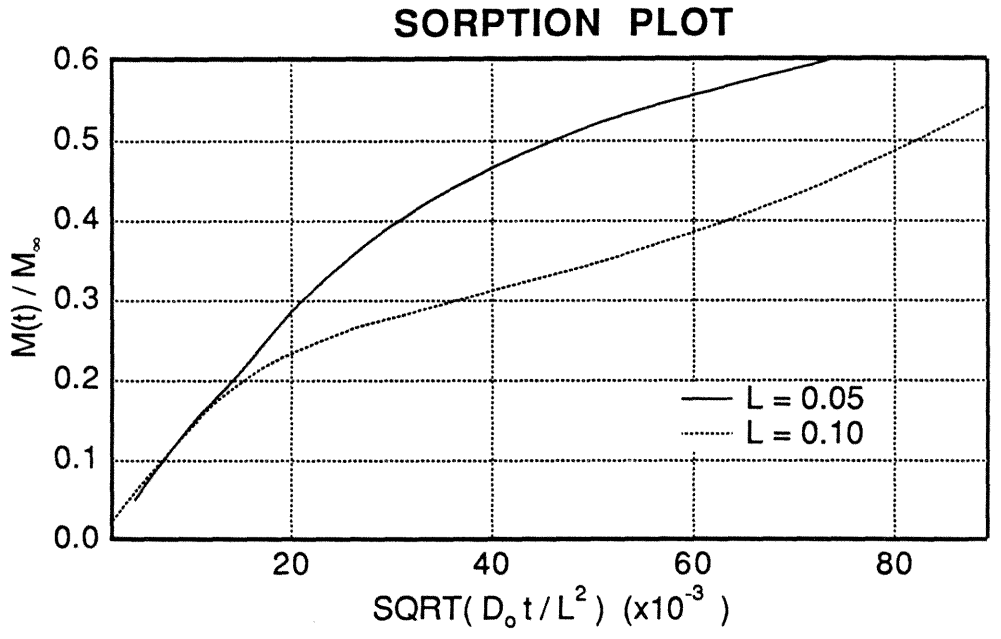


Figure 3.15 Absorption profile for two different thicknesses using the same properties as shown in Fig. 3.8.

## 3.4 Two-Dimensional Problems

As mentioned previously, diffusion experiments are conducted such that the results are assumed to be comparable to one-dimensional (1-D) solutions to Fick's diffusion equation. In this section the consequences of this assumption will be examined by comparing two-dimensional (2-D) solutions, which would more appropriately model typical diffusion experiments, to the corresponding 1-D solutions.

The axisymmetric assumptions for the 2-D problems restrict the deformations, mass flux, and concentration of the cylinder to be only functions of $r$, $z$, and $t$ (see Eqns. (3.1), (3.2), and (3.3)). For convenience the equations are repeated here,

$$u_r = u_r(r,z,t), \quad u_\theta = 0, \quad u_z = u_z(r,z,t) \tag{3.20}$$

$$j_r = j_r(r,z,t), \quad j_\theta = 0, \quad j_z = j_z(r,z,t) \tag{3.21}$$

$$c = c(r,z,t) \tag{3.22}$$

The free surfaces of the cylinder are considered traction free (the normal and shear stresses on the surfaces are zero).

$$\sigma_{zz}(r,\pm L,t) = \sigma_{rz}(r,\pm L,t) = 0; \quad r=[0,R], \quad \forall t \geq 0 \tag{3.23}$$

$$\sigma_{rr}(R,z,t) = \sigma_{rz}(R,z,t) = 0; \quad z=[-L,L], \quad \forall t \geq 0 \tag{3.24}$$

And the concentration boundary conditions are considered to be uniform along the cylinder's surface.

$$c(r,\pm L,t) = 1.0; \quad r=[0,R], \forall t \geq 0 \quad c(R,z,t) = 1.0; \quad z=[-L,L], \forall t \geq 0 \tag{3.25}$$

On the basis of angular symmetry for the above problem, the cylinder can be identified by the rectangular region between $r = [0,R]$ and $z = [0,L]$ and the symmetry boundary conditions are given as

$$u_r(0,z,t) = \sigma_{rz}(0,z,t) = j_r(0,z,t) = 0; \quad z=[0,L], \quad \forall t \geq 0 \tag{3.26}$$

$$u_z(r,0,t) = \sigma_{rz}(r,0,t) = j_z(r,0,t) = 0; \quad r=[0,R], \quad \forall t \geq 0 \tag{3.27}$$

The region for the 2-D problem with the associated boundary conditions can now be depicted as

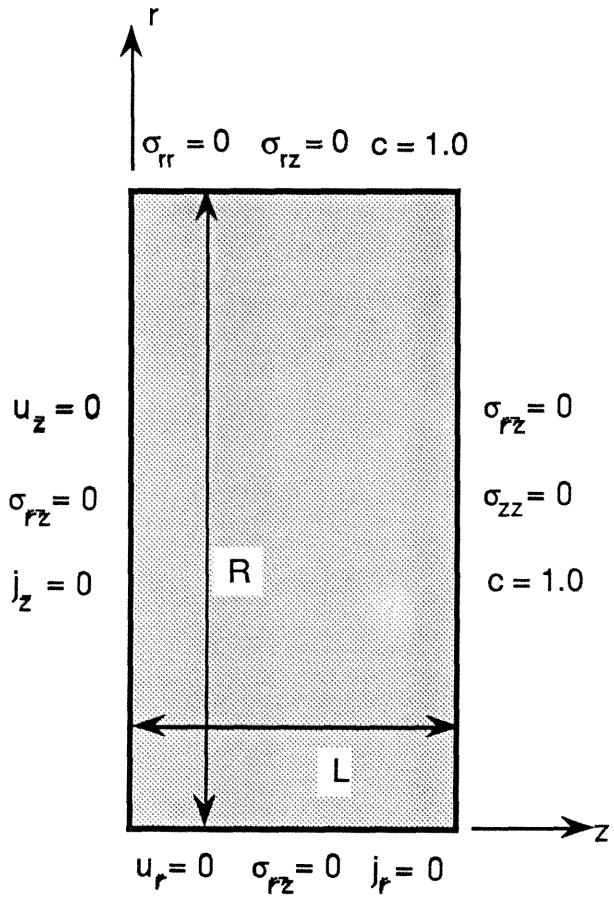


Figure 3.16 Modelled region for the 2-D problems with the associated boundary conditions.

Two-dimensional numerical simulations for both the uncoupled and coupled diffusion problems are computationally intensive and, as a result of available computer time restrictions, not all permutations of the relevant material and geometrical parameters could be analyzed. This study confines the 2-D analyses to basically the same material parameters that were examined in the 1-D section. In most cases this allows a comparison between the two situations. A summary of the 2-D cases that were examined is found in Table 3.2.

| Summary of Two-Dimensional Numerical Analyses | | | | |
|---|---|---|---|---|
| # | Description | Material Properties | Comments | Fig. |
| 6 | Uncoupled diffusion with constant $D$ and elastic material response (Corresponds to Pb. 1). | $D$=0.01, $\Lambda$=0, $K$=1.0, $G$=0.28265 $\alpha$=0.3, $\beta$=0.3 | Examines the effect of 2-D Fickian solution as compared to 1-D cases. Motivates a modified boundary condition. The geometry is $L$=0.05, $R$=[0.005,0.05] with a minimum element size of dz=0.005. | 3.17 3.18 3.19 3.20 3.21 3.22 3.23 |
| 7 | Same as 6 except modified boundary conditions are used. | $D$=0.01, $\Lambda$=0, $K$=1.0, $G$=0.28265 $\alpha$=0.3, $\beta$=0.3 | Examines the effect of modifying the lateral boundary conditions to be impermeable. | 3.24 |
| 8 | Coupled diffusion with constant $D$ and elastic material properties (Corresponds to Pb. 3). | $D$=0.001, $\Lambda$=100, $K$=1.0, $G$=0.28265 $\alpha$=0.3, $\beta$=0.3 | The geometry is $L$=0.05, $R$=0.5 ($R/L$=10) with a minimum element size of dz=0.002. Results appear Fickian as in Pb. 3. | 3.25 3.26 3.27 3.28 3.29 3.30 |
| 9 | Uncoupled diffusion with time shifting of $D$ and elastic material properties (Corresponds to Pb. 4) | $D_o$=0.001, $\Lambda$=0, K=1.0 or 0.6083, $G$=0.283 or 0.0001 $b$=0, $b_d$=30, $f_o$=1.0 $A$=1.0, $B$=0.9, $\alpha$=0.3, $\beta$=0.3 | The geometry is L=0.05, R=0.5 with a minimum element size of dz=0.002. Appearance of Case II behavior for glassy properties. | 3.31 3.32 3.33 3.34 3.35 3.36 |
| 10 | Coupled diffusion with time shifting of D and elastic material properties | $D_o$=0.001, $\Lambda$=100, K=1.0, $G$=0.28265 $b$=0, $b_d$=30, $f_o$=1.0 $A$=1.0, $B$=0.9, $\alpha$=0.3, $\beta$=0.3 | The geometry is L=0.05, R=0.5 with a minimum element size of dz=0.002. | 3.37 3.38 3.39 3.40 |
| 11 | Coupled diffusion with time shifting and viscoelastic material properties (Corresponds to Pb. 5) | $D_o$=0.001, $\Lambda$=100, $K$ and $G$ see Fig. 3.12. $b$=30 or 40, $b_d$= 20 or 30, $f_o$=1.0, $A$=1.0, $B$=0.9, $\alpha$=0.3, $\beta$=$\alpha K$ | An example of the effect of coupled diffusion model. The viscoelastic properties relaxes the pressure field slowing the rate of diffusion into the body. The geometry is L=0.05, R=0.5 with a minimum element size of dz=0.002 | 3.41 3.42 3.43 3.44 3.45 3.46 |

Table 3.2 Summary of the 2-D numerical analyses that were performed.

### 3.4.1 Problem 6 : 2-D Uncoupled Diffusion; Constant D; Elastic Material Properties

For these numerical simulations the diffusion coefficient has a constant value, $D_o$, and the resultant pressure field does not contribute to the mass flux. To examine the effects of two-dimensionality various $R/L$ ratios were analyzed and the actual parameters used to generate these curves can be found in Table 3.2. The consequence of the two-dimensionality on the diffusion process is evident in the sorption plots shown in Fig. 3.17. There it can be seen that as $R/L$ becomes large the 2-D solutions approaches the 1-D case which is depicted as $R/L$ equal to $\infty$.

To evaluate the diffusion coefficient from experimental sorption curves a small time approximation for the 1-D plane sheet solution is typically used. Using this approximation the diffusion coefficient can be expressed as

$$D = \frac{\pi}{4}\Theta^2 \tag{3.28}$$

where $\Theta$ is the initial slope of the "reduced" sorption curve ( $M(t)/M_\infty$ vs $\sqrt{t}/L$ ).

Assuming that all the sorption curves depicted in Fig. 3.17 are from a 1-D plane sheet solution Eqn. (3.28) can used to calculate the "apparent" diffusion coefficient. The error introduced by this 1-D assumption could then be compared to the diffusion coefficient's actual value of $D_o$. The resultant error is shown in Table 3.3 for the various $R/L$ ratios.

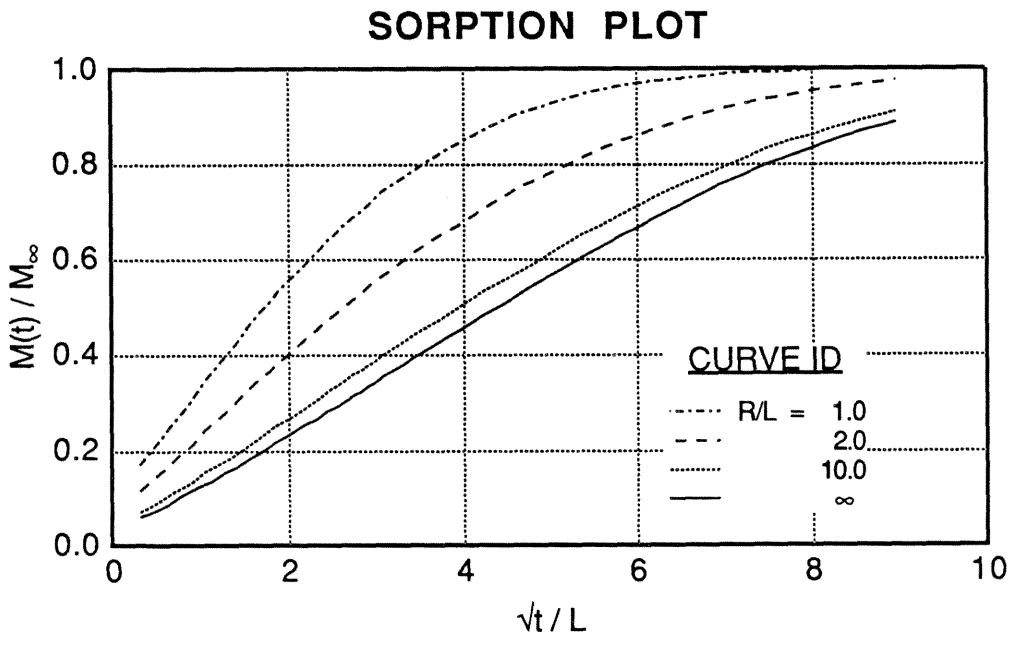


Figure 3.17 Sorption plot for varying R/L for a constant diffusion coefficient $D_0$. If these curves were assumed to be from a 1-D solution, the two-dimensionality would give the appearance of a larger diffusion coefficient as indicated by the larger slope of the curves.

Hence even $R/L$ ratios of 10 to 1 would produce an error of 10%, so care must be taken when using Eqn. (3.28) to reduce sorption experimental data such that the planar area is much greater than the edge or side area. Most sorption experiments use thin films with a large cross-sectional area with typical $R/L$ ratios varying from 20 to 300. For these $R/L$ ratios the 1-D assumption would produce an error of less than 5% which is acceptable in light of the errors introduced by the experimental measurement techniques.

More important is that the resultant pressure and dilatational fields also become two-dimensional in nature and that the effects extend beyond the concentration front. Contour plots for the concentration, pressure, and

dilatation fields at a nondimensional time, $D_0t/L^2 = 0.02$, are presented as a function of $R/L$ in Figs. 3.18, 3.19, and 3.22, respectively.

| Comparison of Diffusion Coefficients for Various R/L | | |
|---|---|---|
| $R/L$ | $D$ (calculated)$/D_0$ | % error |
| 1.0 | 4.207 | 320 |
| 2.0 | 2.152 | 115 |
| 10.0 | 1.100 | 10.0 |
| $\infty$ | 1 | 0 |

Table 3.3 Comparison of diffusion coefficients for various $R/L$ ratios, demonstrating the error by assuming a 1-D solution for a 2-D problem.

The contour plots for the concentration approaches the 1-D solution as $R/L \rightarrow \infty$ confirming the sorption plots shown in Fig. 3.17. What may not be as apparent as a result of the spatial normalization, $r/R$ and $z/L$, is that for this uncoupled case the diffusion front moves at approximately the same speed in both the $r$ and $z$ directions. As the diffusion process becomes coupled the effects of the pressure field and the time shift modified diffusion coefficient would probably alter the speed of the diffusion front in both the $r$ and $z$ directions.

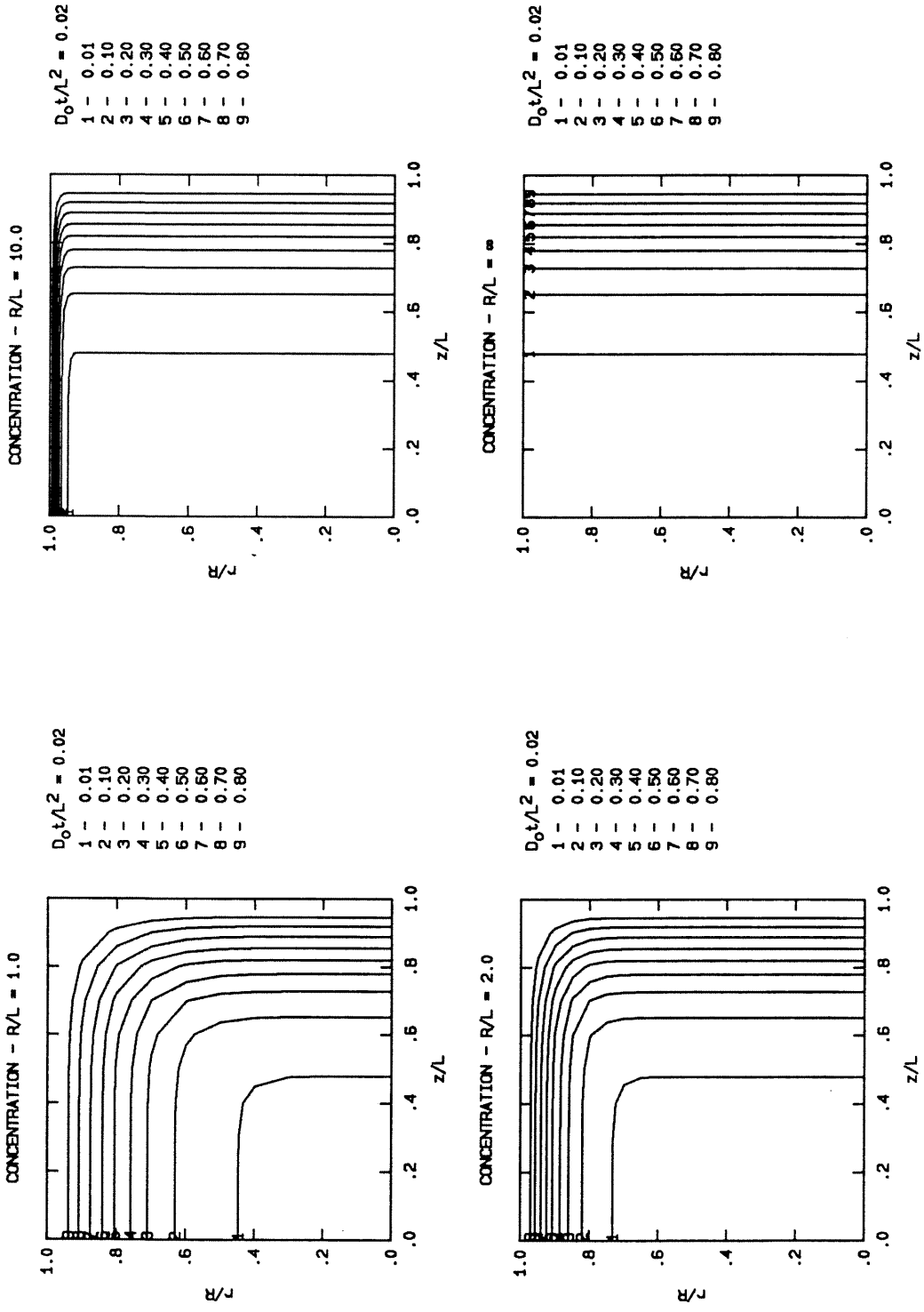


Figure 3.18 Concentration contour plots at $D_o t/L^2 = 0.02$ for various $R/L$ ratios. As $R/L \rightarrow \infty$ (see $R/L = 10$) the results begin to approach the 1-D solution.

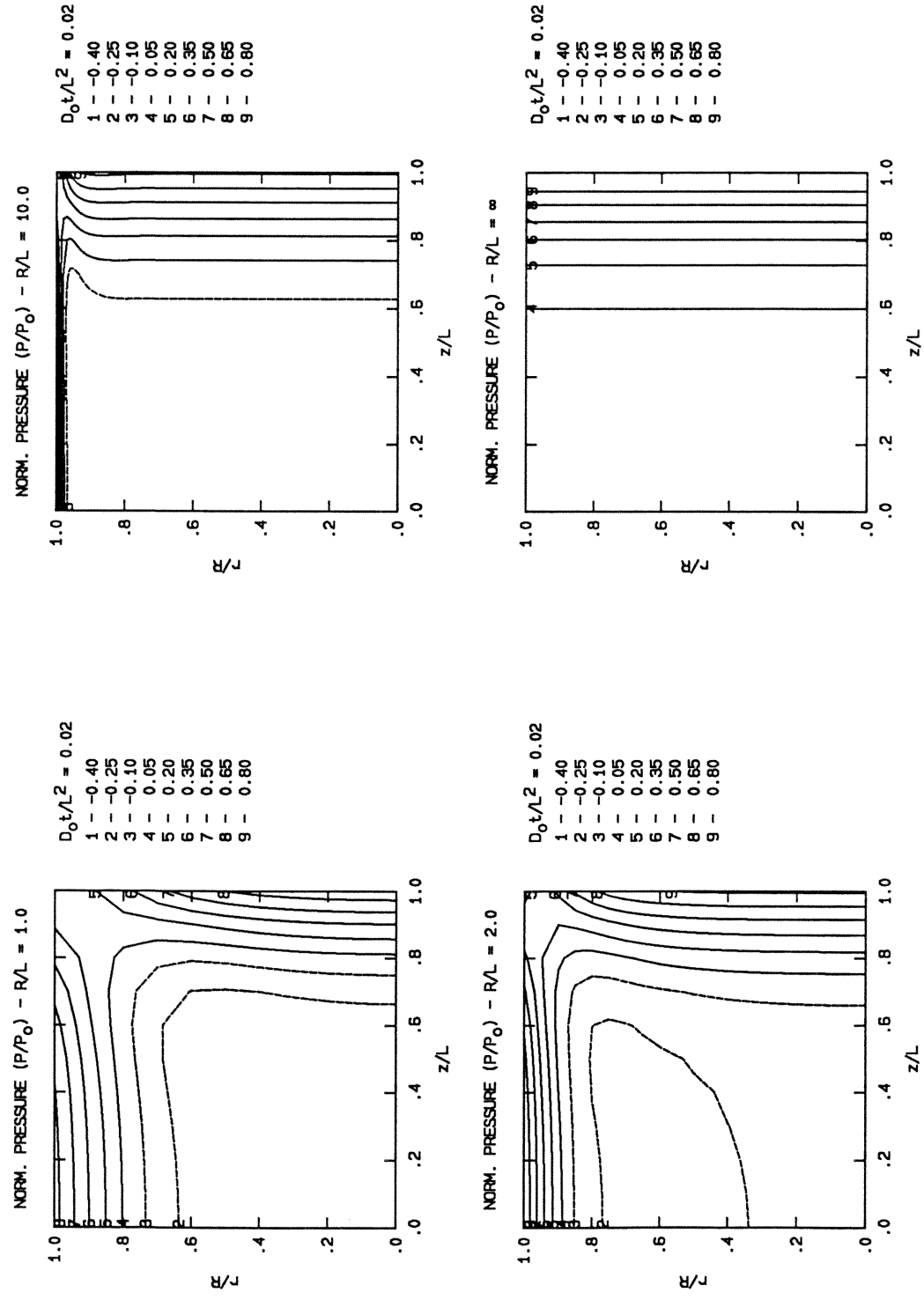


Figure 3.19 Pressure contour plots at $D_o t/L^2 = 0.02$ for various $R/L$ ratios. The pressure has been normalized by $P_o$, the equilibrium pressure value for the corresponding 1-D problem (Problem 1). As $R/L \to \infty$ (see $R/L = 10$) the results become one-dimensional near the region $r = 0$.

The pressure contour plots, Fig 3.19, also become one-dimensional in nature as $R/L$ is increased but does not approach the corresponding 1-D solution. Unlike the 1-D case which has a finite equilibrium pressure value, $P_o$, the 2-D equilibrium pressure is zero. From this observation the decay of the pressure field, as shown in Fig. 3.20, must be a consequence of the two-dimensionality and the traction-free boundary conditions.

From the contour line separation the pressure gradient at $r = 0$ for $R/L$ values of 10 and $\infty$ are nearly the same. This suggests that the 2-D pressure field, like the 1-D pressure field, may be related to the concentration field. This can be seen more clearly in Fig. 3.21 where the concentration profile and a modified pressure profile are plotted at various nondimensional times, $D_o t/L^2$. The modifications to the pressure profile at $r = 0$ includes a normalization by the 1-D equilibrium pressure, $P_o$, and a vertical shift by an additive constant such that at $z = L$ the modified pressure value is unity. Observing that the two profiles in Fig. 3.21 are identical one may suggest that the pressure can be related to the concentration through the following equation

$$P(z,t) = P_o c(z,t) + B(t) \qquad \text{near } r = 0 \tag{3.29}$$

where $B(t)$ is some function of the material parameters, geometry, and time.

Analytically this result can be shown to be true if the displacement field in the region around the axis of the cylinder takes the form

$$u_r = u_r(r,t); \quad u_z = u_z(z,t) \tag{3.30}$$

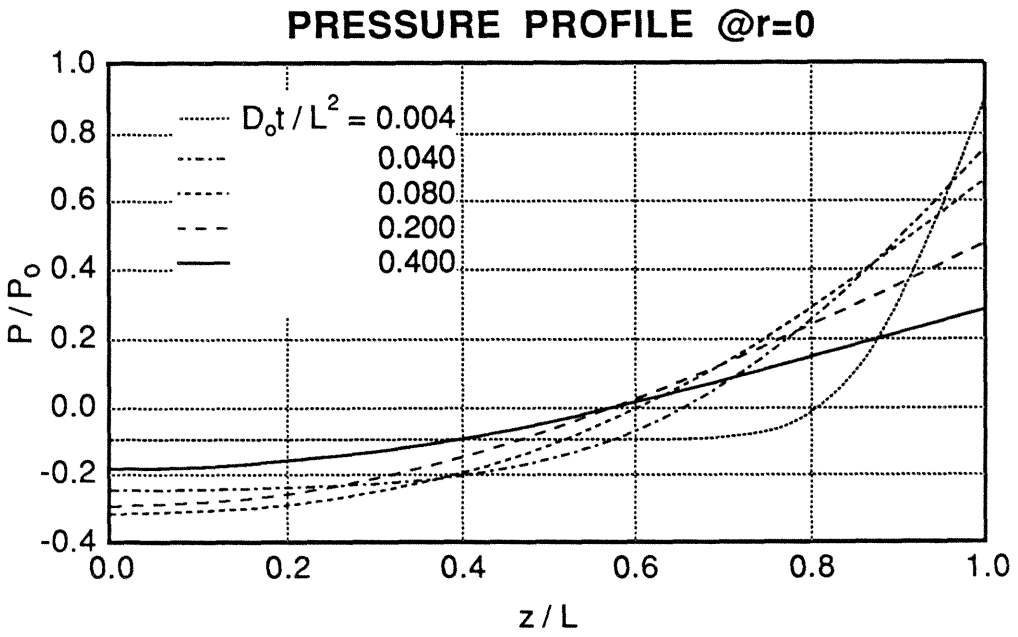


Figure 3.20 Normalized pressure profile for R/L = 10.0 at $r = 0$. $P_0$ is the equilibrium pressure value for the corresponding 1-D case (Problem 1).

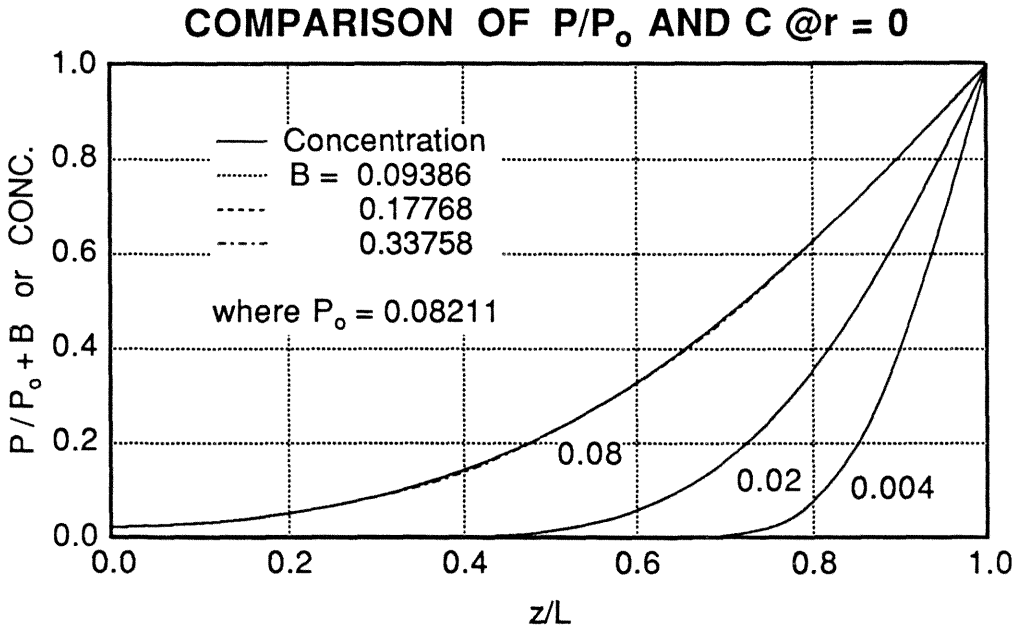


Figure 3.21 The correspondence between the modified pressure and concentration profiles suggest that near $r = 0$ the pressure field is linearly related to the concentration. The numerical values for B and Po are dependent on the input material parameters and geometry that are found in Table 3.2. The numbers on the curves represent a nondimensional time, $D_0t/L^2$.

If this were the case, the pressure field and dilatational field can be shown to be linearly related to the concentration through an equation similar to Eqn. (3.29). However the function $B(t)$ is undetermined by the analysis and must be numerically derived.

In general, unlike the 1-D cases, there is no 2-D analytical solution for the MR problem and therefore the coupled diffusion problem cannot be uncoupled. However near the region $r = 0$, for large $R/L$ values, an equation similar to Eqn. (3.29) may hold for the pressure field, allowing one to "uncouple" the diffusion problem since only the spatial gradient of the pressure field directly enters the diffusion equation.

Contour plots for the dilatation, shown in Fig. 3.22, also become 1-D in nature and, like the pressure field, a normalized dilatation value near $r = 0$ does compare with the 1-D case by just an additive vertical shift. As a result of the traction-free boundary conditions the equilibrium dilatation for the 2-D case is higher than that of the corresponding 1-D problem.

From the above observations for the uncoupled diffusion problem, the coupled diffusion processes may be seriously affected by the change from one to two dimensions. Though both the pressure and dilatation fields become more complicated for this 2-D case, the two fields for large $R/L$ ratios near $r = 0$ may still be linearly related to the concentration field. Thus the added mass flux due to the pressure gradient would be the same for the two cases. The same cannot be said about dilatation because the actual value of the dilatation affects the free-volume fraction and therefore the time shift factor and not the gradient. Also the equilibrium dilatation for the two problems are not equal because of the added constraints impos-

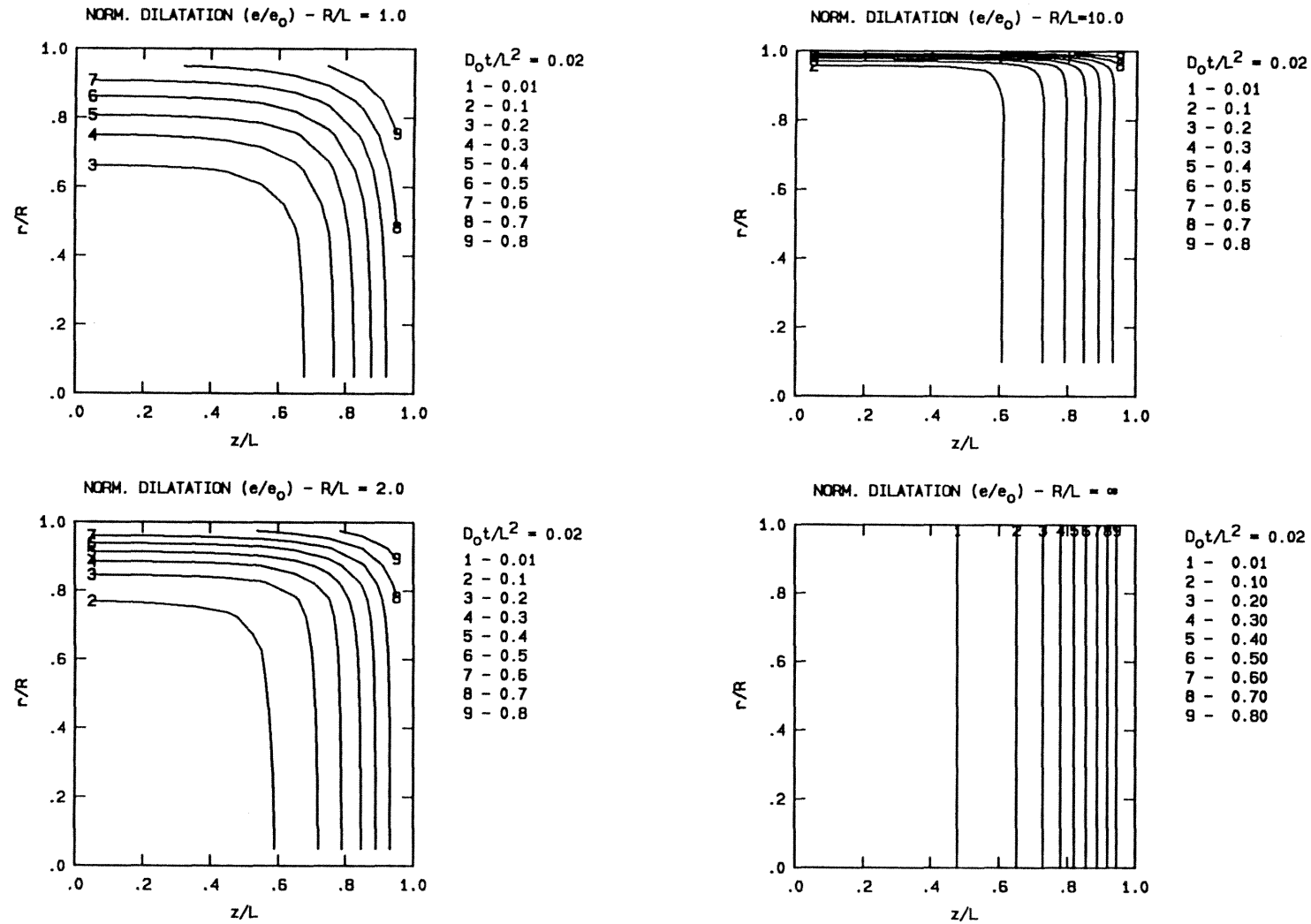


Figure 3.22 Dilatation contour plots at $D_0t/L^2 = 0.02$ for various R/L ratios. As R/L $\rightarrow \infty$ (R/L = 10) the results begin to assume a one-dimensional nature.

ed on the 1-D case. As the effect of time shifting is included in the coupled diffusion problems, the full three-dimensional problem must be considered to accurately capture the dilatation behavior.

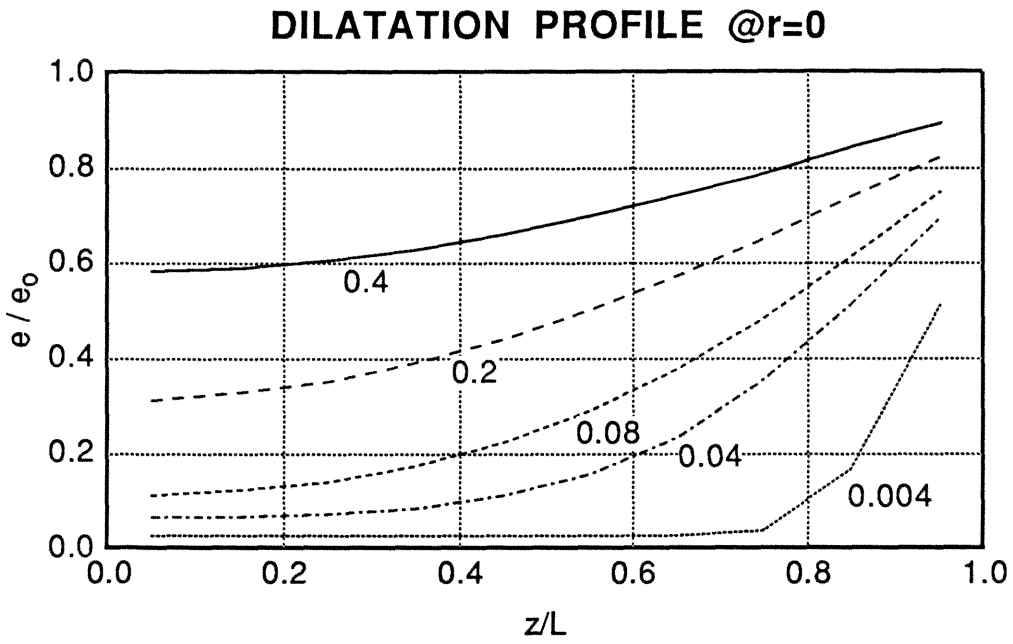


Figure 3.23 Dilatation profile for $R/L$ = 10.0 at $r$ = 0. The numbers on the curves represent nondimensional times, $D_0t/L^2$. The dilatation is plotted from strain values at the one-point Gauss quadrature point and normalized by $e_0$ the 2-D equilibrium dilatation for this problem.

### 3.4.2 Problem 7: 2-D Uncoupled Diffusion; Constant Diffusion Coefficient; Elastic Material Response; Modified Boundary Conditions

In order to capture the proper solution as the concentration front moves, the resulting numerical mesh or elements must be small enough to capture the salient features of the solution. This requirement calls for a fine mesh in both the $r$ and $z$ directions and the resulting matrix equation

will be very large (on the order of 3000 degrees-of-freedom) and computationally expensive, 5-10 Cray YMP units per time step. As $R/L \rightarrow \infty$ the solution becomes one-dimensional and it behooves one not to solve for the concentration front as it moves in the radial direction, since it occupies only a small fraction of the entire region. With this condition in mind one may try to compare the 2-D solutions of the preceding section to a solution for which the lateral surface of the cylinder is considered to be impermeable. In this way, the basic concentration front will move in the axial direction allowing one to forgo the fine mesh restriction in the radial direction. Since the displacement, strain, and pressure fields will still be 2-D the mesh in the radial direction must still be able to accurately capture these fields, but even with this restriction the computational cost can be significantly decreased.

A comparison of the pressure and dilatation contour plots for the full 2-D case versus the modified 2-D problem is shown in Fig. 3.24. The two solutions are shown to be comparable provided one is concerned with the central region of the cylinder, near $r = 0$. As the problem becomes more coupled and nonlinear, the region of comparison will probably still exist, but will be reduced in size.

Keeping these issues in mind, in the following sections the numerical solutions will be performed using the modified boundary condition which is formally given as

$$j_r(R,z,t) = 0; \quad z = [0,L] \quad \forall t \geq 0 \tag{3.30}$$

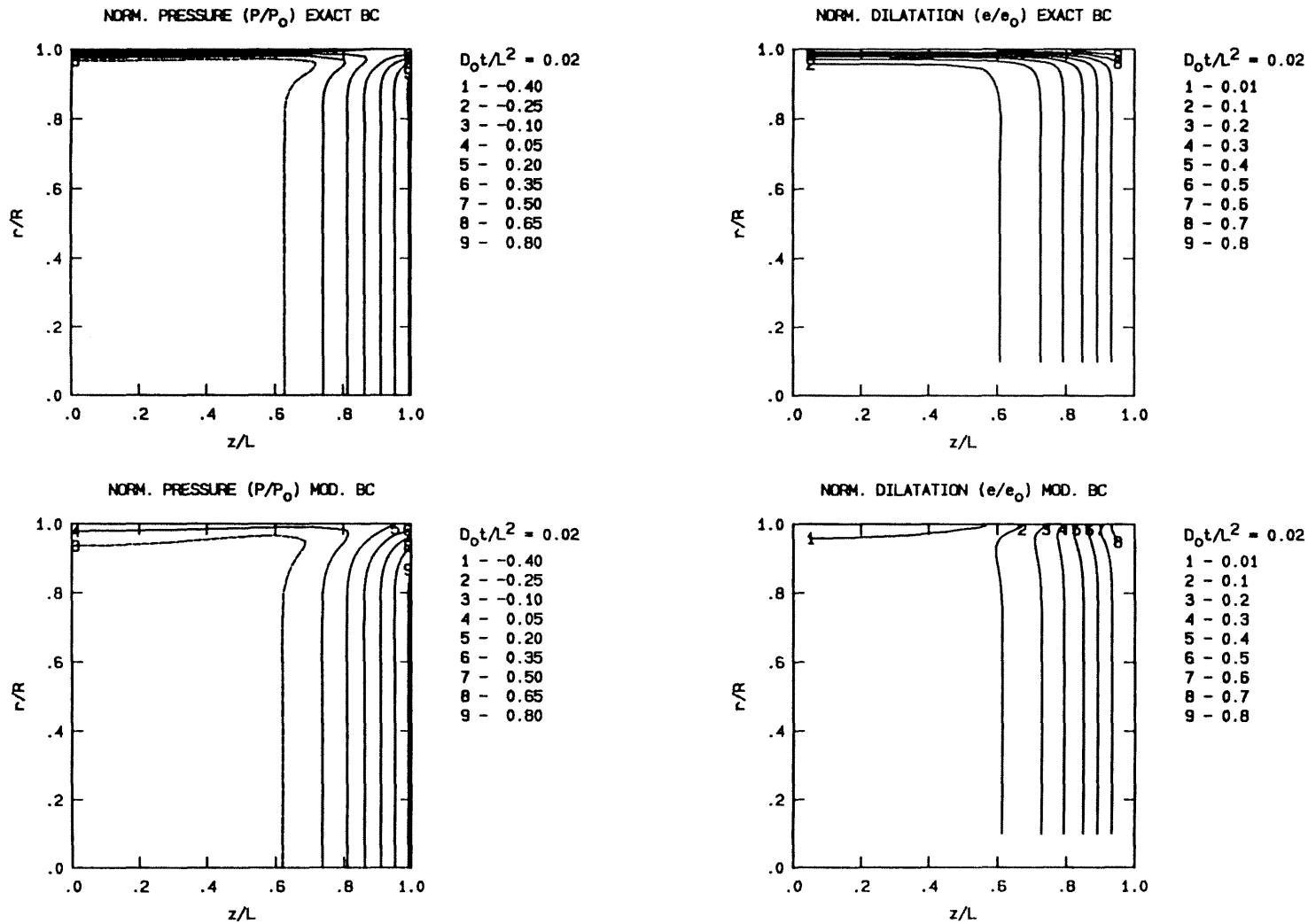


Figure 3.24 Comparison for $R/L = 10$ between the full 2-D problem and the modified boundary condition problem for the pressure and dilatational contour plot at $D_0t/L^2 = 0.02$. The two solutions are comparable provided one is concerned with the region near the axis of the cylinder, $r = 0$.

### 3.4.3 Problem 8 : 2-D Coupled Diffusion; Constant Diffusion Coefficient; Elastic Material Response; Modified Boundary Conditions

For this problem the pressure gradient is included in the diffusion equation, thus coupling the mechanical response to the diffusion process. The diffusion coefficient is assumed to be constant and not modified by the time shift parameter and the material properties are considered to be linearly elastic. The actual values used in this numerical simulation are listed in Table 3.2. An $R/L$ ratio of 10 was used since it approximated the 1-D solution in Problem 6 and because the modified boundary conditions are used only in the region near $r = 0$.

The concentration profile at $r = 0$ is depicted in Fig. 3.25 at several nondimensional times, $D_o t/L^2$. The curves exhibit a slight concavity with respect to the $z$-axis and are similar to the 1-D concentration profile curves in Fig. 3.8.

The pressure profile at $r = 0$ is normalized by the equilibrium pressure, $P_o$, for the corresponding 1-D Problem (Problem 3) and depicted in Fig. 3.26 at several nondimensional times, $D_o t/L^2$. The normalized pressure profile is similar to the concentration profile except that it is vertically shifted by an additive constant (see Fig. 3.27) so the linearity with respect to the concentration (as described in Problem 6) of the pressure field near $r = 0$ still appears to hold.

The dilatation profile at $r = 0$ is depicted in Fig. 3.28 at several nondimensional times, $D_o t/L^2$. The curves are normalized by the equilib-

rium dilatation value of $e_o$ and are similar to the curves in Fig. 3.23 of Problem 6.

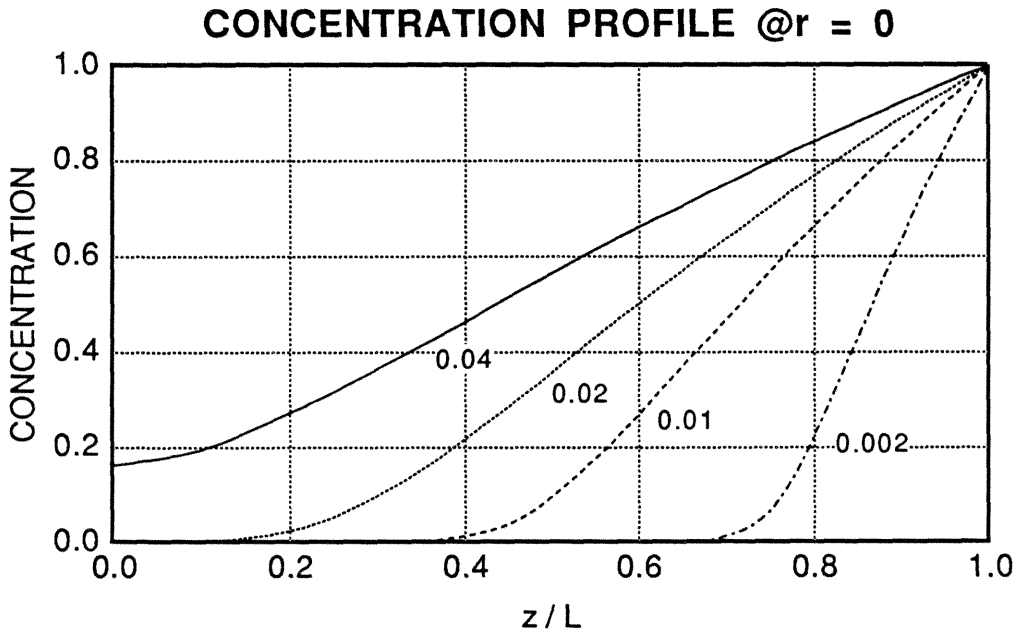


Figure 3.25 Concentration profile for $R/L$ = 10 at $r$ = 0 at several nondimensional times, $D_o t/L^2$.

Depicted in Fig. 3.29 is a comparison of the sorption plots for Problem 8 and Problem 3, the corresponding 1-D solution. Since the pressure gradient is proportional to the concentration gradient by the same factor, $P_o$, the two sorption curves should be comparable, but Problem 8 appears to have a slower absorption rate. An examination of the concentration contour plots, in Fig. 3.30, shows that near the lateral boundary, $r = R$, the concentration front tends to "lag" behind the front at $r$ = 0. This phenomenon is a result of the traction-free boundary conditions, for both the modified and unmodified BC's, which cause the pressure field near the boundary to be reduced (see Fig. 3.18) and thus decrease the mass flux contribution from a pressure gradient.

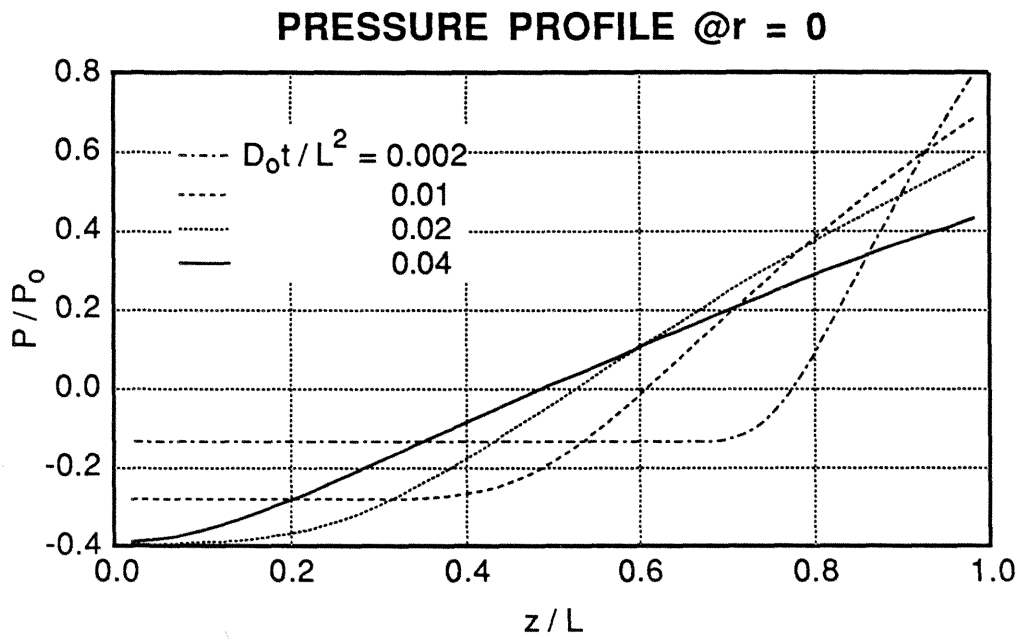


Figure 3.26 Pressure profile at $r = 0$ for $R/L = 10$ at several nondimensional times, $D_0t/L^2$. The value of $P_0$ is the equilibrium pressure for the 1-D case described in Problem 1.

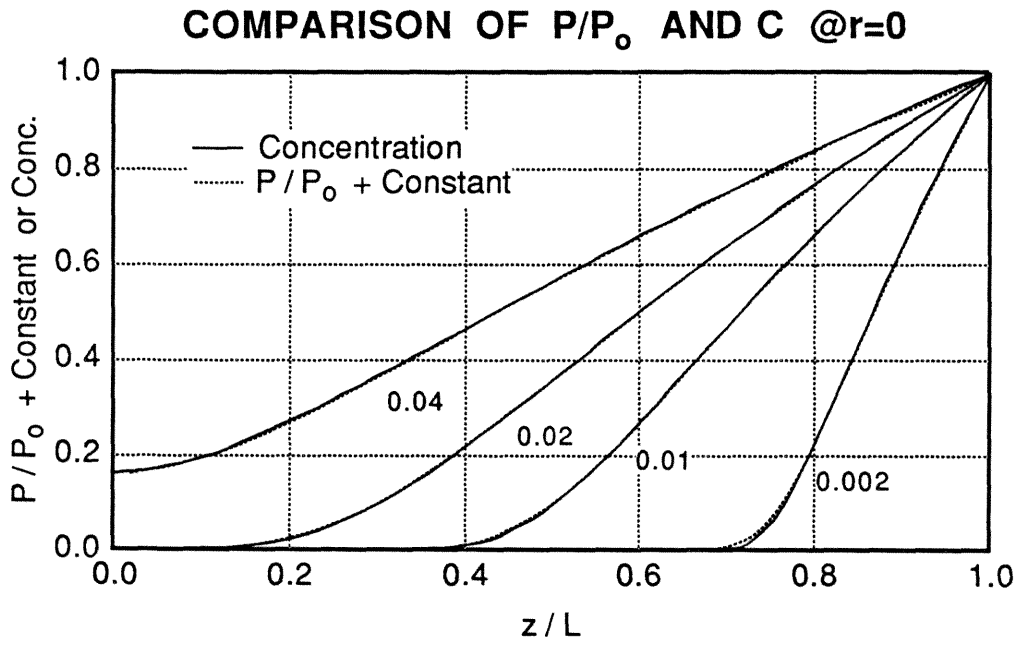


Figure 3.27 Modified pressure profile as compared to the concentration profile. The normalized pressure profiles are shifted vertically by additive constants which are 0.1326, 0.2802, 0.3921, 0.5491 for $D_0t/L^2$ = 0.002, 0.01, 0.02, 0.04, respectively. $P_0$ is the equilibrium pressure for Problem 1.

As mentioned before (Problem 6) the sorption plots between the 1-D cases and the 2-D cases are not truly comparable unless the $R/L$ ratios become very large. The modified boundary conditions alter this statement slightly since sorption curves using the modified BC's do not have the added mass due to the edge effects. In either case the 1-D sorption curves appear to follow the same trends as the 2-D sorption curves using either BC, so for the sake of computational effort the modified BC will still be used and the interpretation of the sorption curves will have to include the contour plot solutions for the concentration.

The similarity between the 1-D and 2-D problem for the concentration profile and sorption plot demonstrates that one may approximate the 2-D problem by the 1-D problem. Also since the concentration profiles and sorption curves are similar for both the one- and two-dimensional cases, the comments made in Problem 3 would also be applicable here. More importantly the lack of uniqueness in these two types of results make it difficult to determine which is the appropriate diffusion model.

However, if the stresses and strains were the focus of attention, the full 2-D problems would need to be modelled due to the significant differences between the two cases.

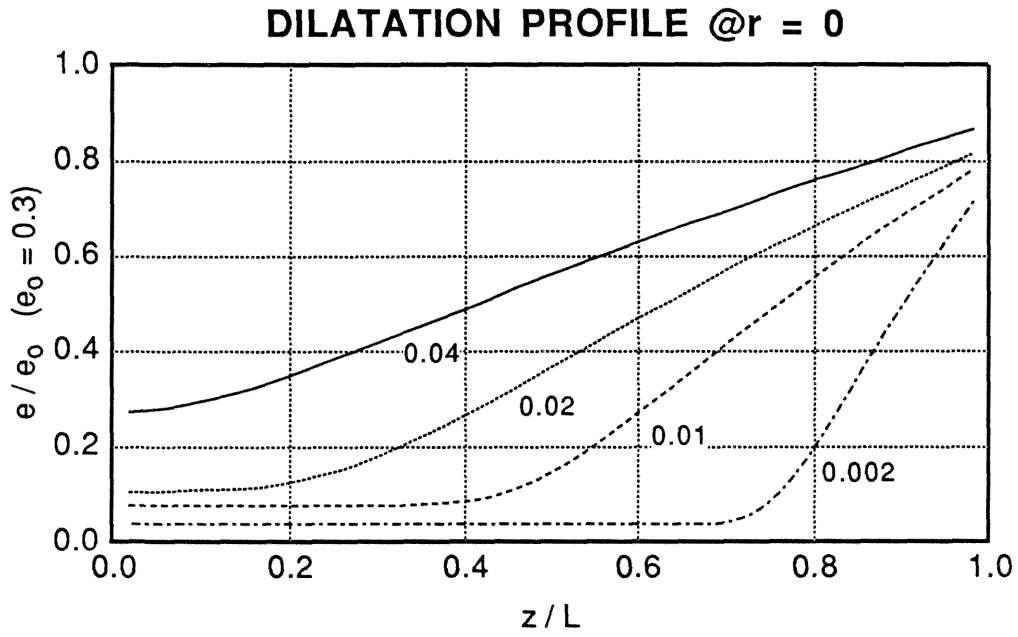


Figure 3.28 Dilatation profile at $r$=0.0 at several nondimensional times, $D_0t/L^2$. The equilibrium dilatation for Problem 8 is denoted $e_0$. The numbers on the curves indicate a nondimensional time, $D_0t/L^2$.

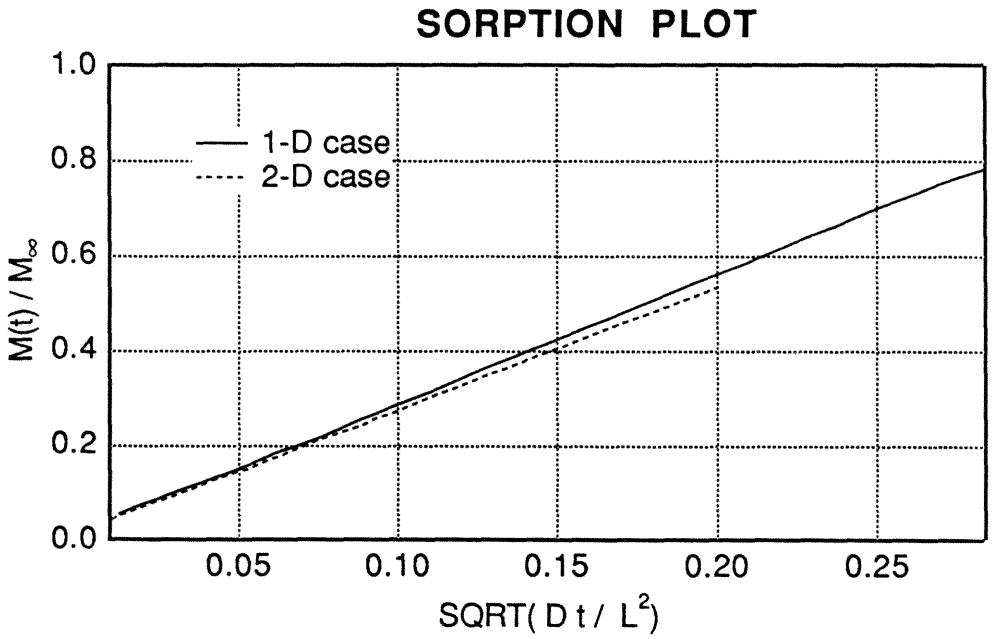


Figure 3.29 Comparison of sorption profiles between the corresponding 1- and 2-D cases.

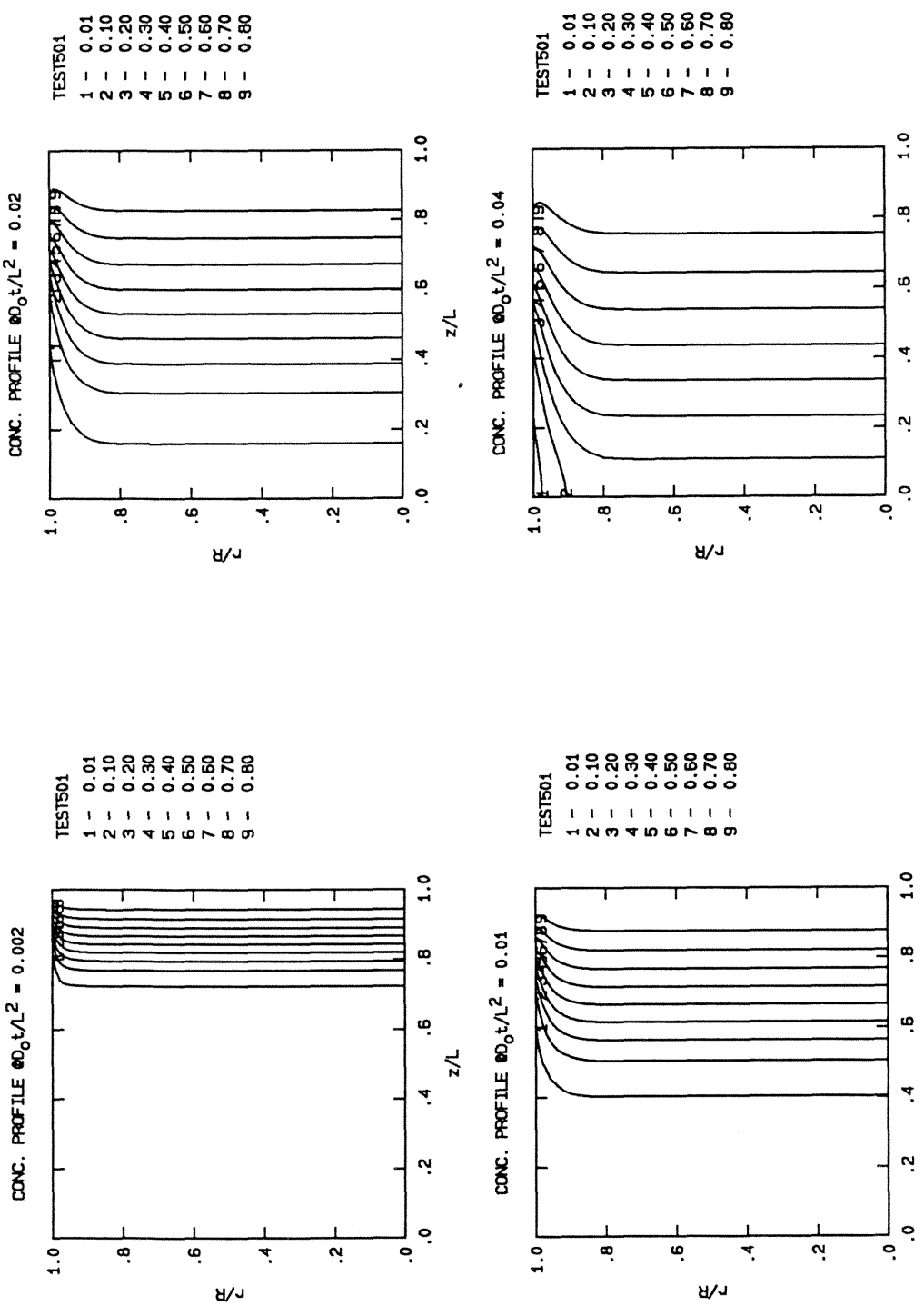


Figure 3.30 contour concentration plots for Problem 8 at several nondimensional "times." Notice that the approximate boundary conditions cause the concentration profile near $r = R$ to "lag" behind the profile near $r$=0.

### 3.4.4 Problem 9: 2-D Uncoupled Diffusion; Time Shift Modified Diffusion Coefficient; Elastic Material Response; Modified Boundary Conditions

In Problem 9 the pressure-induced mass flux was eliminated so that the effect of a time shifting diffusion coefficient could be studied. To minimize the 2-D behavior a $R/L$ ratio of 10 was used and the modified boundary conditions imposed. For this problem two different elastic material properties have been considered: one, values depicting the glassy response of polymer, and two, tthe rubbery response. The modelled material is assumed to represent an uncrosslinked polymer which has a "long" time shear modulus approaching 0 ($G/K \rightarrow 0$) for the rubbery response.

The basic effect of the two different material properties on the mechanical response is that for the rubbery material properties the pressure field is zero and the swelling strain is equal to the dilatation (the mechanical dilatation is zero). In contrast the glassy material properties have pressure and dilatation response which is similar to what has been seen in Problems 6 through 8. Bear in mind that the time shifting is dependent on the free volume of the material, which in turn is assumed to be related to the dilatation. Hence in Problem 9 the effect of the dilatation should become apparent.

The effect of the material properties can be seen in the sorption curve for the two cases, as shown in Fig. 3.31. The glassy sorption curve tends to curve away from the abscissa indicating that the sorption rate is greater than what a typical Fickian diffusion response would be. On the other hand the rubbery sorption curve exhibits the typical Fickian behavior. In

Fig. 3.32 the sorption curves are plotted with respect to time. The glassy sorption curve appears to have, after an initial Fickian behavior where the curve is concave towards the time axis region, a linear (between $0.01 < t < 0.015$) region that is characteristic of Case II behavior. The rubbery sorption curve remains concave toward the time axis.

To examine if the glassy properties lead to Case II behavior, the concentration profiles are plotted and are shown in Figs. 3.33 and 3.34. From Fig. 3.34 the glassy concentration front appears to be moving at a constant rate, another indicator of a Case II diffusion process. The rubbery concentration front shows the typical slowing characteristic of Fickian-type diffusion.

From the observations on the sorption and concentration plots several comments can be made. For the rubbery material properties, the results suggest that a Fickian diffusion process is occurring but is the result of a non-Fickian diffusion model. This again illustrates the nonuniquess that may occur between the proposed model and the Fickian model. The results are similar to those found in Problem 4 and this is a consequence of the dilatation being proportional to the concentration field (see Fig. 3.35). The difference between the diffusion response for the rubbery and glassy material values suggests that the material's ability to "resist" the swelling that occurs during the diffusion process and development of internal stresses, may play a role in the evolution of a Case II response.

For completeness the pressure field for the simulation using the glassy material properties at $r = 0$ cases is shown in Fig. 3.36. The rubbery properties have a pressure field of zero for all times.

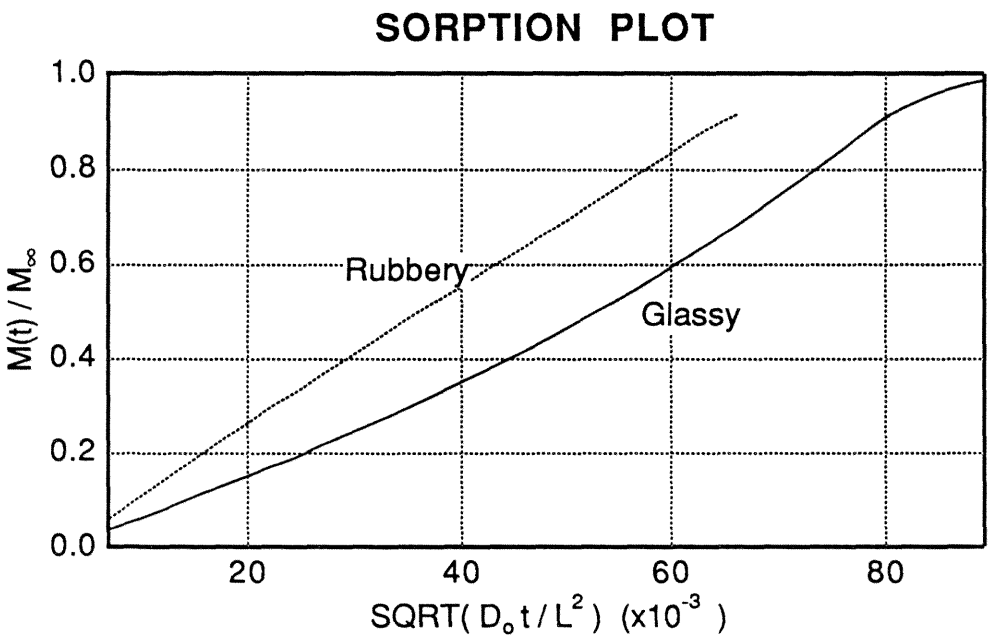


Figure 3.31 Sorption plot for Problem 9 comparing the results of the glassy and rubbery material properties. The glassy sorption profile's convexity indicates that the diffusion process is occurring faster than what is predicted by a typical Fickian diffusion process.

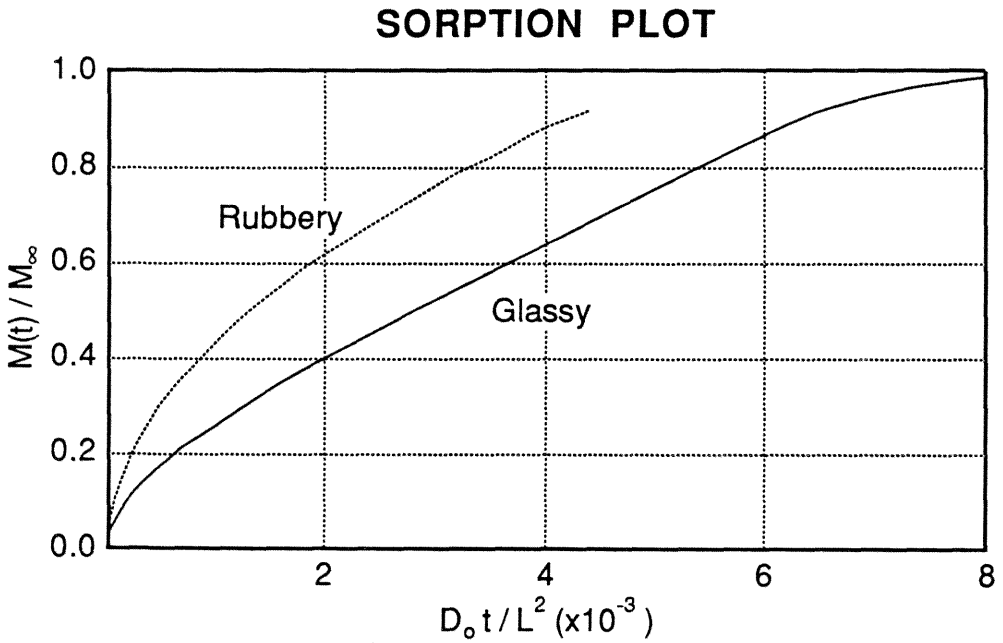


Figure 3.32 Sorption plot versus nondimensional time. Notice the glassy profile becomes linear in the region 0.005< t<0.015, characteristic of Case II behavior.

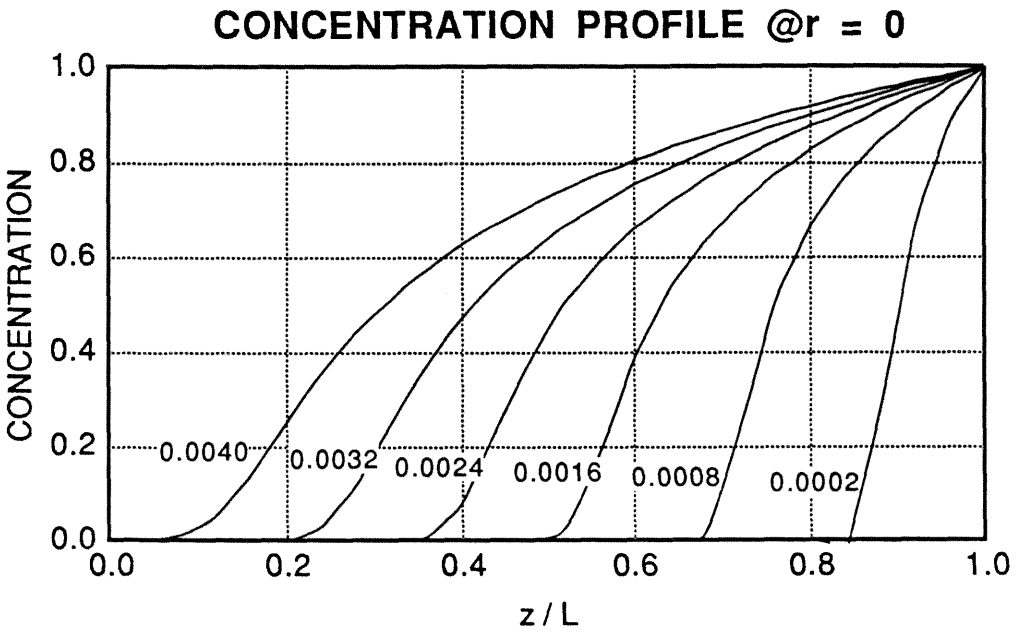


Figure 3.33 Concentration profile at $r = 0$ for the case of glassy material properties. The concentration front appears to be moving at a constant rate, an indicator of Case II diffusion. The numbers on the curves represent nondimensional times, $D_o t/L^2$.

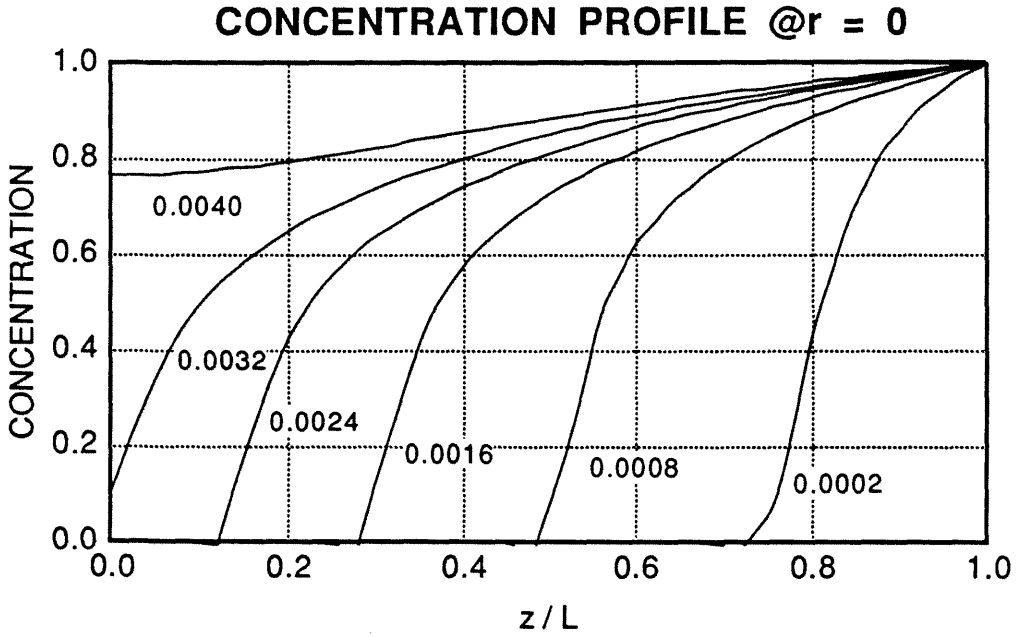


Figure 3.34 Concentration profile at $r = 0$ for the case of rubbery material properties. The concentration front appears to be slowing for this case typifying a Fickian-type response. The numbers on the curves represent nondimensional times, $D_o t/L^2$.

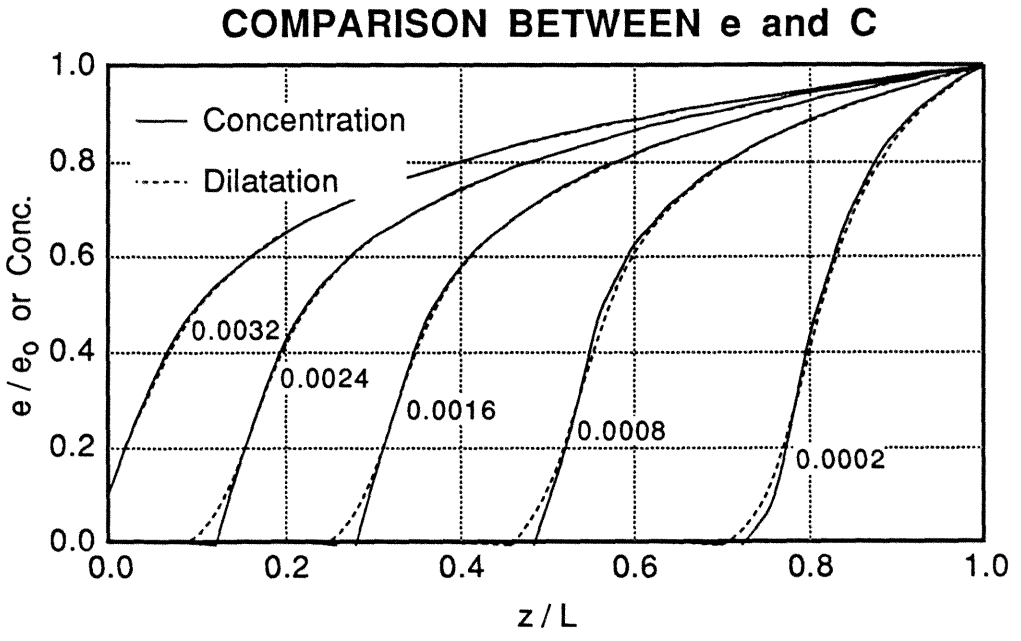


Figure 3.35 Comparison between dilatation and concentration for the rubbery material properties. The $e_0$ is the equilibrium dilatation. The numbers on the curves represent a nondimensional time, $D_0t/L^2$.

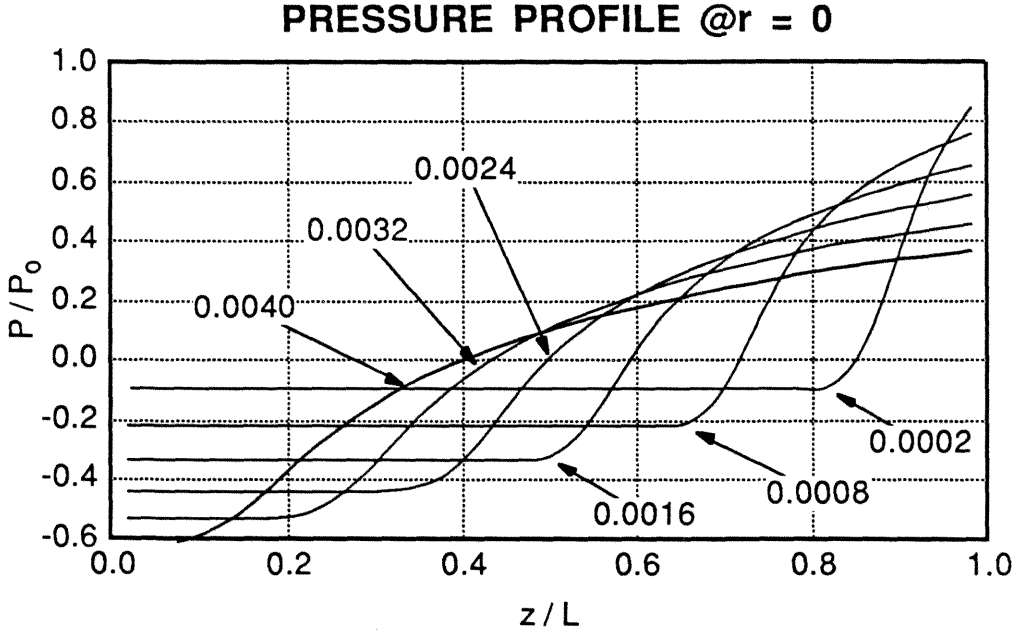


Figure 3.36 Pressure profile at $r = 0$ for a $R/L$ =10. The curves have been normalized by the 1-D equilibrium pressure value, $P_0$ (Problem 3). The numbers on the curves are nondimensional times, $D_0t/L^2$.

### 3.4.5 Problem 10: 2-D Coupled Diffusion; Time Shift Modified Diffusion Coefficient; Elastic Material Properties; Modified Boundary Condition

Problem 10 is similar to Problem 9 except now the pressure-induced mass flux is included in the diffusion process. The sorption curves comparing the uncoupled problem (Problem 9) to the coupled problem (Problem 10) is shown in Fig. 3.37. The addition of the pressure gradient-driven mass flux has accelerated the diffusion process causing the coupled problem to reach equilibrium earlier. The coupled sorption curve still exhibits the upturning behavior indicating that the diffusion process is occurring at a faster rate than a normal Fickian diffusion process.

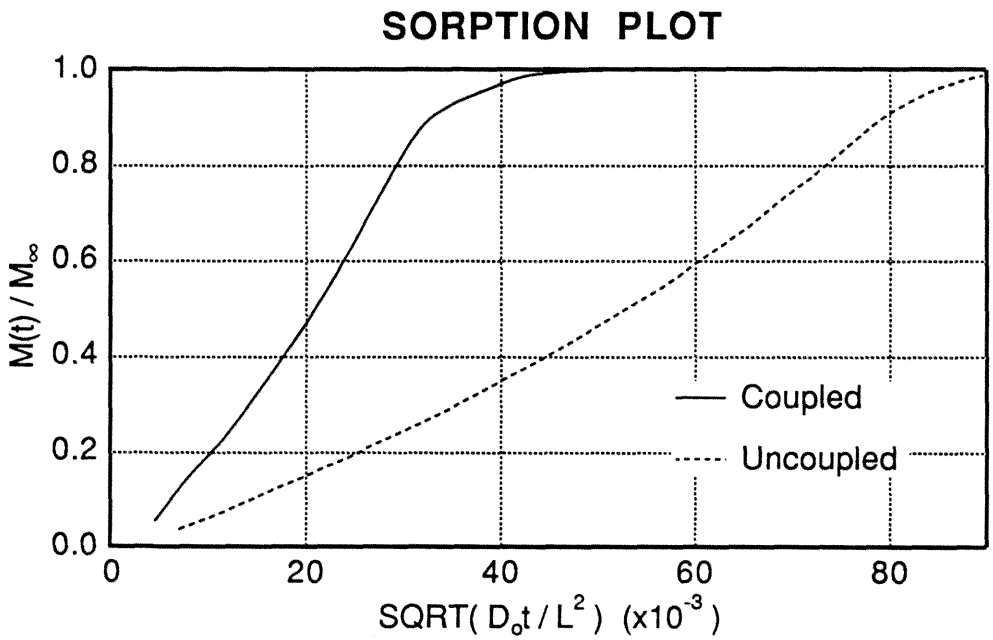


Figure 3.37 Sorption plot comparing uncoupled (Problem 9) versus coupled (Problem 10) diffusion processes. Addition of pressure-driven mass flux accelerates the diffusion process.

The concentration profile is shown in Fig. 3.38 and it appears that the concentration front is slowing as time increases. Hence the process does not exhibit true Case II behavior. The pressure profile, as in the previous elastic cases, is linearly related to the concentration and is shown in Fig. 3.39. Thus the pressure profile is in fact adding to the Fickian nature of the process and the Case II behavior in the coupled case may be obscured by the Fickian-like processes.

For completeness the dilatation profile at r = 0 is shown in Fig. 3.40. The profile resembles Problem 8 in Fig. 3.28.

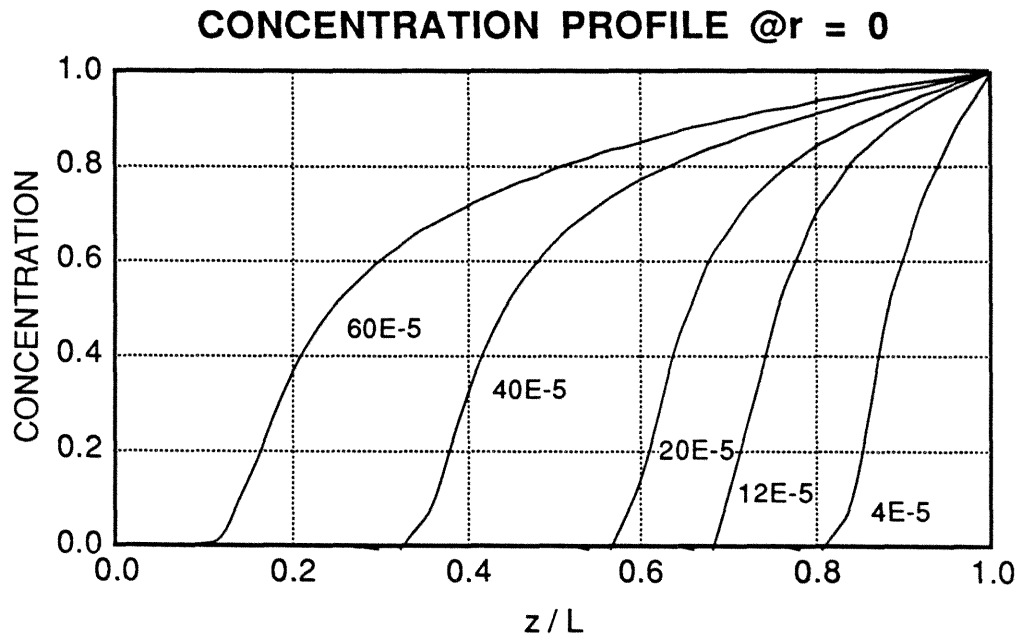


Figure 3.38 Concentration profile at $r = 0$ for Problem 10. The numbers on the curves represent nondimensional times, $D_0 t/L^2$.

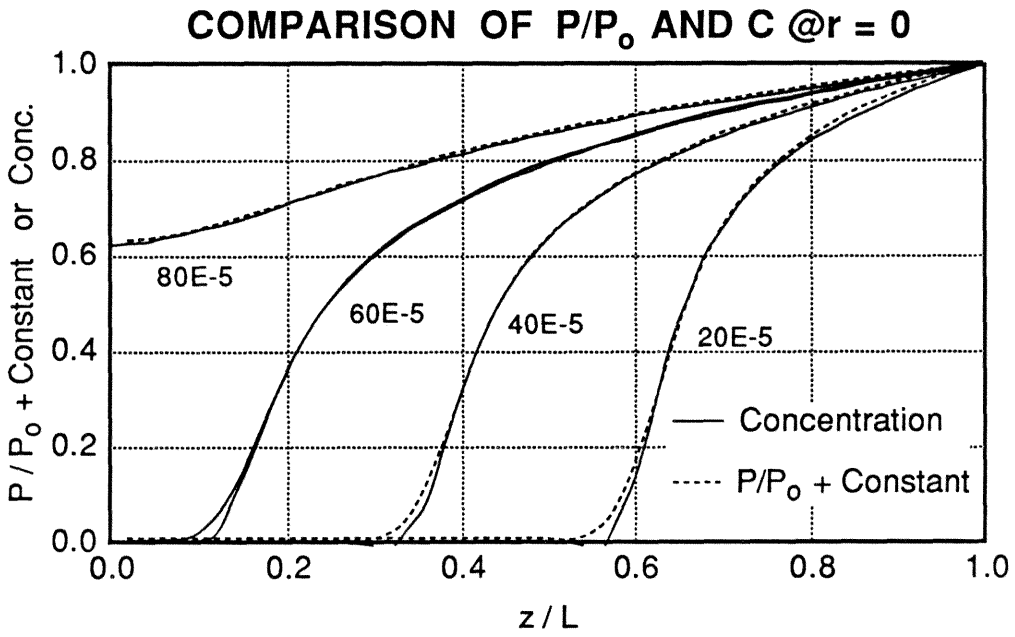


Figure 3.39 Comparison between the concentration profile and the modified pressure profile. The pressure profile is normalized by $P_0$ the 1-D equilibrium pressure and vertically shifted such that at $z = L$ the modified value is 1. The numbers on the curves represent nondimensional times, $D_0t/L^2$.

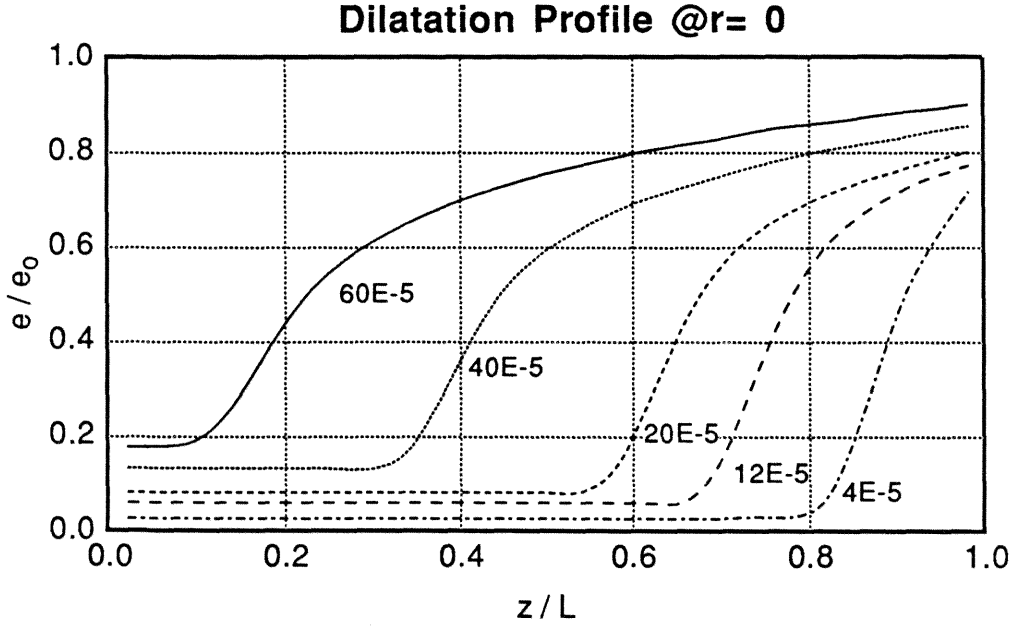


Figure 3.40 Dilatation profile at $r$= 0 for Problem 10. The numbers on the curves represent nondimensional times, $D_0t/L^2$.

### 3.4.6 Problem 11: 2-D Coupled Diffusion; Time Shift Modified Diffusion Coefficient; Viscoelastic Material Properties; Modified Boundary Condition

The fully coupled two-dimensional diffusion problem which incorporates the effects of a nonlinear viscoelastic response is simulated in Problem 11. The material properties for the bulk and shear moduli are the same used in Problem 5 and are again depicted in Fig. 3.41.

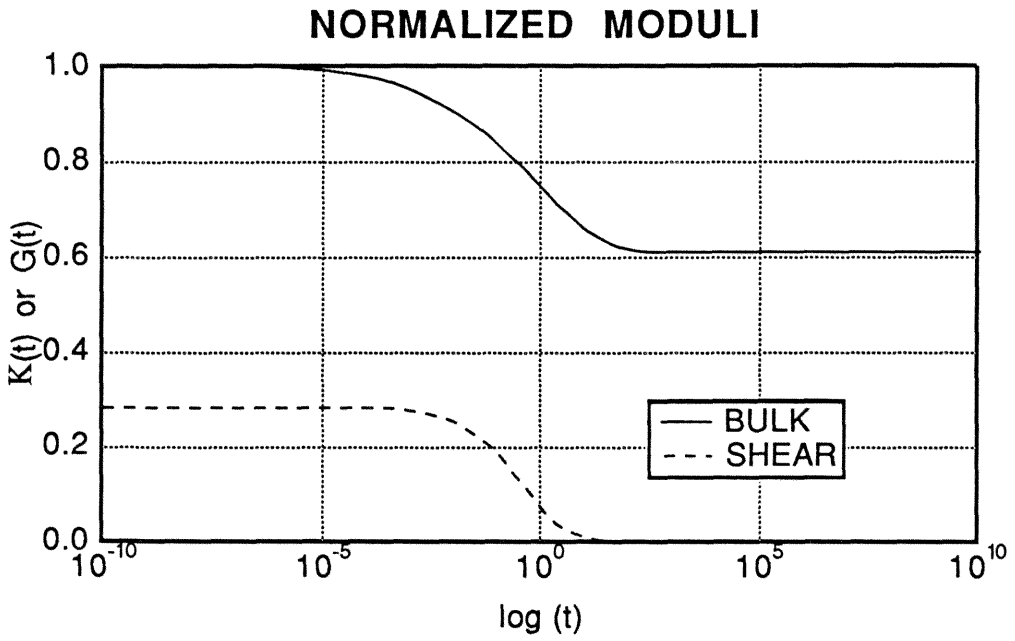


Figure 3.41 Material properties for the bulk and shear behavior used in the following numerical analysis. The properties are for PVAc normalized such that the bulk moduli is 1.0 in the glassy region.

For this problem the parameters $b$ (in Eqn. (1.12)) and $b_d$ (in Eqn. (2.12)) are chosen to enhance the material relaxation or the time shifted diffusion coefficient, respectively. Two different sets of values are used: the first is $b = b_d = 30$ which are the same values used in Problem 5 and the second is $b = 40$ and $b_d = 20$. The effect of the second set is to accelerate the

material relaxation process and to inhibit the time shifting behavior of the diffusion coefficient with respect to the first set of values.

The sorption plots for the two sets are shown in Fig. 3.42 and there the effect of the different sets of $b$-values can be seen. For Curve 1 where $b = b_d = 30$ the response appears to be Fickian for this region of the sorption curve. For the case where $b = 40$ and $b_d = 20$, Curve 2 assumes a non-Fickian sigmoidal shape. The similarity with the sorption curves of Fig. 3.15 can be explained by material relaxation behavior with the chosen $b$-values. For the given length, $L = 0.05$, the sigmoidal shape of Curve 2 is a result of the faster material relaxation rate. This corresponds to the explanation given in Problem 5 where the longer length, $L = 0.1$, which allowed the material to relax during the diffusion process, created the sigmoidal shaped sorption curve.

If sorption curves in Fig. 3.43 are replotted against nondimensional time, as shown in Fig. 3.43, Curve 2 appears to become linear indicating that a Case II diffusion process may be occurring.

Recall that a Case II diffusion process in a plate sheet is identified by three conditions: a linear mass versus time curve, a concentration front which moves at a constant velocity, and a sharp boundary between the swollen and unswollen regions of the polymer. The concentration profiles for Problem 11 are shown in Fig. 3.44 and there one observes that while the concentration profile does not exhibit a sharp front it does appear to move at a constant rate. The constant rate for the concentration front explains the linear behavior of the mass-time sorption plot. Because the concentration does not exhibit a sharp front, the process is termed pseudo-Case II

diffusion. It is conjectured that by altering the input parameters the front can be sharpened to capture true Case II behavior.

In Fig. 3.45 the pressure profile for Curve 2 is depicted for several nondimensional times. The shape of the profiles explains much of the observed anomalous diffusion behavior. At early times the regions with an inverse pressure gradient (due to the viscoelasticity) inhibit the mass flux causing the concentration profile to appear to "stall" in those regions (see the concentration profile at early times) and creates the slowing of the sorption curve. As the pressure field begins to move away from the boundary its shape appears to remain the same, though shifted vertically and horizontally, and the effect is a constant velocity concentration front. These results suggest that a Case II diffusion process initially starts as a Fickian-like diffusion process until the pressure field can relax and move away from the boundary. The pressure field then basically acts near the front of the concentration causing the constant front behavior.

It is expected that if the material were to relax quicker and the effect of the pressure gradient-driven mass flux was enhanced, the concentration front would steepen and give rise to true Case II behavior.

The dilatation profile is shown in Fig. 3.46 for completeness. The curves appear similar to the concentration profile in that they exhibit a sigmoidal shape.

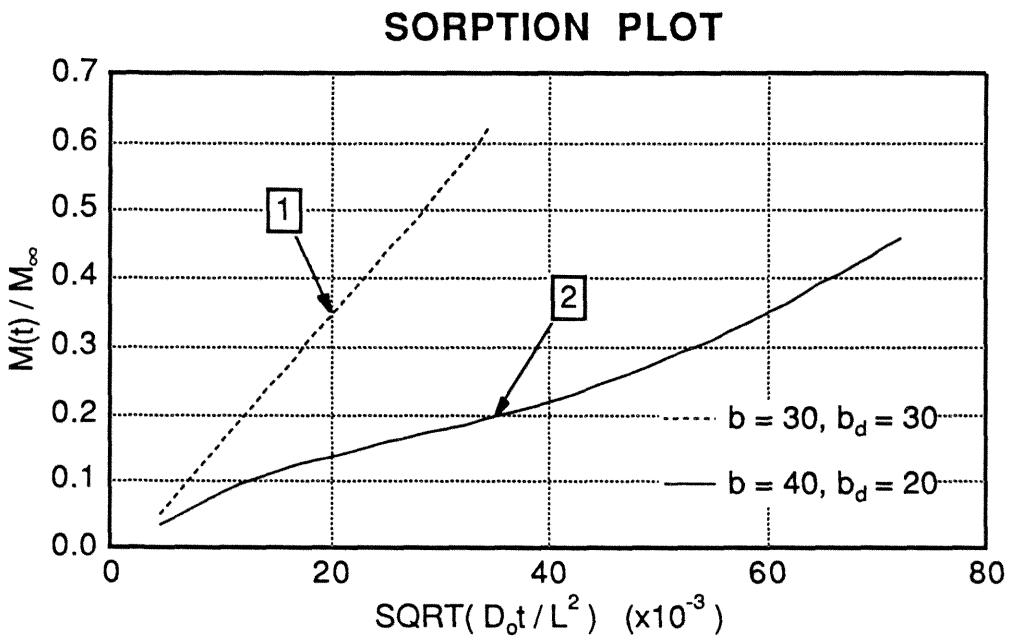


Figure 3.42 Sorption plot for the coupled diffusion process with a time shift modified diffusion coefficient and viscoelastic material properties. The sigmoidal shape of Curve 2 is a result of the higher material relaxation rate caused by the choice of the *b* value.

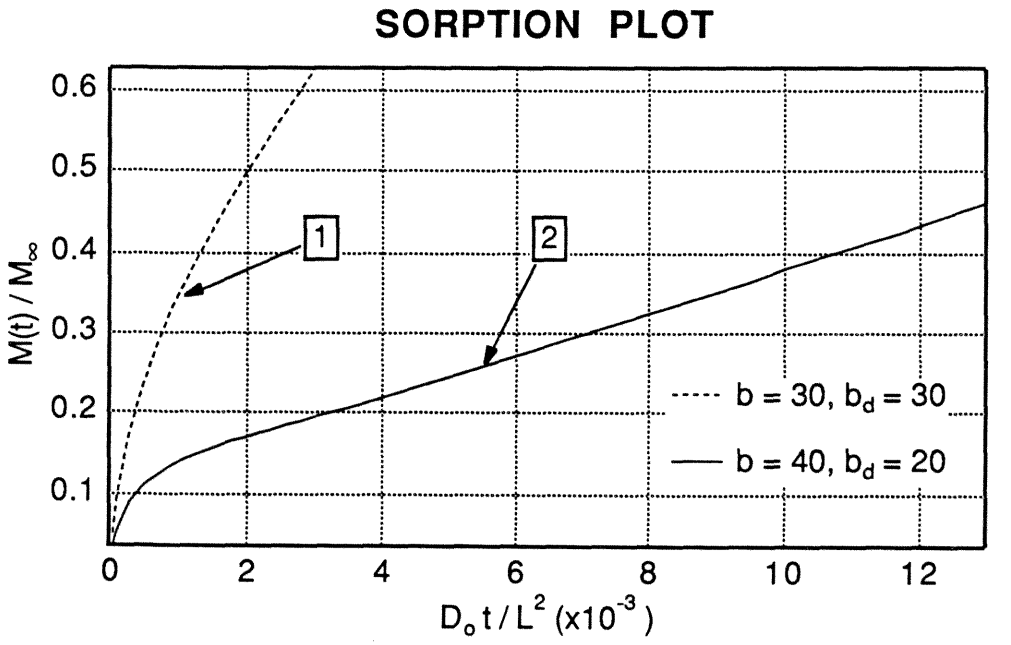


Figure 3.43 Sorption plot for Problem 11 with respect to time. After an initial nonlinear region Curve 2 becomes linear with time indicating a Case II diffusion process.

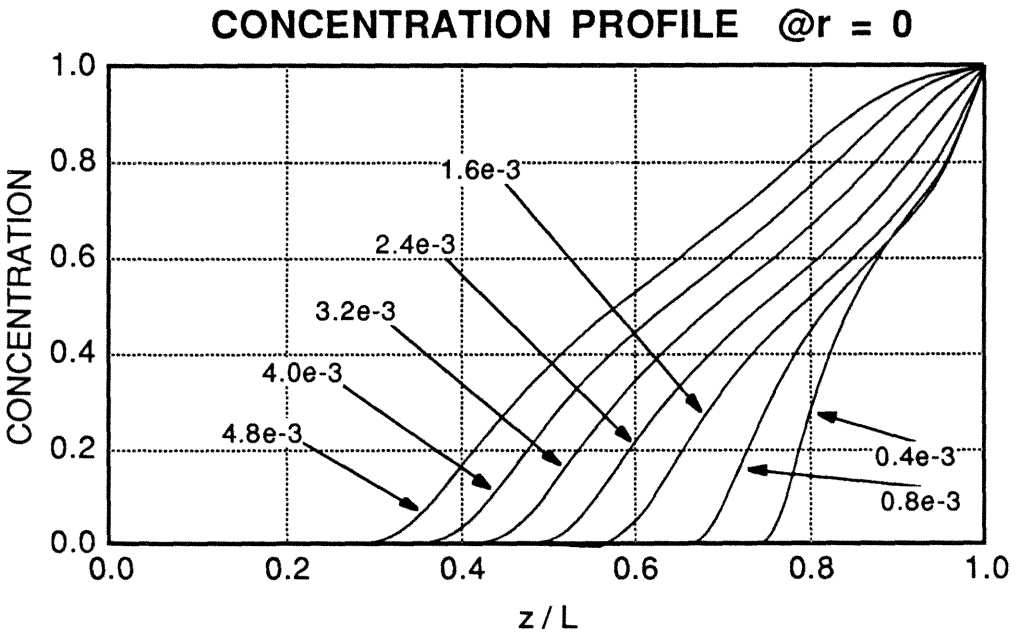


Figure 3.44 Concentration profile at various time steps for Problem 11. Note that at early time sections of the profile appear to stall leading to a sigmoidal shape for the profile. The numbers on the curves reflect the nondimensional time, $D_o t/L^2$.

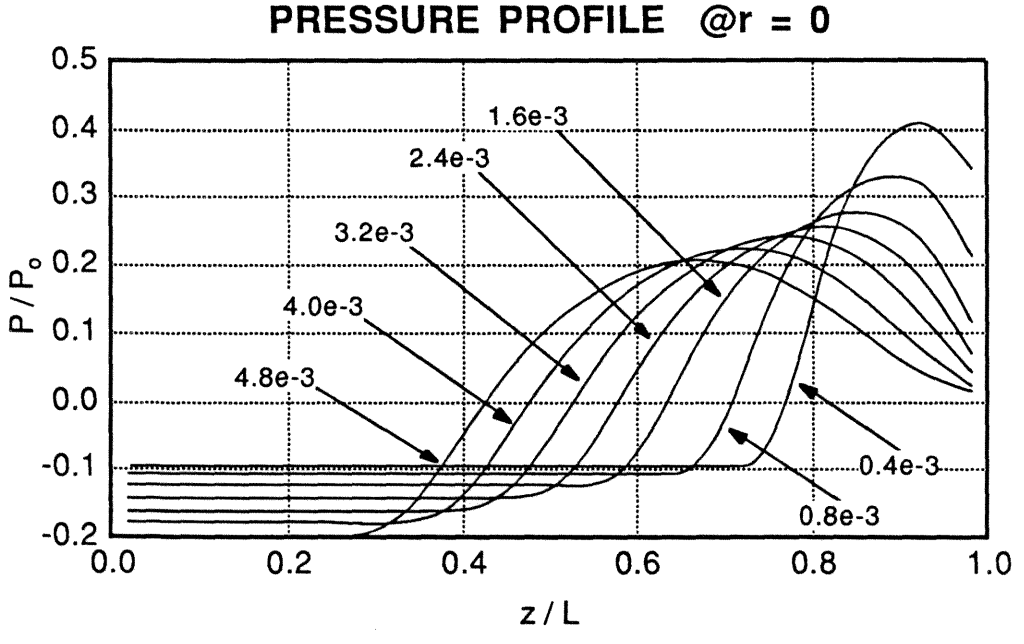


Figure 3.45 Pressure profile at various time steps for Problem 11. The end relaxation is for the most part a result of the material relaxation. The numbers on the curves reflect the nondimensional time, $D_o t/L^2$.

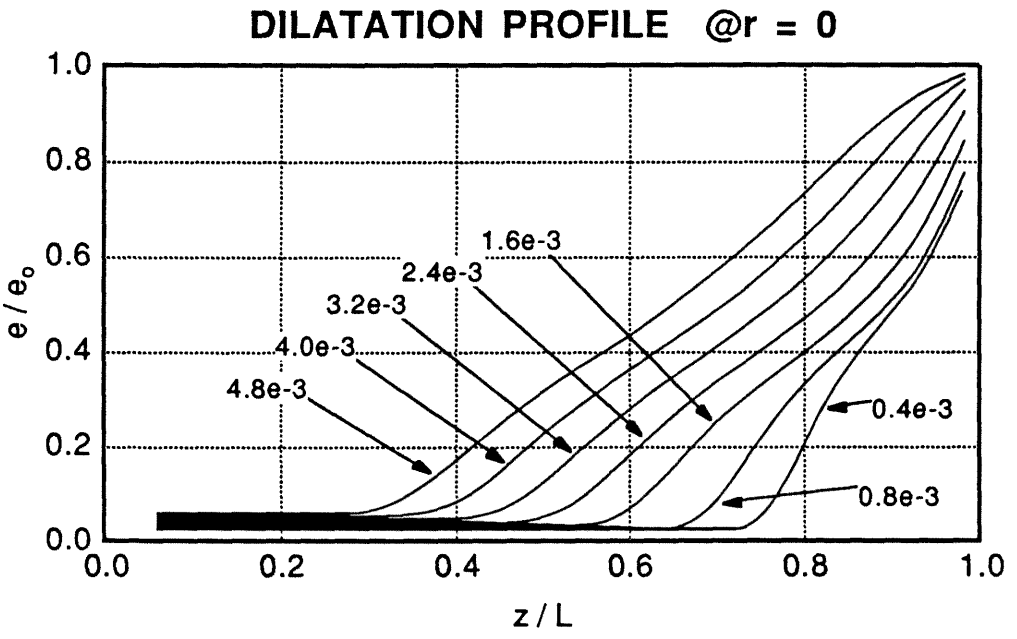


Figure 3.46 Dilatation profile at various time steps for Problem 11. The numbers on the curves reflect the nondimensional time, $D_o t/L^2$.

As with the previous 2-D problems, the concentration profiles (and thus the sorption plots) exhibit similar features to the corresponding 1-D problem (Problem 5). On the other hand, the pressure profiles have lost the additive vertical shift comparability and have different forms.

# Chapter 4
# Conclusions

A non-Fickian diffusion model that incorporates both the effect of internal pressure as an additional mass flux contributor and a free-volume dependent diffusion coefficient has been proposed. The internal pressure is a result of the swelling that occurs as the diluent diffuses into the polymer and a nonlinear viscoelastic constitutive law relates the two quantities. Besides the non-Fickian diffusion equation, the equations of equilibrium and strain-displacement equations also need to be satisfied thus coupling the diffusion process with the mechanical response of the polymer. In the following sections the results of the numerical solutions will be summarized and conclusions put forth about the applicability of the proposed model.

## 4.1 Effect of Elastic Material Properties

For the one-dimensional (1-D) problems, the restricted displacement field and the elastic material properties allow one to solve the mechanical response problem independent of the diffusion process. Here both the pressure and dilatation are found to be directly proportional to the concentration. Likewise the time shift factor that modifies the diffusion coefficient can also be expressed as an explicit function of concentration. These results allow the proposed non-Fickian diffusion model to be expressed as an

equivalent Fickian diffusion process which has the effects of the pressure gradient and time shift factor grouped together to form a concentration-dependent diffusion coefficient.

Similar statements can be made for the two-dimensional (2-D) problems but only for geometries with a large planar surface where the contributions through the edge effects can be ignored. For such geometries the two-dimensional solutions are unidimensional and numerical simulations indicate that the pressure and dilatation are linearly related to the concentration. By assuming an approximate displacement field to hold for such a region, one can show analytically the form of the linear relation up to an additive constant. This linearity with concentration again allows the non-Fickian diffusion model to be expressed as a Fickian diffusion process with a concentration-dependent diffusion coefficient.

The consequence of being able to express the proposed non-Fickian diffusion model as a Fickian equivalent is that typical diffusion experiments may not be able to discern which is the appropriate model. Currently many diluent-polymer systems, where the material properties of the polymer can be assumed to be elastic, are classified as a Fickian diffusion process where in fact a non-Fickian process might be occurring.

A related issue is the comparability of the 1-D and 2-D solutions using either the uncoupled Fickian model or the coupled non-Fickian model. Analytically and computationally the 1-D problems are more tractable so being able to model the diffusion process as one-dimensional would be advantageous. For the Fickian model the 2-D solutions become nearly equivalent to the 1-D solutions provided the geometry has a large

$R/L$ ratio and if only the region near $r = 0$ is considered. These conditions on the specimen geometry would also hold for the non-Fickian model and will be the only conditions considered for the rest of the chapter.

Similar statements can be made for the non-Fickian model though it may not be as clear cut. If only the effect of a pressure-induced mass flux were included the two solutions (one- and two-dimensional) would yield the same concentration profiles and hence sorption curves. The reason being that the pressure profiles for the two cases are different only because of an additive time-dependent constant. Since the pressure field enters the non-Fickian diffusion model through a spatial gradient, the two diffusion models would be equivalent.

The dilatation, on the other hand, affects the free-volume fraction and is dependent on the boundary conditions applied to the region. Hence the time shift modified diffusion coefficient for the 1-D and 2-D problems would be different and thus the diffusion processes would not be comparable. A special exception is when the shear modulus $(G/K) \rightarrow 0$ (typical material behavior for a rubbery uncrosslinked polymer). For this case the pressure field becomes zero, but more importantly the dilatation becomes equal to the swelling strain, $\alpha c$. For this special case the dilatation for both problems are equal and the 1-D solutions become equivalent to the 2-D solutions.

For elastic properties where the shear modulus is not zero only a qualitative comparison can be made. The time shift modified diffusion coefficient would tend to accelerate the diffusion process, hence the general character of the results would be the same for the two solutions.

For the mechanical response, the approximate displacement field used for 2-D problems show that the pressure and dilatation fields are linear with concentration, but does not tell us a priori the amount of the time-dependent additive constant. Thus a 1-D analysis would not be able to define the actual value of the 2-D stresses (pressure) or the strains (dilatation). Again the exception is the special case where the shear modulus is zero and the pressure field is known to be zero here the dilatation (and hence the free-volume fraction) is directly proportional to the concentration.

## 4.2 Effect of Viscoelastic Material Properties

In general with the introduction of viscoelastic material properties both the pressure and dilatation fields for the 1-D and 2-D problems will not be simply proportional to the concentration. This implies that the non-Fickian diffusion model cannot be expressed as a Fickian diffusion process with a concentration-dependent diffusion coefficient.

For this class of material properties, non-Fickian or anomalous diffusion results occur and these are the results that could demonstrate the validity of the proposed model. Actual comparison of the proposed model using "real" material properties have not been performed, but numerical simulations have produced anomalous diffusion results that are typically found in experiments.

As with the elastic results, the 1-D solution is not directly comparable to the related 2-D solution since the time shift factors which are inherently

involved in the use of the nonlinear viscoelastic constitutive law are different. But the two results would again have the same characteristics provided one takes into account the shift in the time scale in which the diffusion process is occurring.

A significant result is that the model, by varying the relaxation rate of the viscoelastic material properties, begins to exhibit Case II-type diffusion behavior. The concentration profiles for the calculated numerical simulations do not exhibit the sharp front associated with the Case II diffusion, but it is conjectured that this may be only a function of the material parameters used to generate the curves.

## 4.3 Final Comments

The proposed model does appear to be able to explain much of the experimental diffusion results ranging from Fickian to non-Fickian (Case II) behavior. The numerical simulations indicate that the proposed diffusion model may be able to span the range by using the appropriate specimen geometry and material properties to model the diluent diffusion behavior. However, in this study no "real" simulations have been performed using "real" material data.

Future work could involve a more comprehensive material parameter study to see if the concentration profile could indeed be sharpened to model Case II diffusion. Another interesting area is studying the effect of the decomposition of the dilatational strains into mechanical and swelling components and the relationship to the free volume. Finally, more exper-

imental work needs to be performed such that the material properties of diluent-polymer systems can be determined. Only when such "real" parameter values are inserted into the model will a check be made of its validity.

# Appendix A
# Finite Element Modelling of the Governing Equations

## A1 Mechanical Response

The method of weighted residuals is used to convert the equilibrium equations to its numerical equivalent, which will later be implemented into the finite element code, FEAP[32]. The equilibrium equations, Eqn. (1.2), are given by

$$\nabla \cdot \underset{\sim}{\sigma}(\underset{\sim}{x},t) + \underset{\sim}{b}(\underset{\sim}{x},t) = \underset{\sim}{0} \tag{A1.1}$$

where $\underset{\sim}{\sigma}(\underset{\sim}{x},t)$ represents the stress field and $\underset{\sim}{b}(\underset{\sim}{x},t)$ the body force at position $\underset{\sim}{x}$ and time $t$.

The weighted residual method begins by dot multiplying Eqn. (A1.1) by a weighting function, $\underset{\sim}{w}$, and integrating the result over a domain $V$

$$\int_V \underset{\sim}{w} \cdot \left\{ \nabla \cdot \underset{\sim}{\sigma}(\underset{\sim}{x},t) + \underset{\sim}{b}(\underset{\sim}{x},t) \right\} dV = 0 \tag{A1.2}$$

Applying the Divergence theorem to the first term of Eqn. (A1.2) and dividing the domain into elements yields the following

$$\sum_{e}^{\acute{e}} \left\{ \int_{V^e} \left\{ \nabla \underset{\sim}{w}^e \cdot \underset{\sim}{\sigma}^e - \underset{\sim}{w}^e \cdot \underset{\sim}{b}^e \right\} dV^e - \int_{\partial S^e} \underset{\sim}{w}^e \cdot \left( \underset{\sim}{\sigma}^e \underset{\sim}{n}^e \right) dS^e \right\} = 0 \tag{A1.3}$$

The superscript $e$ denotes the $e^{\text{th}}$ element and the evaluation of the integrals are now performed over the elemental domain, $V^e$. The elemental surface integral exists only for those elements whose boundary,

$S^e$, originally coincided with the domain's surface, $S$. The vector $\underset{\sim}{n}^e$ is the outward unit normal from the surface, $S^e$.

A generic constitutive law

$$\underset{\sim}{\sigma}^e(\underset{\sim}{x},t) = \underset{\sim}{D}^e(\underset{\sim}{x},t)\underset{\sim}{\varepsilon}^e(\underset{\sim}{x},t) - \underset{\sim}{A}^e(\underset{\sim}{x},t)c^e(\underset{\sim}{x},t) \tag{A1.4}$$

where $\underset{\sim}{D}^e(\underset{\sim}{x},t)$ is a four-tensor and $\underset{\sim}{A}^e(\underset{\sim}{x},t)$ a vector relating the strain and concentration fields to the stress field, respectively, is used to convert Eqn. (A1.3) from a stress formulation into a strain formulation. Cauchy's formula was used to replace the stress field within the surface integral in Eqn. (A1.3) by the appropriate surface tractions, $\underset{\sim}{t}^e$. These operations lead Eqn. (A1.3) to become

$$\sum^{e}\left\{ \int_{V^e}\left\{ \nabla \underset{\sim}{w}^e\cdot \underset{\sim}{D}^e\underset{\sim}{\varepsilon}^e - \nabla \underset{\sim}{w}^e\cdot\left(\underset{\sim}{A}^e c^e\right) - \underset{\sim}{w}^e\cdot \underset{\sim}{b}^e\right\} dV^e - \int_{\partial S^e} \underset{\sim}{w}^e\cdot \underset{\sim}{t}^e\, dS^e \right\} = 0 \tag{A1.5}$$

All field quantities were converted to equivalent matrix expressions and are approximated by the corresponding nodal values through a set of shape functions (see Eqn. (A1.7)).

$$\underset{\sim}{\sigma}^e \Rightarrow \{\sigma\}^e = \begin{Bmatrix} \sigma_{xx} \\ \sigma_{yy} \\ \sigma_{zz} \\ \sigma_{xy} \\ \sigma_{yz} \\ \sigma_{xz} \end{Bmatrix}^e; \qquad \underset{\sim}{\varepsilon}^e \Rightarrow \{\varepsilon\}^e = \begin{Bmatrix} \varepsilon_{xx} \\ \varepsilon_{yy} \\ \varepsilon_{zz} \\ \varepsilon_{xy} \\ \varepsilon_{yz} \\ \varepsilon_{xz} \end{Bmatrix}^e; \qquad \begin{aligned} \underset{\sim}{D}^e &\Rightarrow [D^e] \\ \underset{\sim}{A}^e &\Rightarrow \{A^e\} \\ \underset{\sim}{b}^e &\Rightarrow \{b\}^e \\ \underset{\sim}{t}^e &\Rightarrow \{t\}^e \end{aligned} \tag{A1.6}$$

$$\begin{aligned} \underset{\sim}{u}^e(\underset{\sim}{x},t) &\approx \left[N^e(\underset{\sim}{x},t)\right]\left\{U^e\right\}; \quad \underset{\sim}{\varepsilon}^e(\underset{\sim}{x},t) \approx \left[B^e(\underset{\sim}{x},t)\right]\left\{U^e\right\} \\ c^e(\underset{\sim}{x},t) &\approx \left\langle N^e(\underset{\sim}{x},t)\right\rangle\left\{c^e\right\} \end{aligned} \tag{A1.7}$$

where [*] denotes a M X N matrix, {*} a N X 1 vector, and ⟨*⟩ 1 X N vector.

By restricting the choice of weighting functions to be the same as the shape functions, Galerkin's method, the $i^{th}$ nodal displacement equation can be expressed as

$$\sum_i \Big\{ \int_{V^e} \langle B^e \rangle [D^e][B^e] \{U\}^e dV^e = \int_{V^e} \langle B^e \rangle \{A^e\} \langle N^e \rangle \{c\}^e dV^e + \\ + \int_{V^e} \langle N^e \rangle \{b\}^e dV^e + \\ + \int_{\partial S^e} \langle N^e \rangle \{t\}^e dS^e \Big\} \tag{A1.8}$$

Following standard finite element techniques, the nodal displacement equations for a particular element can be assembled to form the elemental matrices and vectors

$$[K]^e = \int_{V^e} [B^e]^{\mathrm{T}} [D^e][B^e] dV^e \tag{A1.9}$$

$$\{f_c\}^e = \int_{V^e} [B^e]^{\mathrm{T}} \{A^e\} \langle N^e \rangle \{c\}^e dV^e \tag{A1.10}$$

$$\{f_b\}^e = \int_{V^e} [N^e] \{b^e\} dV^e \tag{A1.11}$$

$$\{f_t\}^e = \int_{\partial S^e} [N^e] \{t^e\} dS^e \tag{A1.12}$$

$$\{f_u\}^e = [K]^e \{ \text{ specified nodal displacements } \} \tag{A1.13}$$

Again using standard finite element techniques, the global matrix equations can assembled from the elemental matrices and vectors.

$$[K]\{U\} = \{f_c\} + \{f_b\} + \{f_t\} - \{f_u\} \tag{A1.14}$$

It should be noted that this method of weighted residual yields the same result as the concept of virtual work, if the weighting functions are

chosen to be the same as the shape functions that relate the nodal values to the corresponding interior quantities.

## A1.1 Constitutive Behavior

For an isotropic solid undergoing small deformations, the mechanical response can be described through two independent material functions, for instance the shear modulus $G(t)$ and the bulk modulus $K(t)$. To include the effects of concentration an additional material function $\beta(t)$ is assumed. This is analogous to what is done in thermal viscoelasticity[20], and brief overview follows.

Due to the time-dependence, the stress-strain relationships are now represented as a convolution integral of the form

$$\{\sigma(t)\} = [D^*]\{\varepsilon(t)\} - \{A^*\}c(t) \tag{A1.15}$$

where $[D^*]$ and $\{A^*\}$ are convolution operators, defined as

$$[D]^e = \begin{bmatrix} A_1^* & A_2^* & A_2^* & 0 & 0 & 0 \\ A_2^* & A_1^* & A_2^* & 0 & 0 & 0 \\ A_2^* & A_2^* & A_1^* & 0 & 0 & 0 \\ 0 & 0 & 0 & A_3^* & 0 & 0 \\ 0 & 0 & 0 & 0 & A_3^* & 0 \\ 0 & 0 & 0 & 0 & 0 & A_3^* \end{bmatrix}^e ; \quad \{A\}^e = \begin{Bmatrix} A_4^* \\ A_4^* \\ A_4^* \\ 0 \\ 0 \\ 0 \end{Bmatrix} \tag{A1.16}$$

in which

$$
\begin{aligned}
A_1* &= \int_{-\infty}^{t}\left[K(t-\tau)+\tfrac{4}{3}G(t-\tau)\right]\frac{\partial}{\partial\tau}d\tau \\
A_2* &= \int_{-\infty}^{t}\left[K(t-\tau)-\tfrac{2}{3}G(t-\tau)\right]\frac{\partial}{\partial\tau}d\tau \\
A_3* &= \int_{-\infty}^{t}2G(t-\tau)\frac{\partial}{\partial\tau}d\tau \\
A_4* &= \int_{-\infty}^{t}\tfrac{1}{3}\beta(t-\tau)\frac{\partial}{\partial\tau}d\tau
\end{aligned}
\tag{A1.17}
$$

An element of $[D]$ can be represented as $D_{kl}*(\bullet)$ , where the $*$ denotes the convolution with the argument $\bullet$. As a consequence of the convolutions within the constitutive law the displacement vector cannot be factored from the volume integral, but the shape functions being time independent can; thus the left-hand side (LHS) of Eqn. (A1.8) becomes, in component form,

$$
\begin{aligned}
\text{LHS} &= \int_{V^e} B^e_{ki}D^e_{kl}*\left(B^e_{lj}U^e_j\right)dV^e \\
&= \int_{V^e} B^e_{ki}D^e_{kl}*\left(U^e_j\right)B^e_{lj}dV^e
\end{aligned}
\tag{A1.18}
$$

A component for $\{f_c\}^e$ becomes

$$
f_{ci}{}^e = \int_{V^e} B^e_{ik}A^e_k*\left(c^e_j\right)N^e_j dV^e \tag{A1.19}
$$

## A1.2 Time Integration Scheme

Assuming the three moduli, $G(t)$, $K(t)$, and $\beta(t)$, can be represented as a Prony series of the form.

$$
G(t) = \sum_{i=1}^{L} G_i \exp\left(-\frac{t}{\tau_{Gi}}\right); \qquad K(t) = \sum_{j=1}^{M} K_i \exp\left(-\frac{t}{\tau_{Kj}}\right) \tag{A1.20}
$$

$$
\beta(t) = \sum_{k=1}^{N} \beta_i \exp\left(-\frac{t}{\tau_{\beta k}}\right) \tag{A1.21}
$$

Physically this models the polymer as a number of Maxwell elements connected in parallel and the differential equation for a particular element, say for the $j^{th}$ Prony series term for the bulk modulus, can then be written as follows

$$\frac{\partial P_j}{\partial t} + \frac{1}{\tau_{Kj}} P_j = -\mathrm{K}_j \frac{\partial e}{\partial t} \tag{A1.22}$$

where $P_j$ is the $j^{th}$ pressure contribution due to the strain $e(t)$. An exact solution to Eqn. (A1.22) for a constant strain rate at time $t$ can be expressed as

$$P_j(t) = P_j(0)\exp\left(-\frac{t}{\tau_{Kj}}\right) - K_j\tau_{Kj}\left[1-\exp\left(-\frac{t}{\tau_{Kj}}\right)\right]\frac{de}{dt} \tag{A1.23}$$

and a solution at $t+\Delta t$ can given by

$$\begin{aligned} P_j(t+\Delta t) &= P_j(t)\exp\left(-\frac{\Delta t}{\tau_{Kj}}\right) - K_j\tau_{Kj}\left[1-\exp\left(-\frac{\Delta t}{\tau_{Kj}}\right)\right]\frac{\Delta e}{\Delta t} \\ &= P_j(t)\exp\left(-\frac{\Delta t}{\tau_{Kj}}\right) - K_j^{\tan}\Delta e \end{aligned} \tag{A1.24}$$

Thus the solution at $t+\Delta t$ requires only the solution at the previous time step and the increment in strain during the time step. If the strain rate is not constant then Eqns. (A1.23) and (A1.24) become approximate relations that approach the exact solution as $\Delta t$ is decreased. Hence the convolutions involved in the usual viscoelastic constitutive behavior, which requires that all of the previous solution history be stored, can be replaced by Eqn. (A1.24) provided the material properties are expressible by a Prony series as in Eqns. (A1.19) and (A1.20) and that Eqn. (A1.22) is the differential form for the constitutive behavior.

This time-stepping algorithm is applied to our viscoelastic constitutive behavior and the element matrix equations (see Losi[20]) now take this form

$$[K]^e = \int_{V^e} [B^e]^{\mathrm{T}} [D^e]^{\tan} [B^e] dV^e \tag{A1.25}$$

$$\{f_c\}^e = \int_{V^e} [B^e]^{\mathrm{T}} \{A^e\}^{\tan} \langle N^e \rangle \{\Delta c\}^e dV \tag{A1.26}$$

$$\{f_b\}^e = \int_{V^e} [N^e] \{b^e\} dV^e \tag{A1.27}$$

$$\{f_t\}^e = \int_{\partial S^e} [N^e] \{t^e\} dS^e \tag{A1.28}$$

$$\{f^*(t)\}^e = \{ \text{ additional load due to history } \} \tag{A1.29}$$

$$\{f_u(t)\}^e = \{ \text{ prescribed nodal values } \} \tag{A1.30}$$

where

$$[D^e]^{\tan} = \begin{bmatrix} A_1 & A_2 & A_2 & 0 & 0 & 0 \\ A_2 & A_1 & A_2 & 0 & 0 & 0 \\ A_2 & A_2 & A_1 & 0 & 0 & 0 \\ 0 & 0 & 0 & A_3 & 0 & 0 \\ 0 & 0 & 0 & 0 & A_3 & 0 \\ 0 & 0 & 0 & 0 & 0 & A_3 \end{bmatrix}^e ; \qquad \{A^e\}^{\tan} = \begin{Bmatrix} A_4 \\ A_4 \\ A_4 \\ 0 \\ 0 \\ 0 \end{Bmatrix}^e \tag{A1.31}$$

in which

$$\begin{aligned} A_1 &= \left[\tfrac{4}{3} G^{\tan} + K^{\tan}\right] \\ A_2 &= \left[\tfrac{1}{3} K^{\tan} + \tfrac{2}{3} G^{\tan}\right]; \\ A_3 &= 2G^{\tan} \\ A_4 &= \tfrac{1}{3} \beta^{\tan} \end{aligned} \qquad \begin{aligned} G^{\tan} &= \sum_{i=1}^{L} G_i \frac{\tau_{Gi}}{\Delta t} \left[ 1 - \exp\left( -\frac{\Delta t}{\tau_{Gi}} \right) \right] \\ K^{\tan} &= \sum_{j=1}^{M} K_j \frac{\tau_{Kj}}{\Delta t} \left[ 1 - \exp\left( -\frac{\Delta t}{\tau_{Kj}} \right) \right] \\ \beta^{\tan} &= \sum_{k=1}^{N} \beta_k \frac{\tau_{\beta k}}{\Delta t} \left[ 1 - \exp\left( -\frac{\Delta t}{\tau_{\beta k}} \right) \right] \end{aligned} \tag{A1.32}$$

The element matrices and vectors can then be assembled to form the global matrix equation over the domain at $t+\Delta t$.

$$\begin{aligned}\left[K(t+\Delta t)\right]^{\tan}\left\{\Delta U^{j}(t+\Delta t)\right\} &= \left\{f_c(t+\Delta t)\right\} + \left\{f_b(t+\Delta t)\right\} + \\ &+ \left\{f_t(t+\Delta t)\right\} + \left\{f^{*j}(t+\Delta t)\right\} + \\ &- \left\{f_u(t+\Delta t)\right\}\end{aligned} \tag{A1.33}$$

$$\left\{U^{j}(t+\Delta t)\right\} = \left\{U(t)\right\} + \left\{\Delta U^{j}(t+\Delta t)\right\} \tag{A1.34}$$

the $j^{th}$ superscript indicates that several iterations may be needed to converge to a solution.

## A1.3 Effect of Free Volume or Time Shifting

For nonlinear viscoelasticity the material properties are evaluated at the internal or reduced time $\xi(t)$ denoted by

$$\xi(t) = \int_0^t \frac{d\tau}{\phi(\tau)} \tag{A1.35}$$

The effect on the convolutions is simply replacing the material's time parameter with the internal time. For example, $A_1*$ in Eqn. (A1.16) becomes

$$A_1* = \int_{-\infty}^{t}\left[\tfrac{4}{3}G\big(\xi(t)-\xi(\tau)\big) + \mathrm{K}\big(\xi(t)-\xi(\tau)\big)\right]\frac{\partial}{\partial\tau}d\tau \tag{A1.36}$$

This replacement of the internal time follows through the rest of the derivation and a simple substitution of $t \Leftrightarrow \xi(t)$, where the material properties are being evaluated, are all the changes that occur in the above derivation.

Recalling that the internal time is dependent on the free volume of the material and hence on the stress and strain fields the matrix, Eqn. (A1.33) becomes inherently nonlinear and several iterations may be needed per time step to converge to a solution.

# A2 Diffusion Equation

The diffusion equation to be modelled is given as

$$\frac{\partial c(\underline{x},t)}{\partial t} - \nabla \cdot \underset{\sim}{D}(c)\Big\{ \nabla c(\underline{x},t) + c(\underline{x},t)\underset{\sim}{\Lambda}(c)\nabla p(\underline{x},t) \Big\} = 0 \qquad \text{(A2.1)}$$

where $\underset{\sim}{D}(c)$ is the diffusion coefficient tensor which may be concentration dependent, $\underset{\sim}{\Lambda}(c)$ is a proportionality coefficient tensor, which may also be concentration dependent, and relates the pressure, $p(\underline{x},t)$, gradient to the mass flux of the diluent.

The pressure, $p(\underline{x},t)$, is calculated from the mechanical response portion of the program and can be represented by

$$p(\underline{x},t) = p^{\varepsilon}(\underline{x},t) + p^{c}(\underline{x},t) \qquad \text{(A2.2)}$$

where $p^{c}(\underline{x},t)$ is the component of the pressure that is explicitly dependent on the concentration, $c(\underline{x},t)$. By separating the explicit concentration dependence from the pressure term the numerical scheme tended to converge faster and became more stable. The contribution of the diluent to the pressure can be represented as a summation of N terms corresponding to the Prony series representing $\beta(t)$, (see Eqn. (A1.21)). Each term in the series has a corresponding differential equation whose solution, for the $j^{\text{th}}$ term $p_j^{c}(\underline{x},t)$, and for a constant $\dot{c}(\underline{x},t)$ , can be expressed as

$$p_j^{c}(\underline{x},t) = p_j^{c}(\underline{x},t-\Delta t)\exp(-\Delta t/\tau_{\beta j}) + \beta_j^{\tan}[c(\underline{x},t)-c(\underline{x},t-\Delta t)] \qquad \text{(A2.3)}$$

where

$$\beta_j^{\tan} = \beta_j \frac{\tau_{\beta j}}{\Delta t}\Big[ 1-\exp\big(-\Delta t/\tau_{\beta j}\big) \Big] \qquad \text{(A2.4)}$$

Upon substitution of Eqns. (A2.2) and (A2.3) into Eqn. (A2.1) and a regrouping of terms, one derives the equation that will be actually modelled.

$$\frac{\partial c(\underline{x},t)}{\partial t} - \nabla\cdot\left\{ \underline{\overline{D}}(c)\nabla c(\underline{x},t) + c(\underline{x},t)\underline{\overline{\Lambda}}(c)\nabla\overline{p}(\underline{x},t)\right\} = 0 \qquad \text{(A2.5)}$$

where

$$\underline{\overline{D}}(c) = \underline{D}(c)\left[1 + c(\underline{x},t)\underline{\Lambda}(c)\sum_{j=1}^{N}\beta_j^{\tan}\right] \qquad \text{(A2.6)}$$

$$\underline{\overline{\Lambda}}(c) = \underline{D}(c)\underline{\Lambda}(c) \qquad \text{(A2.7)}$$

$$\overline{p}(\underline{x},t) = \sum_{i=1}^{M} p_i^e(\underline{x},t-\Delta t)\exp\left(-\Delta t/\tau_{Ki}\right) + K_i^{\tan}[e(\underline{x},t)-e(\underline{x},t-\Delta t)] + \\ + \sum_{j=1}^{N} p_j^e(\underline{x},t-\Delta t)\exp\left(-\Delta t/\tau_{\beta j}\right) - \beta_j^{\tan}c(\underline{x},t-\Delta t) \qquad \text{(A2.8)}$$

As with the conversion of the equilibrium equations, the method of weighted residuals is used and Eqn. (A2.8) is multiplied by a weighting function, $w$, and integrating over the domain $V$ yielding

$$\int_V w\frac{\partial c}{\partial t}dV + \int_V w\nabla\cdot\left(\underline{\overline{D}}\nabla c + c\underline{\overline{\Lambda}}\nabla\overline{p}\right)dV = 0 \qquad \text{(A2.9)}$$

Application of the Divergence theorem to the second term and dividing $V$ into elements yields

$$\sum^{e}\left\{\frac{\partial}{\partial t}\int_{V^e} w^e c^e\,dV^e + \int_{V^e}\nabla w^e\cdot\underset{\sim}{\overline{D}}^e\nabla c^e\,dV^e + \right.$$
$$+\int_{V^e}\nabla w^e\cdot c^e\,\underset{\sim}{\overline{\Lambda}}^e\nabla\overline{p}^e\,dV^e -$$
$$\left.+\int_{\partial S^e} w^e\,(\underset{\sim}{\overline{D}}^e\nabla c^e + c^e\,\underset{\sim}{\overline{\Lambda}}^e\nabla\overline{p}^e)\cdot\underset{\sim}{n}^e\,dS^e\right\}=0 \qquad \text{(A2.10)}$$

The coordinate free tensor notation are substituted for their matrix notation equivalent as [*] a M X N matrix, {*} a N X 1 vector, and ⟨*⟩ a 1 X N vector.

The interior values of $p^e(\underset{\sim}{x},t)$ and $c^e(\underset{\sim}{x},t)$ are approximated by the element's nodal values $\{p\}^e$ and $\{c\}^e$ respectively, through a set of shape functions $\langle N^e\rangle$ ( i.e. $c^e(\underset{\sim}{x},t)\approx\bar{c}^e(\underset{\sim}{x},t)=\langle N^e(\underset{\sim}{x},t)\rangle\{c\}^e$). Thus $i^{\text{th}}$ nodal equation, in matrix form, becomes

$$\sum_i\left\{\frac{\partial}{\partial t}\int_{V^e}N_i^e\langle N^e\rangle\{c\}^e dV^e + \int_{V^e}\left\langle\frac{\partial N_i^e}{\partial x}\frac{\partial N_i^e}{\partial y}\frac{\partial N_i^e}{\partial z}\right\rangle[\overline{D}^e][B^e]\{c\}^e dV^e + \right.$$
$$+\int_{V^e}\left\langle\frac{\partial N_i^e}{\partial x}\frac{\partial N_i^e}{\partial y}\frac{\partial N_i^e}{\partial z}\right\rangle[\overline{\Lambda}^e][B^e]\{\overline{p}\}^e\langle N^e\rangle\{c\}^e dV^e +$$
$$\left.+\int_{\partial S^e}N_i^e q_n^e\,dS^e\right\}=0$$

(A2.11)

Assembling into the elemental matrices and vectors

$$[\mathrm{C}]^e = \int_{V^e}\{N^e\}\langle N^e\rangle dV^e \qquad \text{(A2.12)}$$

$$[\mathrm{K}]^e = \int_{V^e}[B^e]^T[\overline{D}^e][B^e]\,dV^e \qquad \text{(A2.13)}$$

$$[\mathrm{G}]^e = \int_{V^e}[B^e]^T[\overline{\Lambda}^e][B^e]\{\overline{p}\}^e\langle N^e\rangle\,dV^e \qquad \text{(A2.14)}$$

$$\{f_q\}^e = \int_{\partial S^e}\{N^e\}q_n^e\,dS^e \qquad \text{(A2.15)}$$

$$\{ f_c \}^e = [ \mathrm{K} ]^e \{ \text{ specified nodal concentrations } \}^e \tag{A2.16}$$

These elemental matrices and vectors can then be assembled to form the global matrix equation over the domain.

$$[\mathrm{C}]\{\dot{c}\} + [\mathrm{K}+\mathrm{G}]\{c\} = \{f_q\} - \{f_c\} \tag{A2.17}$$

## A2.1 Time Integration Method

The time integration scheme used was showed by Wood and Lewis [31] to yield stable and numerically accurate solutions for first-order linear systems. The scheme uses the Three-Step-Gear method (3GM) with a modified Crank-Nicholson (CN) start. The algorithm is shown below.

Three-Step Gear Method for the *n-th* iteration

$$\begin{aligned}
&\left[\frac{1+\gamma}{\Delta t}\mathbf{C} + \mathbf{K}_n(t+\Delta t) + \mathbf{G}_n(t+\Delta t)\right]\left\{ \Delta c^n(t+\Delta t) \right\} = \\
&\qquad \left\{ f^n(t+\Delta t) \right\} + \\
&\qquad \left[ \mathbf{C} \right]\left\{\frac{1+\gamma}{\Delta t}c(t) - \frac{\gamma}{\Delta t'}c(t) - \frac{\gamma}{\Delta t'}c(t-\Delta t)\right\} - \\
&\qquad \left[\frac{1+\gamma}{\Delta t}\mathbf{C} + \mathbf{K}(t+\Delta t) + \mathbf{G}(t+\Delta t)\right]\left\{ c^n(t+\Delta t) \right\}
\end{aligned} \tag{A2.18}$$

where

$$c^{n+1}(t+\Delta t) = c^n(t+\Delta t) + \Delta c^n(t+\Delta t) \tag{A2.19}$$

$$\Delta t' = \text{ Old time increment} \tag{A2.20}$$

$\gamma$ = Weighting parameter; normally equal 0.5 (A2.21)

The modified Crank-Nicholson start approximates the solution at t = $\Delta t/2$ by halving the solution at t = $\Delta t$ as calculated by the CN method. The 3GM uses the "known" solutions at t = 0 and $\Delta t/2$ to obtain a solution at t = $\Delta t$. The solution at t = $2\Delta t$ uses the 3GM with the "known" solutions at t = 0 and $\Delta t$. The CN algorithm for the $n^{th}$ iteration is given by

The CN algorithm for the *n-th* iteration

$$\begin{aligned}\left[ C/\Delta t + \gamma( K+G ) \right]\left\{\Delta c^n(t+\Delta t)\right\} = \\ \gamma\left\{ f^n(t+\Delta t) \right\} + (1-\gamma)\left\{ f(t) \right\} + \\ \left[ C/\Delta t - (1-\gamma)( K+G ) \right]\left\{ c(t) \right\} - \\ \left[ C/\Delta t + \gamma( K+G ) \right]\left\{ c^n(t+\Delta t)\right\}\end{aligned} \quad \text{(A2.22)}$$

where

$$c^{n+1}(t+\Delta t) = c^n(t+\Delta t) + \Delta c^n(t+\Delta t) \quad \text{(A2.23)}$$

$\Delta t'$ = Old time increment (A2.24)

$\gamma$ = Weighting parameter; normally equal 0.5 (A2.25)

Due to the material nonlinearities, $[K]$ and $[G]$ are functions of concentration and a Newton-Ralphson iteration technique is used to update the solution within a time step. Both the Crank-Nicholson and 3-Step Gear remain essentially the same except that the tangent stiffness matrix is used on the left-hand side of the equation. For example the 3GM is now represented as

$$\left[\frac{1+\gamma}{\Delta t}\mathrm{C}+\mathrm{K}_{\mathrm{n}}^{\tan}(t+\Delta t)+\mathrm{G}_{\mathrm{n}}^{\tan}(t+\Delta t)\right]\left\{\ \Delta c^{n}(t+\Delta t)\ \right\}=$$
$$\left\{\ f^{n}(t+\Delta t)\ \right\}+$$
$$\left[\ \mathrm{C}\ \right]\left\{\frac{1+\gamma}{\Delta t}c(t)-\frac{\gamma}{\Delta t'}c(t)-\frac{\gamma}{\Delta t'}c(t-\Delta t)\right\}- \qquad \text{(A2.26)}$$
$$\left[\frac{1+\gamma}{\Delta t}\mathrm{C}+\mathrm{K}(t+\Delta t)+\mathrm{G}(t+\Delta t)\right]\left\{\ c^{n}(t+\Delta t)\ \right\}$$

where (for 2-D problems where $[D^e]$ and $[\Lambda^e]$ are diagonal matrices)

$$\left[\mathbf{K}_{n}^{e}\right]_{ij}^{\tan} = \left[\mathbf{K}_{n}^{e}\right]_{ij} + \int_{V^e}\frac{\partial N_i^e}{\partial x}\frac{\partial \overline{D}_{11}^{e}}{\partial c}\left\langle\frac{\partial N^e}{\partial x}\right\rangle\left\{\ c\ \right\}^{e}N_j^e + \frac{\partial N_i^e}{\partial y}\frac{\partial \overline{D}_{22}^{e}}{\partial c}\left\langle\frac{\partial N^e}{\partial y}\right\rangle\left\{\ c\ \right\}^{e}N_j^e dV^e \qquad \text{(A2.27)}$$

$$\left[\mathrm{G}_{\mathrm{n}}^{\mathrm{e}}\right]_{ij}^{\tan} = \left[\mathrm{G}_{n}^{e}\right]_{ij} + \int_{V^e}\frac{\partial N_i^e}{\partial x}\frac{\partial \overline{\Lambda}_{11}^{e}}{\partial c}\left\langle\frac{\partial N^e}{\partial x}\right\rangle\left\{\ \overline{p}^{e}\ \right\}\left\langle\ N^e\ \right\rangle\left\{\ c^e\ \right\}N_j^e + \frac{\partial N_i^e}{\partial y}\frac{\partial \overline{\Lambda}_{22}^{e}}{\partial c}\left\langle\frac{\partial N^e}{\partial y}\right\rangle\left\{\ \overline{p}^{e}\ \right\}\left\langle\ N^e\ \right\rangle\left\{\ c^e\ \right\}N_j^e\ dV^e \qquad \text{(A2.28)}$$

## A2.2 Free Volume Effect on the Diffusion Coefficient

The diffusion coefficient is modified by the free volume fraction and the effect on the constitutive matrices are as shown in Eqn. (A2.29).

$$\left[D^{*}(c)\right] = \left[\overline{D}(c)\right]/\phi_{d}(c); \qquad \left[\Lambda^{*}(c)\right] = \left[\overline{\Lambda}(c)\right]/\phi_{d}(c) \qquad \text{(A2.29)}$$

The individual elements of $[\overline{D}(c)]$ and $[\overline{\Lambda}(c)]$ will simply be divided by the time shift factor. The modifications are shown below, for one element of the diagonal $[\overline{D}(c)]$ and $[\overline{\Lambda}(c)]$ matrices

$$D^*_{11}(c) = \frac{\overline{D}_{11}(c)}{\phi(c)}; \qquad \Lambda^*_{11}(c) = \frac{\overline{\Lambda}_{11}(c)}{\phi(c)} \tag{A2.30}$$

$$\frac{\partial \overline{D}^e_{11}}{\partial c} = \frac{1}{\phi(c)}\frac{\partial \overline{D}_{11}(c)}{\partial c} + \frac{\overline{D}_{11}(c)}{\phi(c)}\left[\frac{b}{f^2(c)}\frac{\partial f}{\partial c}\right]$$

$$= \frac{1}{\phi(c)}\frac{\partial \overline{D}_{11}(c)}{\partial c} + \frac{\overline{D}_{11}(c)}{\phi(c)}\left\{\frac{b}{f^2(c)}(B-A)\sum_{i=1}^{K}\alpha_i\left[1-\frac{\tau_{\alpha i}}{\Delta t}\left[1-\exp(-\Delta t/\tau_{\alpha i})\right]\right]\right\}$$

$$\frac{\partial \overline{\Lambda}^e_{11}}{\partial c} = \frac{1}{\phi(c)}\frac{\partial \overline{\Lambda}_{11}(c)}{\partial c} + \frac{\overline{\Lambda}_{11}(c)}{\phi(c)}\left[\frac{b}{f^2(c)}\frac{\partial f}{\partial c}\right]$$

$$= \frac{1}{\phi(c)}\frac{\partial \overline{\Lambda}_{11}(c)}{\partial c} + \frac{\overline{\Lambda}_{11}(c)}{\phi(c)}\left\{\frac{b}{f^2(c)}(B-A)\sum_{i=1}^{K}\alpha_i\left[1-\frac{\tau_{\alpha i}}{\Delta t}\left[1-\exp(-\Delta t/\tau_{\alpha i})\right]\right]\right\}$$

The other components of the $[\overline{D}(c)]$ and $[\overline{\Lambda}(c)]$ matrices are modified in a similar fashion.

# A3 Effect of Element Order

Within each diffusion time step the displacements for the mechanical response (MR) problem is solved while holding the concentration field constant. The resultant displacements are then used to calculate the strain (dilatation) and stress (pressure) state. The pressure and dilatation are then used as inputs to the diffusion process (DP). A problem of solution or finite element compatibility occurs when the pressure field is "fed" back into the DP or when the concentration is "fed" into the MR problem. The issue arises because the accuracy of the solutions, either the displacements or the concentrations, is dictated by the shape functions used to define the finite element[17]. As an illustration, the MR element uses an displacement formulation and the stresses are basically derived from the derivatives of the resultant displacements. The implications of this are, first, that a linear finite element (an element which can capture a linear variation in the displacement) can at best only describe a constant stress (pressure) state. Likewise, a parabolic element can at best only capture a linear variation in the stress (pressure). Therefore when the pressure values are "fed" into the DP element, they must reflect the correct variation from which they were derived.

Since the pressure enters the diffusion equation through its spatial gradient, if a linear element were used to solve the MR problem, the resultant gradient in pressure should be zero. Hence to have any effect on the DP problem a parabolic or higher order element must be used in solving for the MR displacements.

In a similar vein the concentration enters the MR problem through the constitutive law (which relates the stresses and strains), thus to have a consistent representation, the elemental variation in concentration should be the same as that for the stresses and strains.

These two compatibility issues can be resolved by using two different ordered elements for each of the two problems, the order of an element is the type of solution field that the element can capture accurately. Hence a first order or linear element can capture accurately a linear variation in the solution. To resolve the compatibility issue, the DP element selected should be one order less then that of the MR element. For this study, in an effort to balance solution accuracy against computational effort, a parabolic 8-noded quadralateral element is used for the MR displacement solution (see Fig. A3.1A). (A parabolic 8-noded quadralateral element can accurately capture a parabolic variation in the displacement field.) Once this choice was made the compatibility requirement leads one to choose a linear 4-noded quadralateral element to solve for DP problem (see Fig. A3.1B). (A linear 4-noded quadralateral can accurately capture a linear variation in concentration.)

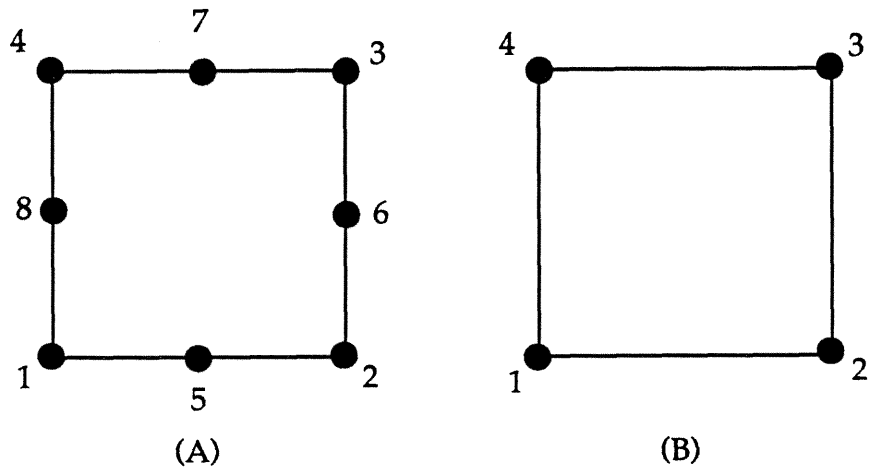


Figure A3.1 (A) a parabolic 8-noded element which can capture a parabolic variation of the nodal parameter. (B) A linear 4-noded element which can capture a linear variation of the nodal parameter.

The numerical implementation involved in using different ordered elements is fairly simple. The elements are defined using the same nodal positions (i.e., the finite element mesh of the region is the same for both problems). But during the formulation of the stiffness matrix for the DP element, linear shape functions are used to define the matrix, the nondiagonal elements of the row and columns for the midpoint nodes (nodes 5, 6, 7, 8) are set to zero, and the diagonal position is set to unity. This alteration causes the matrix equation solver not solve for the midpoint nodes of the element. After the corner nodal concentration values are determined (nodes 1, 2, 3, 4) the midpoint nodes are then calculated by linear interpolation using the corner nodal values as a reference. In this manner the concentration field for the 8-noded element is forced to be linear.

Unlike the displacements, the pressure values (for a parabolic 8-noded element) are evaluated at the Gauss points of the element where they are most accurate. But in the formulation of the DP finite element the nodal pressure values are needed. To accomplish this and to maintain the

pressure field accuracy, the Gauss point-derived pressure values are then smoothed to the nodal position using a technique decribed in the next section.

## A4 Pressure Smoothing Technique

To smooth the pressure values evaluated at the element's Gauss points to the nodal position; a technique described by Hinton and Campbell[14] is used. An abrigded description of their work is shown here.

For each element a smoothing matrix $[S]^e$ is formed and is given by

$$[S]^e = \int_V \left\{N^e\right\}\left\langle N^e\right\rangle dV^e \tag{A4.1}$$

where $\left\{N^e\right\}$ are the shape functions used to define the element.

The "forcing" vector consists of the Gauss point-determined pressure values as is represented as

$$\{F\}^e = \int_{V^e} \left\{N^e\right\} P^e dV^e \tag{A4.2}$$

The evaluation of the volume integrals are performed by Gaussian integration where the pressure values are known.

Following standard finite element techniques to assemble the element matrices and forcing vectors, a global smoothing matrix equation is derived

$$[S]\{P\} = \{F\} \tag{A4.3}$$

where $\{P\}$ is the vector representing the nodal pressure values.

The actual evaluation of the nodal pressure values is relatively cheap since $[S]$ does not change throughout the problem. Hence once $[S]$ is inverted the pressure values can be solved by

$$\{P\} = [S]^{-1}\{F\} \tag{A4.4}$$

This smoothing scheme was evaluated in one-dimension by using a 3-node parabolic element to evaluate the MR problem and the pressure smoothing was performed using a linear element. The results comparing the derivatives of the exact and "smoothed" pressure fields are shown in Figs. A4.1 and A4.2. In Fig. A4.1 the exact pressure is linear within the region and, as expected, the smoothed pressure captures the variation exactly. The exact pressure field in Fig. A4.2 varies parabolically and the "smoothed" pressure field can only approximate the solution, but as more elements are added the solution converges to the exact value.

It is assumed that similar behavior will occur for a two-dimensional problem so the numerical scheme incorporated in this study uses an 8-noded parabolic quadralateral element to evaluate the MR problem and the pressure smoothing will be performed by using a 4-noded linear quadralateral element.

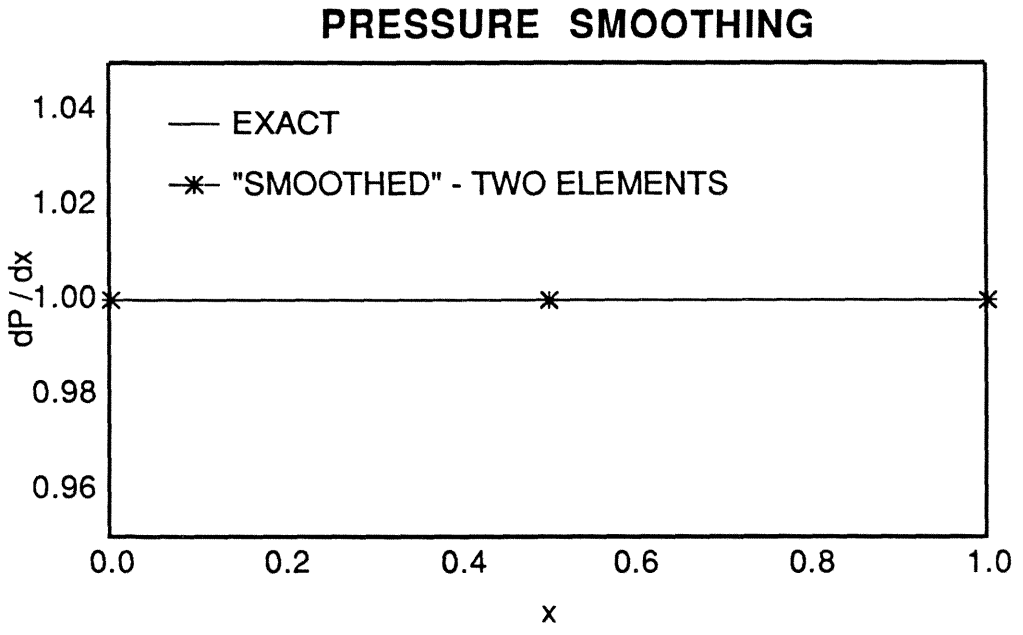


Figure A4.1 MR problem solved using parabolic elements and where the pressure field is "smoothed" using linear elements. The exact pressure field is $P(x) = x$.

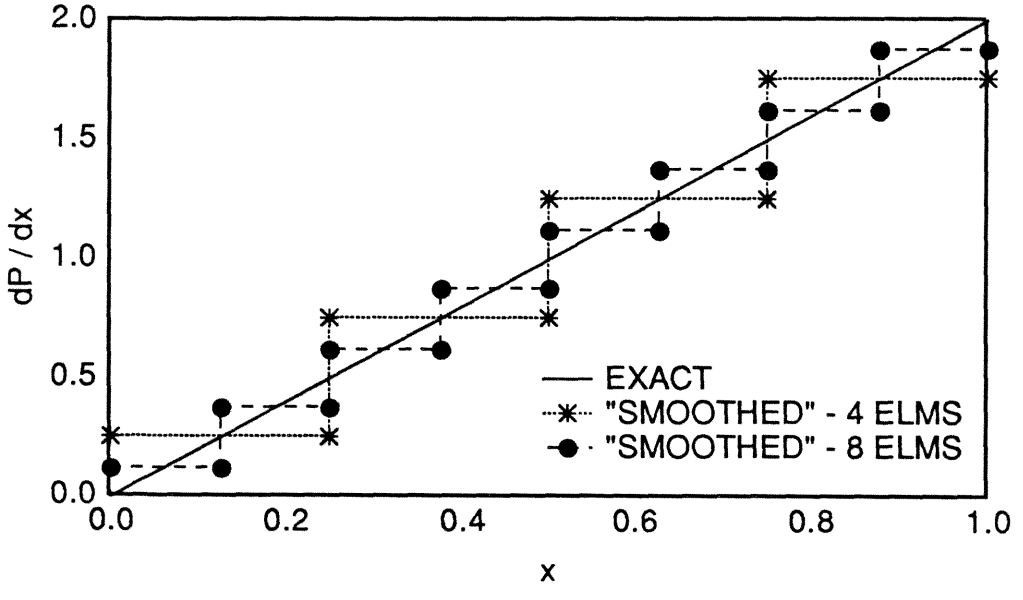


Figure A4.2 MR problem solved using parabolic elements and where the pressure field is "smoothed" using linear elements. The exact pressure field is $P(x) = x^2$.

# References


1. Aitken, A., and Barrer, R. M., "Transport and Solubility of Isometric Paraffins in Rubber," *Trans. Faraday*, **51**, pp. 116-130 (1955).
2. Bearman, R. J., "On the Molecular Basis of Some Current Theories of Diffusion," *J. Phys. Chem.*, **65**, pp. 1961-1968 (1961).
3. Cohen, M., and Turnbull, D., "Molecular Transport in Liquids and Glasses," *J. Chem. Phys.*, **31**, pp. 1164-1169 (1959).
4. Cox, R. W., and Cohen, D. S., "A Mathematical Model for Stress-Driven Diffusion in Polymers," *J. Poly. Sci., Poly. Phys.*, **27**, pp. 589-602 (1989).
5. Crank, J., "The Mathematics of Diffusion," Oxford Press, London, (1956).
6. Crank, J., and Park, G. S., "Diffusion in Polymers," Academic Press, Inc., New York, NY, (1968).
7. Doolittle, A. K., "Studies in Newtonian Flow. II. The Dependence of the Viscosity of Liquids on Free Space," *J. Appl. Phys.*, **22**, pp. 1471-1475 (1951).
8. Ferry, J. D., "Concentrated Solutions, Plasticized Polymers, and Gels," in *Viscoelastic Properties of Polymers*. Wiley & Sons, Inc., New York, NY. pp. 486-544 (1980).
9. Ferry, J. D., "Dependence of Viscoelastic Behavior on Temperature and Pressure," in *Viscoelastic Properties of Polymers*. Wiley & Sons, Inc., New York, NY. pp. 264-320 (1980).
10. Fujita, H., "Diffusion in Polymer-Diluent Systems," in *Fortschr. Hochpolym.-Forsch.* **3**, pp. 1-47 (1961).

11. Gall, T.P., Lasky, R.C., and Kramer, E.J., "Case II Diffusion: Effect of Solvent Molecule Size," *Poly.*, **31**, pp. 1491-1499 (1990).

12. Gillat, O., and Broutman, L. J., "Effect of an External Stress on Moisture Diffusion and Degradation in a Graphite-Reinforced Epoxy Laminate," *Adv. Comp. Mat.*, **ASTM STP 658**, pp. 61-83 (1978).

13. Hayes, M. J., and Park, G. S., "The Diffusion of Benzene in Rubber; Part 1. Low Concentrations of Benzene," *Trans. Faraday*, **51**, pp. 1134-1142 (1955).

14. Hinton, E., and Campbell, J. S., "Local and Global Smoothing of Discontinous Finite Element Functions Using a Least Squares Method," *Int. J. Num. Meth. Eng.*, **8**, pp. 461-480 (1974).

15. Knauss, W. G., and Kenner, V. H., "On the Hygrothermomechanical Characterization of Polyvinyl Acetate," *J. Appl. Phys.*, **51**, pp. 5131-5136 (1980).

16. Knauss, W. G., and Shimabukuro, S. R., High Temperature Adhesive Systems, Contract N00014-85-C-0881; HAC. Ref. No. F7896, Hughes Aircraft Company Electro-Optical & Data Systems Group (1986).

17. Knauss, W. G., and Shimabukuro, S. R., High Temperature Adhesive Systems, Contract N00014-85-C-0881; HAC. REF. NO. F7896, Hughes Aircraft Company, Electro-Optical & Data Systems Group (1988).

18. Lefebvre, D. R., Dillard, D. A., and Ward, T. C., "A Model for the Diffusion of Moisture in Adhesive Joints; Part I: Governing Equations," *J. Adhes*, **27**, pp. 1-18 (1989).

19. Long, F. A., and Richman, D., "Concentration Gradients for Diffusion of Vapors in Glassy Polymers and Their Relation to Time Dependent Diffusion Phenomena," *J. Am. Chem. Soc*, **82**, pp. 513-519 (1960).

20. Losi, G., "Nonlinear Thermoviscoelastic Behavior of Polymers", Ph'd Thesis, California Institute of Technology, Pasadena, CA (1990).

21. Prigogine, I., "Introduction to Thermodynamics of Irreversible Processes," Wiley & Sons, New York, NY (1961).

22. Shmorhunt, M., Jamieson, A. M., and Simha, R., "Free Volume Changes in Epoxy Adhesives During Physical Ageing; Fluorescence Spectroscopy and Mechanical Stress Relaxation," *Poly.*, **31**, pp. 812-817 (1990).

23. Thomas, N. L., and Windle, A. H., "A Deformation Model for Case II Diffusion," *Polym.*, **21**, pp. 613-619 (1980).

24. Thomas, N. L., and Windle, A. H., "A Theory of Case II Diffusion," *Polym*, **23**, pp. 529-542 (1982).

25. Tirrell, M., and Malone, M. F., "Stress-Induced Diffusion of Macromolecules," *J. Poly. Sci., Poly. Phys. Ed.*, **15**, pp. 1569-1583 (1977).

26. Tyrrell, H. J. V., "Diffusion and Heat Flow in Liquids," Butterworth & Co., Inc., Washington D.C (1961).

27. Vrentas, J. S., and Duda, J. L., "Diffusion in Polymer-Solvent Systems. I. Reexamination of the Free-Volume Theory," *J. Poly. Sci., Poly. Phys. Ed.*, **15**, pp. 403-416 (1977).

28. Vrentas, J. S., and Duda, J. L., "Molecular Diffusion in Polymer Solutions," *AIChE Jour.*, **25**, pp. 1-24 (1979).

29. Weitsman, Y., "A Continuum Diffusion Model for Viscoelastic Materials," *J. Phys. Chem.*, **94**, pp. 961-968 (1990).

30. Williams, M. L., Landel, R. F., and Ferry, J. D., "The Temperature dependence of Relaxation Mechanisms in Amorphous Polymers and Other Glass-forming Liquids," *J. Amer. Chem. Soc.*, **77**, pp. 3701 (1955).

31. Wood, W. L., and Lewis, R. W., "A Comparison of Time Marching Schemes for the Transient Heat Conduction Equation," *Int. J. Num. Meth. Eng.*, **9**, pp. 679-689 (1975).

32. Zienkiewicz, O. C., and Taylor, R. L., "Ch15 - Computer Procedures for Finite Element Analysis," in *Finite Element Method*. McGraw Hill, pp. 436-495 .